

# Cellular Automata Technique for Computational Electromagnetics

Ming Zhang

A thesis

Presented to the University of Manitoba  
in partial fulfilment of the requirements for the degree  
of Doctor of Philosophy  
in  
Electrical Engineering

Winnipeg, Manitoba, Canada 2002

©Ming Zhang 2002



National Library  
of Canada

Acquisitions and  
Bibliographic Services

395 Wellington Street  
Ottawa ON K1A 0N4  
Canada

Bibliothèque nationale  
du Canada

Acquisitions et  
services bibliographiques

395, rue Wellington  
Ottawa ON K1A 0N4  
Canada

*Your file Votre référence*

*Our file Notre référence*

The author has granted a non-exclusive licence allowing the National Library of Canada to reproduce, loan, distribute or sell copies of this thesis in microform, paper or electronic formats.

The author retains ownership of the copyright in this thesis. Neither the thesis nor substantial extracts from it may be printed or otherwise reproduced without the author's permission.

L'auteur a accordé une licence non exclusive permettant à la Bibliothèque nationale du Canada de reproduire, prêter, distribuer ou vendre des copies de cette thèse sous la forme de microfiche/film, de reproduction sur papier ou sur format électronique.

L'auteur conserve la propriété du droit d'auteur qui protège cette thèse. Ni la thèse ni des extraits substantiels de celle-ci ne doivent être imprimés ou autrement reproduits sans son autorisation.

0-612-79917-4

**THE UNIVERSITY OF MANITOBA**  
**FACULTY OF GRADUATE STUDIES**  
\*\*\*\*\*  
**COPYRIGHT PERMISSION PAGE**

**CELLULAR AUTOMATA TECHNIQUE FOR  
COMPUTATIONAL ELECTROMAGNETICS**

**BY**

**Ming Zhang**

**A Thesis/Practicum submitted to the Faculty of Graduate Studies of The University  
of Manitoba in partial fulfillment of the requirements of the degree  
of**

**DOCTOR OF PHILOSOPHY**

**MING ZHANG ©2002**

**Permission has been granted to the Library of The University of Manitoba to lend or sell copies of this thesis/practicum, to the National Library of Canada to microfilm this thesis and to lend or sell copies of the film, and to University Microfilm Inc. to publish an abstract of this thesis/practicum.**

**The author reserves other publication rights, and neither this thesis/practicum nor extensive extracts from it may be printed or otherwise reproduced without the author's written permission.**

## ABSTRACT

Lattice Gas Automata (*LGA*) can be considered as an alternative to the conventional differential equation description of problems in electromagnetics. *LGAs* are discrete dynamical systems that are based on a microscopic model of the physics being simulated. The basic constituents of an *LGA* are discrete cells. These cells are interconnected according to certain symmetric requirements to form an extremely large regular lattice. The cells of an *LGA* are extremely simple, requiring only a few bits to completely describe their states. Even though they are simple, the collective behaviour of *LGA* microscopic systems is capable of exhibiting those behaviours described by partial differential equations for real physical systems. The inherent parallelism and simplicity of *LGA* algorithms make them ideally suited to implementation in a parallel processing architecture which can be effectively realized with special-purpose cellular automata machines. The objective of this research is to explore and develop the potential of cellular automata as mathematical tools for electromagnetic modelling.

In two-dimensional applications, a new *HPP*-type mixture *LGA* algorithm is presented for modelling wave propagation in inhomogeneous media. It can be analytically shown that change in sound speed of an *LGA* can be achieved by incorporating rest bits at a lattice site, as well as moving or interaction bits. It will also be shown that a simple mixture *LGA* will behave according to the linear scalar wave equation. Thus, by making an analogy between a fluid and two-dimension electromagnetic field parameters, we can utilize this simple particle interaction paradigm as a tool for two-dimensional inhomogeneous electromagnetic problems.

However, the problem of developing *LGA* vector models for modelling three dimensional electromagnetic phenomena is more difficult since there is no a direct analogy between fluid and three-dimensional vector electromagnetic fields. By considering the inherent property of electromagnetic fields, an *LGA* vector algorithm for modelling three-dimensional vector electromagnetic fields is constructed. We show how, in the macroscopic limit, the three-dimensional Maxwell's equations can be derived from the *LGA* vector model.



## Acknowledgments

First of all I would like to express my sincere gratitude to my supervisor, Dr. Greg Bridges, for his guidance, patience, continuous encouragement, helpful discussion and friendship throughout the course of this research. I deeply appreciate the help of Dr. N. Simons, Dr. A. Sebek, Dr. L. Shafai and Dr. Southern and all the staff of the Electrical and Computer Engineering Department.

I would also like to thank my friends and fellow graduate students, particularly Nikhil and Dino, for their friendship and their help whenever I needed.

Special thanks are due to my friend, Richard Ellis and his family, who have always been eager to provide all kind of help for me and for my family since the first day we landed in Winnipeg. They made us feel at home every Christmas and Chinese New Year party.

I would like to thank my parents, parents-in-law, my two sisters (Hong and Feng Zhang) and their family for their faith and encouragement. Special thanks to my wife Lihua, my daughter Cathy for their patience and support.

Finally, all this would have not been possible without the steady and substantial support from my father, who insisted that I leave him to complete this degree even though he was suffering of a terrible heart attack in China.

# Contents

Abstract	i
Acknowledgments	ii
Table of Contents	iii
List of Figures	vi
List of Tables	viii
Acronyms and Symbols	ix
<b>1 Introduction</b>	<b>1</b>
<b>2 Lattice Gas Automata</b>	<b>11</b>
2.1 Introduction - - - - -	11
2.2 Two Dimensional Lattice Gas Models - - - - -	12
2.2.1 The <i>HPP</i> Model - - - - -	12
2.2.2 The <i>FHP</i> Model - - - - -	14
2.2.3 Mixture Models of <i>HPP</i> or <i>FHP</i> - - - - -	17
2.2.4 Microdynamic and Macroscopic Observables - - - - -	19
2.2.4.1 Microdynamic States of <i>LGAs</i> - - - - -	19
2.2.4.2 Microdynamics of <i>LGAs</i> - - - - -	22
2.2.4.3 Dynamical description for <i>HPP LGA</i> - - - - -	23

2.2.4.4 Dynamical description for <i>FHP</i> - - - - -	24
2.2.4.5 Dynamical description for Mixture Model - - - - -	25
2.2.4.6 Conserved Quantities of Two Dimensional <i>LGAs</i> - - -	26
2.3 Three-Dimensional Lattice Gas Model - - - - -	27
2.3.1 Three-Dimensional Lattice Gas Model - - - - -	27
2.3.2 Dynamic States of 3-d Vector <i>LGA</i> - - - - -	33
2.3.3 Dynamic Description of 3-d Vector <i>LGA</i> - - - - -	34
2.3.4 Conserved Quantities of 3-d Vector <i>LGA</i> - - - - -	36
2.4 Macroscopic Observables - - - - -	37
2.5 Review of Lattice Gas Theory - - - - -	40
2.5.1 Collision Operator - - - - -	40
2.5.2 Semi-Detailed Balance and Ensemble Average - - - - -	44
2.5.2.1 Ensemble Average - - - - -	44
2.5.2.2 Semi-Detailed Balance and Equilibrium Distribution - -	46
2.6 <i>CAM</i> -8 Cellular Automata Machine - - - - -	47
<b>3 Mixture Lattice Gas Automata</b>	<b>50</b>
3.1 Introduction - - - - -	50
3.2 Theoretical Analysis for the Mixture Model - - - - -	51
3.2.1 Lattice Boltzmann Equation - - - - -	51
3.2.2 The Equilibrium Distribution - - - - -	52
3.2.3 Chapman-Enskog Expansion and Conservation Laws - - - -	59

3.2.3.1 Mass Conservation - - - - -	60
3.2.3.2 Momentum Conservation (Euler Equation) - - - - -	63
3.2.4 Undamped Sound Wave - - - - -	65
3.2.5 Sound Speed and Dielectric Constant - - - - -	66
3.3 Numerical Simulations and Results - - - - -	70
<b>4 Three - Dimensional Vector Lattice Gas Automata</b>	<b>89</b>
4.1 Introduction - - - - -	89
4.2 Macrodynamics and Solution for <i>3-d vector LGA</i> - - - - -	90
4.3 Macroscopic Property and Conserved Quantity- - - - -	98
4.4 <i>3-d</i> Vector <i>LGA</i> and Maxwell's Equations - - - - -	102
4.4 Results of Numerical Experiments - - - - -	111
<b>5 Summary and Proposed Works</b>	<b>120</b>
5.1 Preliminary Benchmarks - - - - -	120
5.2 Main Contributions - - - - -	124
5.3 Discussion and Proposed Future Works - - - - -	125
<b>6 Reference</b>	<b>129</b>
<b>Appendix A</b>	<b>135</b>
<b>Appendix B</b>	<b>147</b>

## List of Figures

2.1	Operation on the <i>HPP</i> gas automaton over a single time step - - - - -	12
2.2	Collision rules for the <i>HPP LGA</i> - - - - -	13
2.3	Operation on the <i>FHP</i> gas automaton over a single time step - - - - -	15
2.4	Examples of possible <i>FHP</i> lattice collision rules - - - - -	17
2.5	<i>LGA</i> rule with three weighted rest particles- - - - -	19
2.6	<i>LGA</i> mixture model with $b_r$ probabilistically weighted rest particles -	19
2.7	<i>LGA</i> rule with $b_r$ probabilistically weighted rest particles - - - - -	22
2.8	A small portion of a three-dimensional cubic lattice - - - - -	29
2.9	Four polarization vectors of a given velocity vector - - - - -	29
2.10	One example of the collision rules for the positive vector lattice gas automata - - - - -	31
2.11	One example of the collision rules for the negative vector lattice gas automata - - - - -	32
2.12	Twelve particles of the three-dimensional vector <i>LGA</i> - - - - -	33
2.13	Macroscopic quantities as obtained through spatial averaging of microscopic states over a region $R$ - - - - -	39
2.14	Basic operations of CAM_8 - - - - -	49
3.1	Theoretical results for dielectric constants $\epsilon_r$ versus the combinations of rest particle mixture ratios- - - - -	69

3.2 Time domain waveforms for model 1 - - - - -	77
3.3 Equilibrium for the models with two rest particles - - - - -	77
3.4 Propagation speed for the two mixture models - - - - -	78
3.5 Snapshot of gaussian plane wave propagating through a dielectric solid cylinder with $\epsilon_r = 5$ (radius $a = 20l$ ) - - - - -	82
3.6 Snapshot of gaussian plane wave propagating through a dielectric solid cylindrical shell with $\epsilon_r = 21$ (inner radius $a=80l$ and outer radius $b=100l$ ) - - - - -	83
3.7 Time-domain electric field intensity inside the dielectric cylinder with a) $\epsilon_r = 5$ and b) $\epsilon_r = 21$ - - - - -	84
3.8 Time-domain electric field intensity inside a dielectric cylindrical shell with a) $\epsilon_r = 5$ and b) $\epsilon_r = 21$ - - - - -	85
3.9 Cross section of human torso model for a 3.4 mm resolution lattice used in the LGA simulation. Permittivity values for eight different tissues range from $\epsilon_r = 6$ for fat to $\epsilon_r = 62$ for blood - - - - -	86
3.10 Image of the instantaneous field intensity for harmonic plane wave incidence on the cross section of the human torso model at 975MHz - -	88
4.1 Gaussian pulsed plane wave propagating in a cavity - - - - -	115
4.2 Transient electric field intensity( $f = 0.5$ ) of Gaussian pulsed plane wave- - - - -	116
4.3 Transient electric field intensity( $f = 0.7$ ) of Gaussian pulsed plane wave- - - - -	117
4.4 $TM_{111}$ Mode wave propagating in a cubic cavity - - - - -	118
4.5 Time-Domain electric field intensity in a cavity excited by $TM_{111}$ - -	119

## List of Tables

3.1a	Collision Model 1: case A	73
3.2a	Collision Model 2: case A	73
3.1b	Collision Model 1: case B	74
3.2b	Collision Model 2: case B	74
3.1c	Collision Model 1: case C	74
3.2c	Collision Model 2: case C	74
3.1d	Collision Model 1: case D	75
3.2d	Collision Model 2: case D	75
3.3	Body cross-section model	87

## Acronym and Symbols

<i>CA</i>	=	Lattice Gas Automata;
<i>LGA</i>	=	Lattice Gas Automata;
<i>HPP</i>	=	Initials of the inventors of Hardy, Pazzi and Pomeau;
<i>HPP LGA</i>	=	An lattice gas automata with square unit cell;
<i>FHP</i>	=	Initials of the inventors of Frisch, Hasslacher and Pomeau;
<i>FHP LGA</i>	=	An lattice gas automata with hexagonal unit cell;
<i>CAM-8</i>	=	A special-purpose computation hardware for cellular automata simulation;
<i>TLM</i>	=	Transmission Line Matrix;
<i>FDTD</i>	=	Finite difference time-domain;
$n_i (x, t)$	=	Two-dimensional binary (bit) variables at position $x$ of the <i>LGA</i> at time $t$ ;
$n^\dagger(x, t)$	=	A complete set of bit variables $n_i (x, t)$ located at site $x$ and time $t$ ;
$\omega_i(x, t)$	=	Two-dimensional collision operators located at site $x$ and time $t$ ;
$S_{K i}(x, t)$	=	Three-dimensional binary (bit) variables at located at site $x$ and time $t$ , propagating in $K$ direction and polarized $i$ ;
$\omega_{Ki}(x, t)$	=	Three-dimensional collision operators located at site $x$ and time $t$ ;



$\langle \rangle$	=	Ensemble averages over lattice;
$N_i(\mathbf{x}, t)$	=	Mean population binary (bit) variable $i$ at position $\mathbf{x}$ of the <i>LGA</i> at time $t$ ;
$\Omega_i(\mathbf{x}, t)$	=	Ensemble average of collision operator $i$ at position $\mathbf{x}$ of the <i>LGA</i> at time $t$ ;
$N^\dagger(\mathbf{x}, t)$	=	Ensemble average of $n^\dagger(\mathbf{x}, t)$ ;
$N_i^{eq}(\mathbf{x}, t)$	=	Mean population of binary (bit) variable $i$ at equilibrium;
$\mathbf{u}$	=	Flow velocity of fluid;
$\rho$	=	Particle density of fluid;
$c_s$	=	Sound speed of fluid;
$d$	=	Particle density per cell;
$d_k$	=	Rest particle density per cell;

---

## Chapter 1. Introduction

The objective of this research is to explore and develop the potential of cellular automata as mathematical tools for electromagnetic modelling. Investigation of electromagnetic phenomena have conventionally been based on partial differential equations, Maxwell's equations. Two general techniques can be applied to the solution of Maxwell's equations. These are analytical and numerical methods. Numerical methods can be further classified in two classes[1]. The first involves the numerical solution of integral-equation formulations and the second involves the numerical solution of differential-equation formulations.

Analytical techniques are limited to specific geometries, which conform to specific coordinates systems[2]. It is generally not possible to obtain complete solutions to an arbitrary problem. In most cases one must resort to a variety of numerical approaches with the aid of digital computers.

Integral-equation formulations are obtained through the use of source representations for the unknown field distributions. A detail review of numerical methods based on integral-equation formulations of electromagnetic field problems can be found in [1,3,4]. Using physical or physical-equivalent sources (corresponding to electrical and magnetic currents and densities), and a Green's function (to take into account any analytically solvable geometrical aspects of the problem [5]), a mathematical statement can be made in the form of an intergral equation. The unknowns are usually current and charge densities, and are deter-

---

mined through the discretization of the mathematical formulation using the Method of Moments or Boundary element method for example. The discretization is limited within defined regions or on their surfaces with finite geometric dimensions. This usually results in a system with a dense matrix equation.

Differential-equation formulations involves the determination of approximate solutions by direct approximation of Maxwell's equations. The direct approximation can be considered as the formulation which applies Maxwell's equations locally. Due to the locality of the formulations, it is capable of treating medium heterogeneities, nonlinearities, and time variations in a straightforward manner. A detailed review of these methods can be found in [6,7,8]. The numerical solution of these equations is obtained via the application of techniques such as the time-domain finite-element, time-domain finite-difference, and transmission-line matrix methods. Since Maxwell's equations are satisfied throughout the entire spatial domain of a problem, the region of discretization is all space in which a non-zero field distribution exists. For a open region problems, an absorbing boundary condition(ABC) is required to limit the spatial domain of the problem to a finite size and enforce the radiation condition on the field distributions.

Based on the spatially discrete form of the mathematical formulations, selection of time or frequency domain for the solution is required. Solutions to the time dependent formulations described above (time-domain finite-elements and finite-difference) yield transient solutions for a given excitation. For certain electromagnetic compatibility and electromagnetic interference (EMC/EMI) problems, the transient response analysis is required. For most antenna application and radar-cross-section analysis, however, frequency domain

---

results are desired due to their time harmonic excitation (single frequency).

Although many differences in the above techniques appear, computation is not directly considered in the development of the numerical models. The assumption is made that the implementation (programming and hardware) will be performed on a general-purpose computer. This is partially due to the availability, flexibility, and low-cost of general-purpose computers. The computers can, however, represent such formulations only approximately. While formulations involve continuous variables, digital computers can only treat discrete digital quantities. The real numbers that correspond to continuous variables in the formulations must be represented on the computer by packets of bits, typically in the form of 32- or 64-bit numbers in floating point format. In current computational physics, much effort has been spent both to show that, with sufficiently fine grids, solutions to continuum equations can be found, and also to study error in these solutions[9,10]. For many complex applications, computational physics increasingly requires computational resources. For instance, high-performance computers are often measured in terms of the rate at which they can carry out the floating points operations needed. The situation leads to view that the traditional formulation of physical problems in terms of differential equations is not a computationally reasonable representation of physical phenomena and alternative representation should be pursued[9,10].

The Cellular Automata (CA) approach is a departure from traditional formulation. It may offer a more efficient computational technique. A cellular automaton consists of discrete lattice cells. Each cell takes on a finite set of discrete values. Thus the system can be described by binary variables. The values of each cell are updated in a sequence of discrete timesteps according to logical rules which depend only on the values of cells in a local

---

neighbourhood. The inherent parallelism and simplicity of processing elements make cellular automata attractive for simulating and studying physical processes. In the early 1980's, Wolfram demonstrated that, even with very simple rules, it is possible for cellular automata to exhibit complex dynamical behaviour [10]. Often these behaviours show striking similarities to the forms observed in many natural systems. Toffoli [11] noted the phenomena and indicated that cellular automata can serve as models to simulate many complex physical and mathematical systems. Some examples include studies of time-reversible automata [12], quantum lattice-gas models for the many-particle Schrodinger equation [13] and simulation of cellular automata for quantum field problem [14].

One of the most remarkable results of studies on cellular automata was the successful application of the lattice gas automata (*LGA*) (a class of cellular automata to be introduced later in this chapter) to the modelling of fluid dynamics [15,16,17]. This was the first concrete example of a cellular automata model reproducing partial-differential equations (Navier-Stokes equations) in the macroscopic limit. Frisch, Hasslacher, and Pomeau showed how the Navier-Stokes equations could be derived from a microdynamics consisting of an artificial set of rules for collision and propagation of identical particles. Since then, many authors and researchers modified, refined and extended cellular automata approaches in different areas involving many interesting ramifications in hydrodynamics. *LGA* gave rise to some new ideas for constructing models to predict certain complex fluids, including fluid mixtures involving multiphase flows, phase transitions and complex turbulent phenomena of fluids [17,18,19,20].

Research efforts have been made by some authors toward modelling electromagnetic phenomena with cellular automata approaches. For example, Bornholdt and Tatalias [21]

---

presented some background information and strategies for the development of possible rules regarding the modelling of scalar waves. Thiele [22] discussed the optimal parallel architecture of cellular automata for simulating electromagnetic phenomena. However, concrete examples about computational experiments or details regarding the application to modelling electromagnetic phenomena are not available. Recently, N. Simons and G. Bridges *et al.* successfully exploited the use of lattice gas automata for the analysis of complex electromagnetic field problems. In their papers [23,24] and N. Simons' Thesis [25], they presented concrete algorithms for two-dimensional *HPP LGA* [26] models, and implemented these models on the *CAM-8* cellular automata machine (*CAM*) [27]. Experiments for some electromagnetic field problems were carried out using the machine. Their experimental results showed correct quantitative behaviour and reasonable accuracy. Based on their basic *LGA* algorithm, they extended the theory to modelling electrically large and spatially inhomogeneous two-dimensional electromagnetic field problems, such as the interaction of an electromagnetic wave with complex biological systems. Their work [28] showed how an *LGA* algorithm is capable of simulating inhomogeneous dielectric structures with a wide range of dielectric constant. Most recently, initial success in modelling three-dimensional electromagnetic field problems has been achieved [29]. Several three-dimensional vector *LGA* models have been developed for the modelling of electromagnetic phenomena.

Exploitation of cellular automata as a mathematical tool for electromagnetic modelling includes three main aspects. These aspects can be considered in the following progression:

- Development of a specific lattice gas automata model.

- 
- Implementation on a cellular automata machine (CAM).
  - Simulations on the CAM and analysis of the model.

The development of an *LGA* model involves finding an optimal microscopic dynamic description for the physical system(s) in terms of a cellular automata algorithm. An *LGA* is a discrete dynamic system which consists of a lattice of identical cells. The time evolution of the system is governed by a local dynamic law (or rule) which acts on all cells simultaneously in parallel, and is the same throughout space for all times. Such a description involves the specification of a rule. This rule determines how the state of each cell at the next timestep can be determined by the current states of a finite number of its neighbours. In addition to this basic lattice gas format, other properties such as the geometrical symmetry of the lattice, reversibility and conservation of some physical quantities may also be imposed. The most important problem when developing a lattice gas model is the specification of a rule that yields the desired underlying physical phenomena while maintaining these constraints.

Computational experiments are intended to be carried out on cellular automata machines (CAMs) which are specifically designed for simulating cellular automata. The latest machine available is the *CAM-8* [27]. *CAM-8* is implemented with simple 16-bit logical operations at each of 32 million computing sites (cells). It can perform 200 million site updates per second. This performance is equivalent to that of a *Connection Machine* or a *Cray* supercomputer, but the *CAM-8* can be used to simulate cellular automata at a fraction of the cost of using a *Connection Machine* or *Cray* supercomputer [30]. Thus the machine provides an ideal computational environment for cellular automaton modelling of complex

---

electromagnetic field problems.

The final step in the above progression, simulation on a CA followed by analysis of the model(s), is required to study the macroscopic behaviour in a physical system. This can be done by considering values of collective quantities, such as particle density or momentum density, or other macroscopic quantities (polarization and so on). These are obtained by averaging over a large lattice region. If the CA model(s) is well constructed, one can expect that the collective behaviour should be capable of exhibiting that behaviour described by partial differential equations for a real physical system. In addition to observing the macroscopic behaviour, the validity of CA model(s) can be analysed by considering some fundamental physical principles such as reversibility, conservation laws and so on. This is because, if a CA model is explicitly constructed, each step or feature of the construction is specifically designed to have particular known consequences relating to these principles. As well, a study of spurious behaviour and non-dualities has to be considered. The former, due to the *LGA* algorithm, causes a problem of spurious conservation laws [31,33], while the latter, resulting from the lattice discretization, leads to the anisotropy of a physical field represented by an *LGA* model.

Another very important aspect in developing an *LGA* approach in computational physics is the provision of a mathematical analysis of the *LGA* model. This analysis is based on using fundamental physical principles to demonstrate how a simple *LGA* model can be used to simulate a real physical system, and determining the limitations of the *LGA* model. Much development in this direction has been done in the modelling of fluid dynamics [31,32,33,34], but only a few efforts [28,29] have been made in computational electromagnetics. One of the most important aspects of the research is to provide the provision of math-



---

emational analysis and demonstrate that our *LGA*s models are indeed solving the requisite partial differential equations.

In two dimensional cases, the analysis involves proving the validity of the simplest *HPP LGA* for modelling electromagnetic propagation and scattering in lossless inhomogeneous media, and deriving a comprehensive expression for the sound speed defined on our mixture lattices. This expression indicates how to model the media with different sound speeds, analogous to the modelling of different dielectric constants in lossless inhomogeneous media of electromagnetics.

The problem of developing *LGA* vector models for modelling three dimensional electromagnetic phenomena, and providing physical interpretation for these models, is more challenging than two-dimensional *LGA* models, where a great number of theoretic analyses have been done for applications to fluid dynamics. Some concepts, methods and simulating algorithms of these analyses have been used in two-dimensional electromagnetic modelling. For three-dimensional modelling, initial success has been achieved by setting up a vector *LGA* model which conserves energy and polarization. Some simulation experiments for some electromagnetic problems have been designed and carried out. These show close agreement with those results obtained using the traditional numerical electromagnetic method. A theoretical analysis in the three-dimensional case has been made by using *LGA* theory and the mathematical method, which is similar to the Transmission Line Matrix Method (*TLM*) method[8,35]. This analysis shows how the three dimensional *Maxwell's* equations can be derived from the model.

Chapter 2 of the thesis introduces cellular lattice gas automata (*LGA*), and reviews some of the models that have been developed and used to model computational electromagnetic

---

problems. In this chapter, the basic format of these models and their applications in two and three-dimensional problems are presented. Microscopic and macroscopic descriptions of these *LGA* models are then given. Some of the basic concepts of *LGA* theory, such as ensemble average, detailed and semi-detailed balance and the equilibrium particle distribution function, are also briefly discussed. Finally, in chapter 2, an introduction to the *CA* machine is presented. A *CA* machine is equipped with special hardware to undertake cellular automaton simulation.

A mixture *LGA* model which is not limited to a uniform or a concrete configuration of rest particles is presented in chapter 3. Detailed analysis is developed to show how this model can be applied to the simulation of two-dimensional electromagnetic phenomena in lossless inhomogeneous media. In the analysis, fundamental principles of geometric symmetry of the lattice, equilibrium distribution of particles are considered.

The damping effect associated with the viscosity of the *LGA* can generally not be analogously used to model the conductivity coefficient of lossy media for the wave attenuation in electromagnetics[28]. Thus, the analysis will be concentrated on the modelling of linear wave behaviour, and ended up with an *Euler's* equation [31,33]. Results for particle density and sound speed obtained from specially designed numerical experiments are compared with the theory to confirm the validity of the model. A great number of simulations using various mixture models for the electromagnetic wave propagation in inhomogeneous media has been finished by other researchers, D. Cule [36] and N.Adnani[37]*et al.* Some of these simulation results are reported in the thesis. Electromagnetic wave interaction with a human cross section model as simulated by D. Cule[36] is presented as an application of the mixture model to the modelling of complex inhomogeneous structures.

---

In chapter 4 one of the important inherent properties of three-dimensional electromagnetic fields is considered. An *LGA* vector model is constructed by endowing each abstract particle not only with the unit mass and propagating velocity vector, but also with unit polarization. The rules governing the interactions among these particles conserve particle's polarization which relate to electromagnetic field vectors in macroscopic limit. A theoretical analysis is developed using *LGA* theory, the Chapman-Enskog expansion, and appropriate mathematical methods. The analysis gives a first-order solution for the *LGA* system. The solution is then used to show how, in the macroscopic limit, three-dimensional Maxwell's equations can be derived. Some applications of the model to vector electromagnetic propagation are presented, and the resulting values are compared with those obtained by using the *TLM* method.

In chapter 5, a summary of the research is given. An initial benchmark about the issues such as computational stability, accuracy, and complexity are briefly discussed by making a comparison between a lattice gas automata and *TLM* method. We then suggest further studies and possible solution methods or approaches.

---

## Chapter 2. Lattice Gas Automata

### 2.1 INTRODUCTION

Recently, cellular Automata has received more and more attention in physics. Of the greatest current interest are the lattice gas automata *LGA*[38]. The term *LGA* refers to the class of cellular automata that obey specific collision and advection rules; *i.e.* some conservation properties are enforced[38]. *LGA* were used first for the simulation of fluid dynamics, where the bits of a cell mimic the movements of particles.

The basic constituents of an *LGA* are discrete cells. These cells are interconnected according to certain symmetric requirements to form an extremely large regular lattice. Only a few variables (bits) are needed to describe the states of each cell. These bits mimic the interacting particles and their evolution. The primary characteristic of an *LGA* is this: it evolves in discrete timesteps and its cells are simultaneously updated according to a simple rule that satisfies some conservation properties.

Sections 2.2 and 2.3 discuss both *LGA* models and concrete forms used in the modelling of two and three-dimensional electromagnetic problems. Microscopic and macroscopic descriptions of these *LGA* systems are then introduced in these sections. As a preparation for the following theoretical analysis, a brief review of lattice gas theory (ensemble average, detailed and semi-detailed balance and equilibrium particle distribution) is given in section 2.4. A brief introduction to *CA* machines is presented in section 2.5.

## 2. 2 TWO Dimensional Lattice Gas Model

### 2.2.1 The *HPP* Model

The geometric structure of a basic cell of a two-dimensional *HPP* lattice is square with unit spacing  $l$  (size of the cell). *HPP* represents the initials of Hardy, Pazzis and Pomeau [26], the inventors of the model. Fig.2.1 shows a small portion of a lattice (without rest particles). Each cell has four links, with each link representing a possible velocity or momentum state (moving particle has unit mass) in which a moving particle can exist. Particles obey an exclusion principle, that is, only one moving particle is allowed to reside in a particular velocity or momentum state. Therefore each cell in the lattice can contain up to a maximum of four moving particles. The lattice operates in two phases; a collision phase in which the particles interact and the state of each cell is updated, and an advection phase in which particles are passed to adjacent cells, as shown in Fig.2.1.

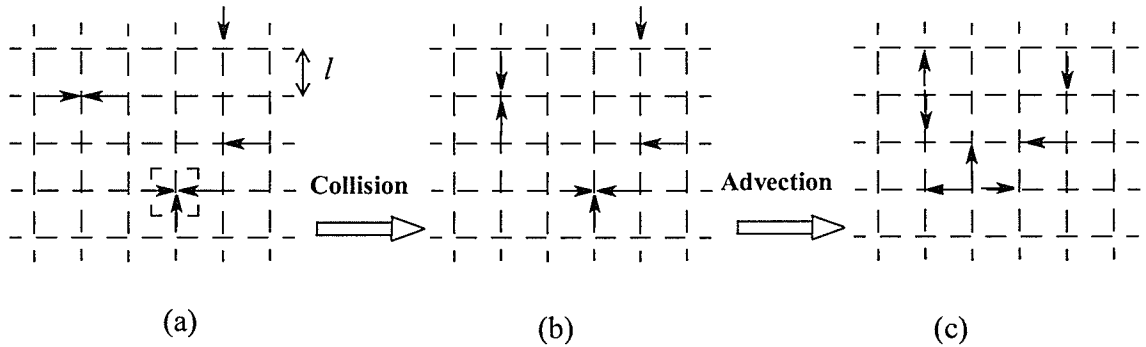
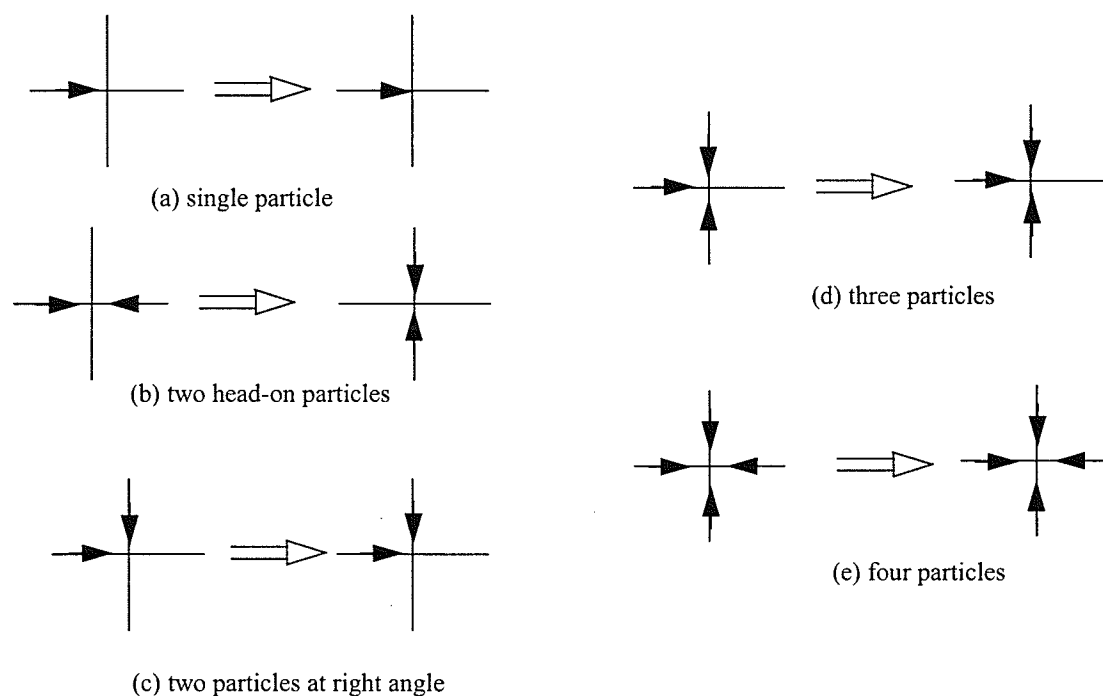


Fig.2.1: Operation of the *HPP* gas automaton (a small portion) over a single time step. In (a), the state of the lattice is shown before collisions. In (b), the state of the lattice is shown after the collisions have taken place. In (c), the particles have been transferred to adjacent cells.

The summarization of the collision events associated with the *HPP* model is given in

Fig.2.2. A transformation of momentum states occurs only when two and exactly two particles arrive at a site from opposite directions (head-on collision). The result of the collision is two particles in the momentum state orthogonal to the initial pair and previously unoccupied. For all other possible cases - a single particle, two particles at right angles, three particles, or four particles- the particle configuration remains unchanged after the collisions. They can be simply treated as passing through one another. Collisions in the *HPP* model conserve mass and momentum locally (within each cell), and thus conserve them globally.



Figs.2.2. Collision rules for the *HPP LGA*. Only two particles in opposing velocity states result in a transformation of velocity states. There are  $2^4 = 16$  total rules.

These can all be obtained by rotation of the above.

It is worthwhile to note that the dynamics of the *HPP* model is invariant under all discrete transformations that conserve the square lattice. These transformations include discrete translations, rotations by  $90^\circ$  and mirror symmetry. The *HPP* rule shown in Fig.2.2 is

---

characterized by the invariance of  $90^\circ$  rotations. Thus there are a total of 16 collision rules associated with this model. The *HPP* model is able to model the *Euler's* equation and yield correct sound speed for the media. However, it is not able to model the complete Navier-Stokes equation and it gives incorrect viscosity[16]. This is due to non-physical extra conservation inherent to the square lattice and a low symmetry of the lattice.

### 2. 2. 2 The *FHP* Model

The residing lattice of the *FHP* model is triangular with unit lattice constant  $l$  as shown in Fig.2.3. This structure is a variant of the above *HPP* model and was first introduced by Frisch, Hasslacher, and Pomeau [15,16]. The important characteristic of this model is that it has a larger invariance group. It is able to yield the standard Navier-Stokes equations and give a correct expression for viscosity. On the lattice, each cell is now connected with six neighbours. Thus, six bit variables per cell are required to specify the velocity or momentum states (without rest particles). Updating again involves two phases: collision and advection.

In this model, collisions that result in a change in the momentum of particles are only associated with two situations: two head-on particles and three particles which enter a site in the symmetric arrangement shown in Fig.2.4. The two-body collisions have two possible outcomes. Each outcome occurs with equal probability of  $1/2$  to maintain symmetry

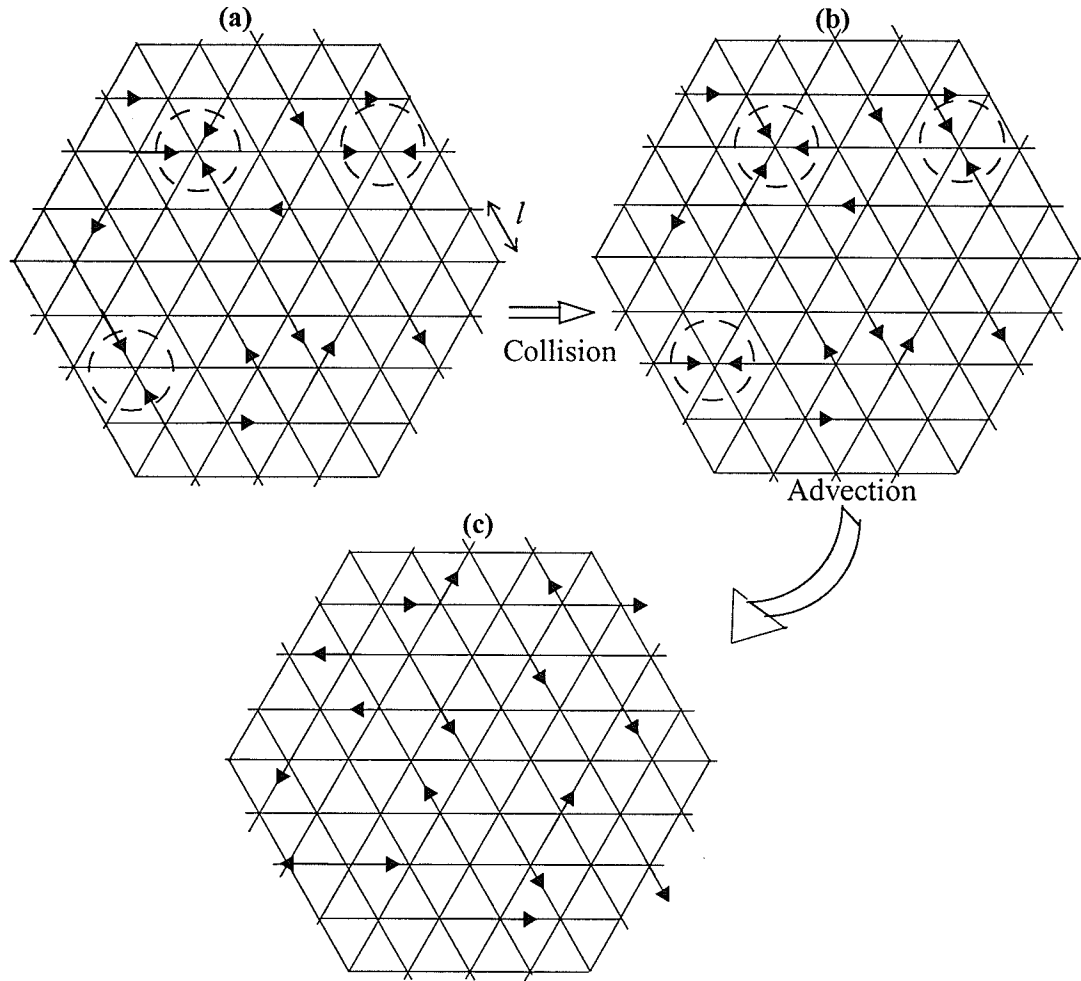


Fig.2.3: Operation on the *FHP* gas automaton over a single time step. In (a), the state of the lattice is shown before the collisions occur. In (b), the state of the lattice is shown after the collisions have taken place (two head-on and one triple collisions outlined with circles). In (c), the particles have been transferred to adjacent cells.

It can be observed that the triangular lattice has the invariant discrete transformations: rotations by  $\pi/3$  and mirror symmetry with respect to a lattice line. Under the transformations the dynamical characteristics of the *FHP* models are invariant. It should also be noted that, in the model, head-on collisions conserve, in addition to total particle number (mass), the



---

difference of particle numbers in any pair of opposite directions. This leads to a spurious conservation law. The large-scale dynamics of such a model will differ drastically from ordinary hydrodynamics unless the spurious effect is removed. To achieve this, one can introduce the three particle collision as shown in Fig.2.4b, or incorporate rest particles (with zero velocity). A model with the rest particles has the desired property, which allow us to control different sound speeds, analogous to different dielectric constants in the modelling of electromagnetic problem. The details of a lattice gas model with rest particles will be discussed in the following subsections.

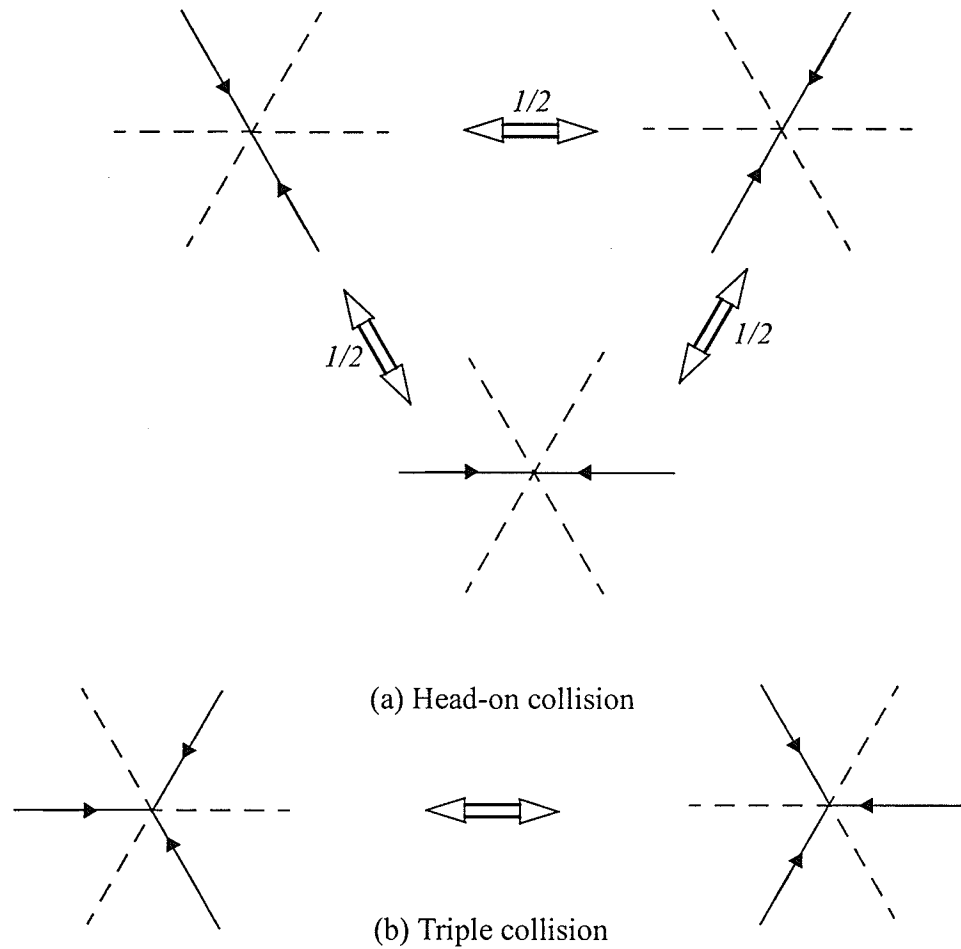


Fig.2.4: Examples of possible *FHP* lattice collision rules. (a): Head-on collision. (b): Triple collision.

### 2. 2. 3 Mixture Model of *HPP* or *FHP*

An *LGA* model without zero-velocity “rest particles” as depicted in the previous subsections can only yield a uniform sound speed. To enable the *LGA* lattice to model media with different sound speeds (analogous to modelling different dielectric constants in electromagnetics), certain rest particles are incorporated within sites of the lattice. It will be seen in the

---

analysis in chapter 3 that there are only a few restrictions (conservations of mass and momentum, and semi-detail balance) imposed on constructing such mixture models, and thus there are many ways for them to be employed. One can also specify that certain regions of the lattice have different rest particle numbers and masses. Thus the energy exchanges between moving and rest particles in the regions are different, and a lattice with different sound speeds can be realized. This inhomogeneous lattice model was first introduced in [23]. It is called a mixture model. In the subsection, the configuration and the notation of the model will be given, and the analysis will be developed in Chapter 3.

In Fig.2.5, one of many rest particle models is shown, where a stack (length of the stack is 3) of particles of various masses(4, 8 and 16) can be created. For example, a rest particle of mass 4 is created when four unit mass moving particles collide and where there is initially no mass 4 rest particle. Alternatively, if a mass 4 rest particle already exists at a site, and there are no initial moving particles, four moving particles will be created after the collision phase, and the rest particle will be annihilated.

In principle, one can extend the stack to an arbitrary length,  $b_r$ , and use a spatial distribution of different rest particle models such that  $b_r$  is a function of position, or even incorporate stochastic rules which probabilistically allow rest particles to be created or annihilated. Therefore, we can construct a mixture *LGA* in a very general way. Fig.2.6 shows some example cells of a mixture model with  $b_r$  probabilistically weighted rest particles, where  $p_k^r (k = 1, \dots, b_r)$  describes the creation or annihilation probability of the rest particle with mass  $m_k$ . The  $p_k^r$  also could be a spatial or temporal function. The details of

the model will be discussed in the next subsection.

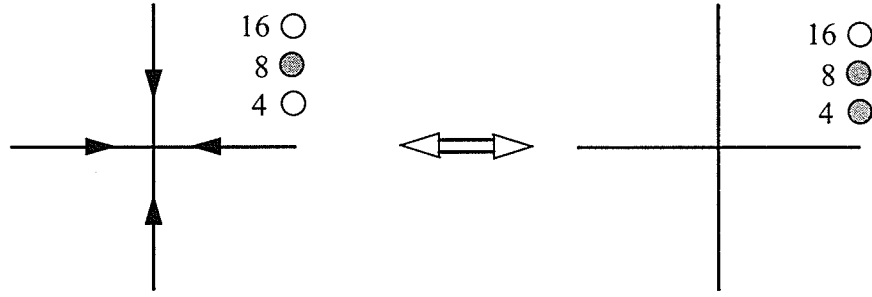


Fig.2.5: *LGA* rule with three weighted rest particles

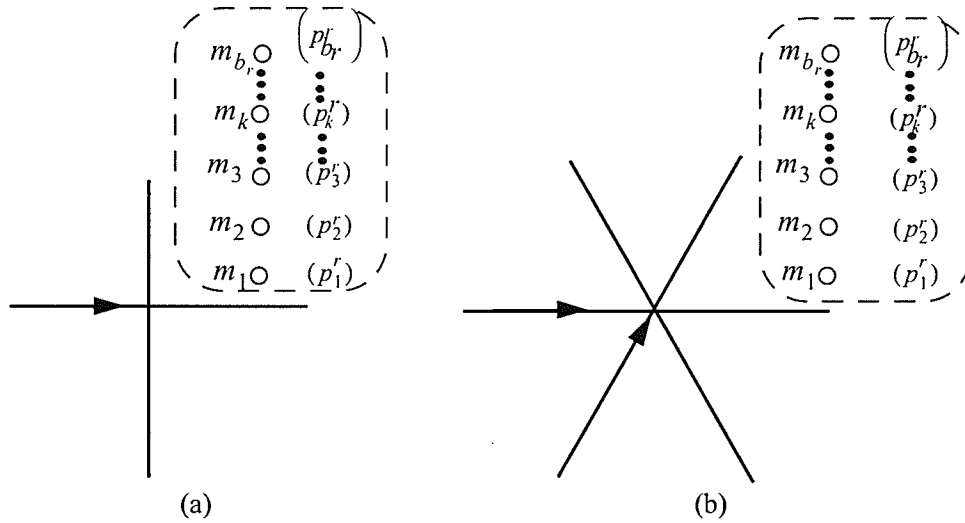


Fig.2.6: *LGA* mixture model with  $b_r$  probabilistically weighted rest particles  
(a): *HPP* two-dimension mixture model.(b): *FHP* two-dimension mixture model.

## 2.2.4 Microdynamics and Macroscopic Obersevarbles

### 2.2.4.1 Microdynamic states of *LGAs*

A lattice gas automata is generally described by a set of Boolean variables (bits) and a

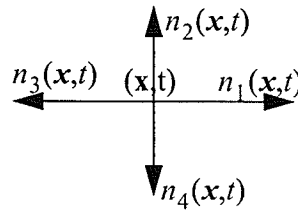
set of time-independent rules. The set of binary (bit) variables  $n_i(x, t)$  ( $i = 1, \dots, N_l$ ) is associated with bit  $i$  of the cell at position  $x$  of the *LGA* at time  $t$ . The bit variable  $n_i(x, t)$  takes values 1 or 0, representing the presence or absence of the particle in the  $i$ th velocity state (or other physical quantity) at a particular site and time  $t$ .  $N_l$  is the maximum number of particles which the cell can hold. This number is determined by the exclusion principle (only one particle is allowed to reside in a particular state) and all possible particle states per cell. The notation of particle states in terms of bit variables for each of the above models is given below.

#### ***A: HPP lattice gas***

The *HPP* has four possible velocity states per cell. Four bits,  $n_i(x, t)$  ( $i = 1, 2, 3, 4$ ), are used to describe these states. The four velocity vectors correspond to the four link vectors and can be calculated by:

$$c_i = l \left[ \cos \frac{\pi}{2}(i-1) \hat{x} + \sin \frac{\pi}{2}(i-1) \hat{y} \right] \quad (i = 1, 2, 3, 4). \quad (2.1)$$

where  $l$  is the characteristic length spacing (cell size) and  $l e_i \equiv c_i$  and  $e_i = \pm \hat{x}, \pm \hat{y}$ . For example, for the case of  $i = 1$ ,  $c_1 = l \hat{x}$ . Thus the bit  $n_1(x, t)$  represents the presence or absence of the particle moving along positive  $x$ -direction and at site  $x$  and time  $t$ .



### ***B: FHP lattice gas***

In the *FHP* lattice, six bits( $n_i(x, t) \quad i=1, \dots, 6$ ) per cell represent six velocity states. The six velocity vectors are associated to the six link vectors (see Fig.2.4) and can be calculated by:

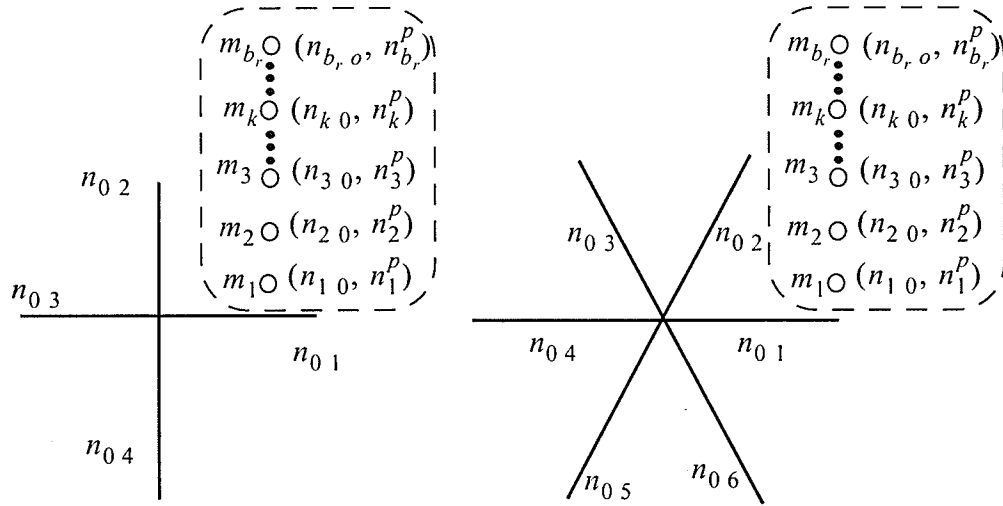
$$c_i = l \left[ \cos \frac{\pi}{3}(i-1) \hat{x} + \sin \frac{\pi}{3}(i-1) \hat{y} \right] \quad (i=1, \dots, 6). \quad (2.2)$$

### ***C: Mixture HPP or FHP model***

A mixture model is capable of modelling different materials. The model is constructed by incorporating rest particles with moving particles in a particular lattice site. For each rest particle, one extra bit should be added to represent its states. In what follows, we use two subscript variables  $n_{i,k}$  to represent the particle states in the mixture lattice. The first subscript,  $i$ , is used to describe the velocity of particles and the second one,  $k$ , represents the mass of the particles. For the rest particle,  $i \equiv 0$ , and the moving particle (unit mass)  $k \equiv 0$ . This notation will be used throughout the remainder of the thesis.

Fig.2.7 shows mixture *HHP* and *FHP* models, both with an arbitrary stack  $b_r$  (the maximum number of rest particles per cell). We define two new sets of bit variables in each cell of the lattice. The first set  $\{n_{o,k}, k=1, \dots, b_r\}$  is used to describe the states of rest particles. For example, if the bit  $n_{o,k}$  is on ( $=1$ ) or off ( $=0$ ), a rest particle of mass  $m_k$  is present or absent. The second set  $\{n_k^p, k=1, \dots, b_r\}$  contains stochastic bit variables. At each cell and each time step, any stochastic bit  $n_k^p$  is randomly sampled to determine whether or not a

rest particle with mass  $m_k$  ( $k = 1, \dots, b_r$ ) may be created or annihilated. These random bits have the average values of  $\langle n_k^p \rangle = p_k$  ( $k = 1, \dots, b_r$ ). Here, the average value  $p_k^r$  serves as the creation or annihilation probability of the rest particle  $m_k$ , and these values satisfy the limitations of  $p_{k+1}^r \leq p_k^r$  and  $\sum_{k=1}^{b_r} p_k^r \leq 1$ .



(a): HPP two-dimension mixture model

(b): FHP two-dimension mixture model

Fig.2.7: LGA rule with  $b_r$  probabilistically weighted rest particles

#### 2.2.4.2 Microdynamics of the LGAs

The notations for the different models introduced above will be retained throughout the rest of the thesis. In the following subsection, we desire to obtain mathematical descriptions of the microdynamics of the LGAs. In an LGA, the dynamic states of particles are character-

ized by their binary bit variables at each timestep. The dynamical state of a particle at the next timestep ( $t + \Delta t$ ) depends on the current state of the particle itself, and the states of its neighbouring particles. In the case where the particle does not interact with its neighbours, the moving particle just passes through its current residing cell and keeps its original dynamical state, while the rest particles with zero-velocity do not advect over time. If the interaction with its neighbouring particles occurs, the dynamical state of the particle is changed according to the collision rules. In what follows, we present the dynamical description for each of the *LGA* models discussed in the previous sections.

#### 2. 2. 4. 3 Dynamical description for *HPP LGA*

The dynamical equations for a *HPP* lattice gas can be obtained according to the collision rules shown in Fig.2.2, where the states for the four moving particles are characterized by bit variables  $n_1$ ,  $n_2$ ,  $n_3$  and  $n_4$ , respectively. These equations are:

$$n_1(x+l, y, t + \Delta t) = n_1(x, y, t) + \omega_1, \quad (2.3)$$

$$n_2(x, y+l, t + \Delta t) = n_2(x, y, t) + \omega_2, \quad (2.4)$$

$$n_3(x-l, y, t + \Delta t) = n_3(x, y, t) + \omega_3, \quad (2.5)$$

$$n_4(x, y-l, t + \Delta t) = n_4(x, y, t) + \omega_4, \quad (2.6)$$

where  $\omega_i(x, y, t)$  ( $i=1, 2, 3$  and  $4$ ) are the four collision operators of the model. These operators take the values of  $\pm 1$  or  $0$ , and are given by

$$\omega_1(x, y, t) = \omega_3(x, y, t) = \overline{n_1 n_3 n_2 n_4} - \overline{n_2 n_4 n_1 n_3}, \quad (2.7)$$

$$\omega_2(x, y, t) = \omega_4(x, y, t) = -\omega_1(x, y, t), \quad (2.8)$$



where the symbol  $\bar{n}_i = 1 - n_i$  stands for the complement of bit  $n_i$ .

These four microdynamical equations can be written in a compact form, that is

$$n_i(\mathbf{x} + \mathbf{c}_i, t + \Delta t) = n_i(\mathbf{x}, t) + \omega_i \quad (2.9)$$

and the compact form of the collision operators  $\omega_i(\mathbf{x}, t)$  is given by

$$\omega_i(\mathbf{x}, t) = \overline{n_i n_{i+2} n_{i+1} n_{i+3}} - \overline{n_{i+1} n_{i+3} n_i n_{i+2}}, \quad (2.10)$$

where the index  $i$  is defined as module four, i.e.,  $i+4=i$ .

#### 2.2.4.4 Dynamic description of *FHP*

It is easy to extend the microdynamic formalism to the *FHP* lattice gas. Based on the collision rules illustrated in Fig.2.4, the microdynamic equations can be written as:

$$n_i(\mathbf{x} + \mathbf{c}_i, t + \Delta t) = n_i(\mathbf{x}, t) + \omega_i. \quad (2.11)$$

where  $i = 1, 2, \dots, 6$ , and the collision operator can be obtained as

$$\begin{aligned} \omega_i(\mathbf{x}, t) = & \xi \overline{n_i n_{i+2} n_{i+3} n_{i+5} n_{i+1} n_{i+4}} + (1 - \xi) \overline{n_i n_{i+1} n_{i+3} n_{i+4} n_{i+2} n_{i+5}} \\ & - \overline{n_i n_{i+3} n_{i+1} n_{i+4} n_{i+2} n_{i+5}} + \overline{n_i n_{i+2} n_{i+4} n_{i+1} n_{i+3} n_{i+5}} - \overline{n_i n_{i+2} n_{i+4} n_{i+1} n_{i+3} n_{i+5}} \end{aligned} \quad (2.12)$$

Here,  $\xi$  is a random bit which is sampled at each lattice site and timestep with the average value  $\langle \xi \rangle$ . The average values  $\langle \xi \rangle$  and  $\langle 1 - \xi \rangle$  represent the respective probabilities that the head-on colliding particles are to be rotated clockwise and counter-clockwise. Note that the subscript  $i$  is defined as module six. If  $\langle \xi \rangle$  is chosen not to be 0.5 then the media will be chiral. Several other possible models for chiral phenomena have been studied [31,32].

#### 2. 2. 4. 5 Dynamic description of the Mixture Model

For the mixture *HPP* or *FHP* lattice gas (shown in Fig.2.7), the microdynamic equations can be formally written as:

(a) for the moving particles ( $i=1, 2, \dots, b_m$ ):

$$n_{i0}(\mathbf{x} + \mathbf{c}_i, t + \Delta t) = n_{i0}(\mathbf{x}, t) + \omega_{i0}(n^\dagger(\mathbf{x}, t)) , \quad (2.13)$$

(b) for the rest particles ( $k=1, 2, \dots, b_r$ ):

$$n_{ok}(\mathbf{x}, t + \Delta t) = n_{ok}(\mathbf{x}, t) + \omega_{ok}(n^\dagger(\mathbf{x}, t)) , \quad (2.14)$$

where  $b_m$  is the maximum number of moving particles per cell. The symbol  $n^\dagger(\mathbf{x}, t)$  stands for the complete set of bit variables located at site  $\mathbf{x}$  and time  $t$ . Explicitly, the collision operator  $\omega_{i0}(n^\dagger(\mathbf{x}, t))$  is the shorthand for  $\omega_{i0}(n_{10}(\mathbf{x}, t), \dots, n_{b_m0}(\mathbf{x}, t), n_{o1}(\mathbf{x}, t), \dots, n_{ob_r}(\mathbf{x}, t))$ . We are not going to give the explicit forms of the collision operators here, since there is a great variety of forms that can be obtained by designing different interactions between the moving and rest particles. In chapter 3, it will be seen that the details of the collision rules are important in hydrodynamic applications [31,34], but not for the modelling of the electromagnetic waves in no-loss media. The dielectric constant (analogous to the speed of sound in a lattice gas) is a macroscopic physical quantity and is not sensitive to these details either. However, the viscosity of the *LGA* can generally not be analogously used to model the conductivity coefficient of lossy media, except for some special problems. In the problems, the geometric structure are simple and excited with steady excitations[29].

Thus, for the wave attenuation in those problems in electromagnetics the details of the collision rules become very important.

#### 2.2.4.6 Conserved Quantities of Two Dimensional *LGAs*

A characteristic feature of *LGAs* is the presence of some form of conservation. In a two-dimensional lattice gas model, mass and momentum are conserved in each collision, *i.e.*, at the microscopic level. As a result, after propagation, mass and momentum are conserved macroscopically. At each cell in a collision event, conservation of mass and momentum can be expressed in terms of the collision operators as

$$\sum_i \omega_i(n^\dagger) = 0, \quad (2.15)$$

and

$$\sum_i c_i \omega_i(n^\dagger) = 0. \quad (2.16)$$

This implies important conservation relations for lattice gas automata:

$$\sum_i n_i(t + \Delta t, \mathbf{x} + \mathbf{c}_i) = \sum_i n_i(t, \mathbf{x}), \quad (2.17)$$

and

$$\sum_i n_i c_i(t + \Delta t, \mathbf{x} + \mathbf{c}_i) = \sum_i n_i c_i(t, \mathbf{x}), \quad (2.18)$$

where the equations (2.15) and (2.16) give the conservations of mass and momentum in bit form, and indicate that the conservation laws are independent of spatial position and timestep. In what follows, some examples for models are discussed for conservation.

In *HPP* model, from the equations (2.7) and (2.8), it follows that,

$$\omega_1 + \omega_2 + \omega_3 + \omega_4 = 0 \quad (2.19)$$

$$(\omega_1 - \omega_3)\hat{x} = 0 \quad (2.20)$$

$$(\omega_2 - \omega_4)\hat{y} = 0, \quad (2.21)$$

where the equation(2.19) indicates the conservation of mass while (2.20) and (2.21) represent the conservation of momentum in the  $x$  and  $y$  directions respectively. At the microscopic level, the conserved quantities could be defined in terms of the bit variables at a particular site. For instance, in the case of the mixture two-dimensional *LGA* described in Section 2.2.3, the mass and the momentum are calculated by equations (2.22) and (2.23) respectively.

$$m_{local} = \sum_{\substack{i=1 \\ (k=0)}}^{b_m} m_o n_{i,o} + \sum_{\substack{k=1 \\ (i=0)}}^{b_r} m_k n_{o,k} n_k^p, \quad (2.22)$$

$$\mathbf{u}_{local} = \sum_{\substack{i=1 \\ (k=0)}}^{b_m} m_o n_{i,o} \mathbf{c}_i. \quad (2.23)$$

In the expression of (2.22) the first term is summed over for the moving particles (unit mass  $m_o = 1$ ) and the second term is over rest particles.

## 2.3 Three-Dimensional Lattice Gas Model

### 2.3.1 Three-Dimensional Vector *LGA* Model(3-d *LGA*)

In this subsection, a three-dimensional Fermi-type vector *LGA* model is constructed to model three-dimensional electromagnetic field problems. The residing lattice is cubic with

the length  $l$  as illustrated in Fig.2.8. Unlike the previous two-dimensional models, the vector model incorporates polarization with each particle. This concept is quite different than the scalar particle models of fluid dynamics. We assume that, in the vector model, each particle has unit mass, polarization vector  $e$  (associated with electrical field in the macroscopic limit) and velocity  $k$ . Each cubic cell has six links, with each representing a possible velocity  $k$ . In addition, each velocity state associates with four polarization vectors  $e$ s. Thus there are a total of 24 particles in a cell, each particle propagating in the direction of velocity  $k$  and polarized in the state of  $e$ . If we denote these six velocity vectors by  $k \in \{\pm\hat{X}, \pm\hat{Y}, \pm\hat{Z}\}$ , the corresponding four polarizations can be expressed as: for  $k = \pm\hat{X}$ ,  $e \in \{\pm\hat{y}, \pm\hat{z}\}$ , for  $k = \pm\hat{Y}$ ,  $e \in \{\pm\hat{x}, \pm\hat{z}\}$  and for  $k = \pm\hat{Z}$ ,  $e \in \{\pm\hat{x}, \pm\hat{y}\}$ . Fig.2.9. shows a case of four particle propagating in  $-z$  direction  $k = -\hat{Z}$ , polarized in  $\pm\hat{x}$  and  $\pm\hat{y}$  directions. Furthermore, the relation between polarization vector  $e$  and velocity  $k$  for each particle is defined to satisfy  $k \times e = h$ , where the vector  $h$  is defined as an inherent magnetic vector associated with each particle. Note that only two of these three vectors are independent. Hence each state of particle is characterized by two vectors  $(k, e)$ .

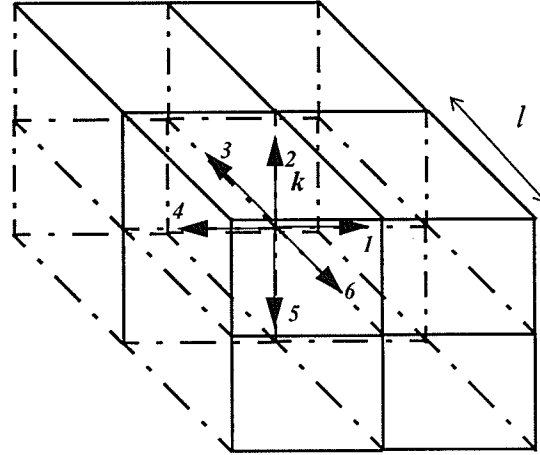


Fig.2.8: A small portion of a three-dimensional cubic lattice.

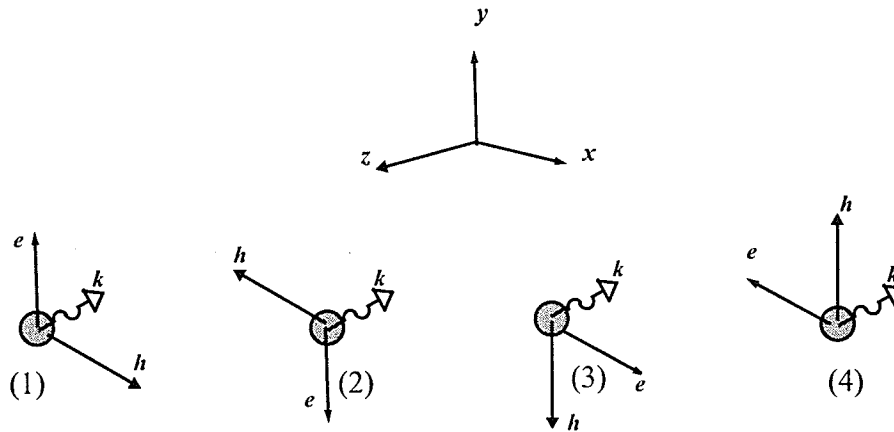


Fig.2.9 Four polarization vectors of a given velocity vector. (1): up-polarization. (2):down-polarization. (3): right-polarization. (4):left-polarization. Here  $k$  is the velocity vector of particles, and  $e$  and  $h$  are the polarization and magnetic vectors, respectively.

To specify the states of the vector model, we need a total of 24 bits per cell (there is a total of 6 velocities and 4 polarizations per velocity) to describe the particle states. When

---

constructing collision rules for the model, two types of the two-body collision events have been considered. The first type is the head-on collision. The interaction configuration between two particles is defined to be the same as that used in the *HPP* or *FHP* models. In the three-dimensional vector *LGA* model, however, the head-on collisions conserve the polarization  $e$  and the magnetic vector  $h$  (Figs.2.10a and 2.11a). The other type is the right-angle collision. In this case, collisions occur if and only if exactly two particles enter a cell at right angles. The collisions result in the exchange of the vector  $h$  between the two incoming particles, and each of two outgoing particles leaves the cell in the direction opposite to its initial direction as shown in Figs.2.10b and 2.11b. Again, these collisions conserve polarization vector  $e$  and magnetic vector  $h$ .

By investigating the above rules, we note that, due to the collisions, a particle with positive polarization can never be changed into a particle with negative polarization because of the conservation of polarization. Thus all particles on the lattice can be classified into independent positive and negative polarization particle groups. On an infinite homogeneous lattice, the positive particles do not interact with the negative particles even on the same lattice, and each group of particles obey the collision rules independently. If the lattice is truncated at, for example, boundaries of objects, then the two-group particles can be coupled. However in the situation of perfect magnetic conducting (PMC) boundaries, these two group particles can still remain uncoupled. A PMC boundary condition can be modelled by forcing the tangential magnetic field along the boundary to be zero. Particles incident on a magnetic conductor are reflected onto the same group (*i.e.*, a positive particle is reflected onto the positive group and a negative particle back onto the negative group)[21,25]. Hence, when modelling an electromagnetic field problem with PMC boundaries, we need only one (positive or

negative) of two group particles such that the vector model can be simplified to two (positive or negative) polarizations  $es$  per velocity as shown in Fig.2.12, requiring a total of only 12 particles per cell. If a PEC boundary is required, the coupling between those two particle groups is required. The concrete implementation of PEC boundary is described by N. Simons[25]. Thus, a total of 24 particles per cell is needed to describe the states. Two questions remain to be answered: are there any other types of collision events? And, if there are, what is the effect of these collision events on the dynamics and macroscopic behaviour (electromagnetic phenomena)?

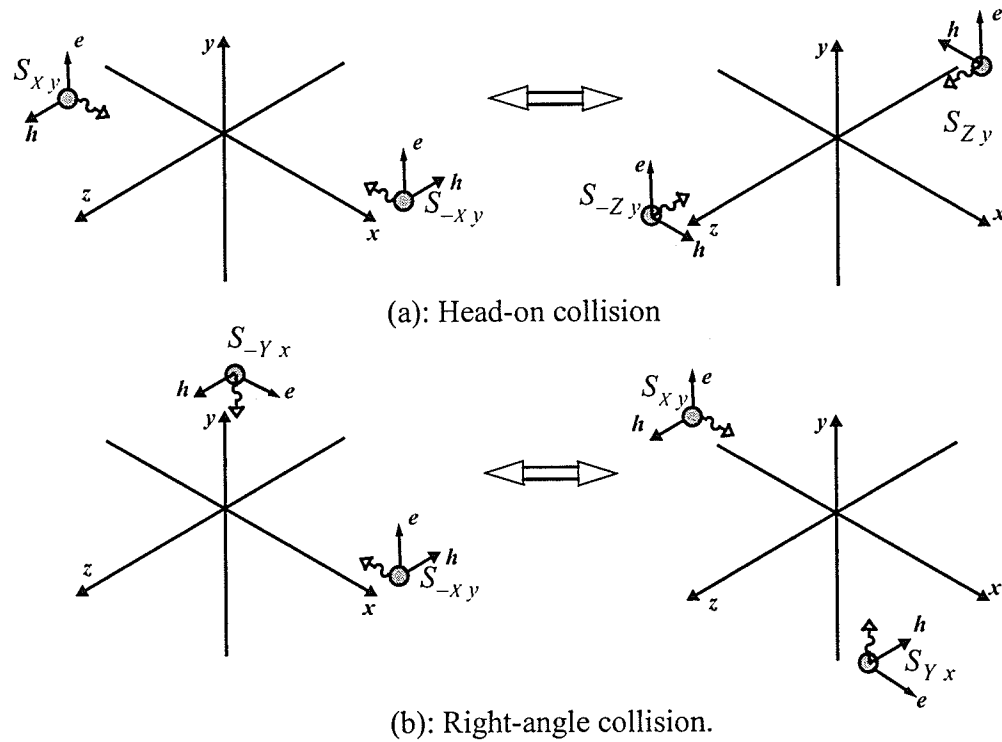


Fig.2.10: One example of the collision rules for the positive vector lattice gas automata. The collision rules conserve the mass, polarization and the physical quantities  $h$ .



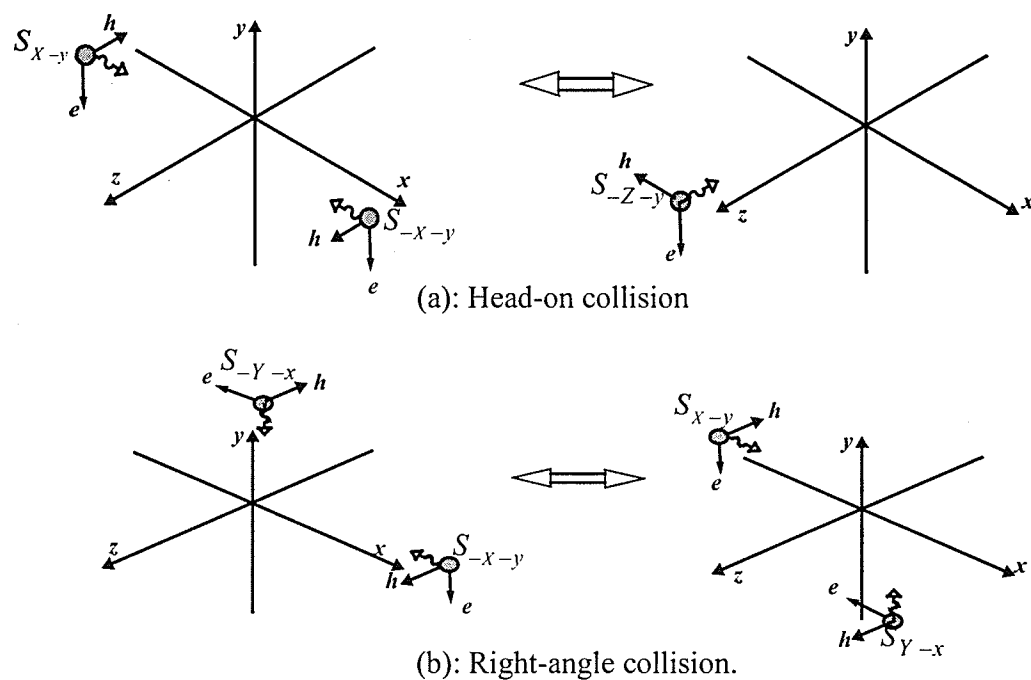


Fig.2.11: One example of the collision rules for the negative vector lattice gas automata. The collision rules conserve the mass, polarization and the physical quantities  $h$ .

### 2.3.2 Dynamic States of 3-d Vector LGA

For the three dimension cubic lattice shown in Figs.2.8 and 2.12, the two-subscript bit variable  $S_{Ki}$  describes the state of a particle, where the first index  $K$  indicates the  $k$ th velocity vector, with  $K$  taking the value in the set of  $\{\pm X, \pm Y, \pm Z\}$ , and the second index  $i$  stands for the  $i$ th polarization related to the  $K$ th velocity. Explicitly the set of bits can be written as:

$(S_{-Xy}, S_{-Xz}, S_{Xy}, S_{Xz}, S_{-Yx}, S_{-Yz}, S_{Yx}, S_{Yz}, S_{-Zx}, S_{-Zy}, S_{Zx}, S_{Zy}, S_{Zx}, S_{Zy}, S_{Zx}, S_{Zy})$ . For example the bit  $S_{-Xy}$  represents the presence or absence of the particle moving along  $-\hat{X}$  direction and polarized in  $y$ -direction at site  $x$  and time  $t$ .

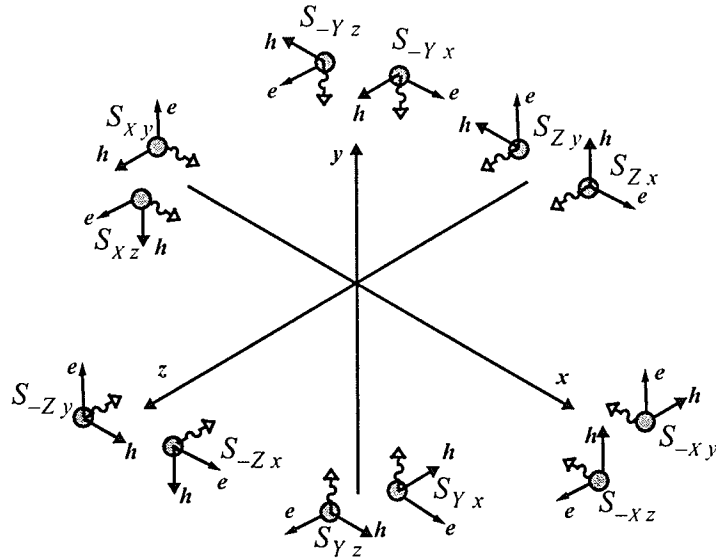


Fig.2.12: Twelve particles of the three-dimensional vector LGA.

### 2.3.3 Dynamic Description of 3-d Vector LGA

For the simplified 3-d vector lattice gas shown in Fig.2.12, two types of collision rules for head-on collisions and right-angle collisions have been defined and shown in Fig.2.10. It is noted that the rules are characterized by  $\pm 90^\circ$  rotational symmetry with respect to the three axes,  $\hat{x}$ ,  $\hat{y}$  and  $\hat{z}$ . This means that the rules are invariant when input particle configurations are performed with any of the rotational transformations. Hence we have a total of 6 collision rules for each type. To obtain the dynamic description, first consider the change in a particular bit  $S_{x,y}(\mathbf{x}, t)$  due to collisions. The bit represents a particle travelling in the  $\hat{x}$ -direction and polarized in the direction of  $\hat{y}$ . At the next timestep  $(t + \Delta t)$ , the state of the particle will be changed to the state of  $S_{x,y}(x + l, y, z, t + \Delta t)$  due to the two collision events, head-on or right-angle, as illustrated in Figs.2.10(a) and 2.10(b). The microscopic dynamics for the particle could be written as

$$S_{x,y}(x + l, y, z, t + \Delta t) = S_{x,y}(x, y, z, t) + \omega_{x,y}^{head} + \omega_{x,y}^{right},$$

where  $\omega_{x,y}^{head}$  and  $\omega_{x,y}^{right}$  are the operators describing the contributions respectively from the head-on and right-angle collisions, and obtained as

$$\omega_{x,y}^{head} = S_{z,y} S_{-z,y} \overline{S_{x,y} S_{-x,y}} - \overline{S_{-x,y} S_{x,y}} \overline{S_{z,y} S_{-z,y}},$$

and

$$\omega_{x,y}^{right} = S_{-x,y} S_{-y,x} \overline{S_{y,x} S_{x,y}} - \overline{S_{-x,y} S_{-y,x}} \overline{S_{y,x} S_{x,y}}.$$

In the same way, we note that the change of any particle state in the model can always

be associated with two collision events (a head-on and a right-angle event). We combine these two events as pairs to describe the change of a particular particle state. Hence, we have a total of twelve such event pairs, listed in Appendix A. Referring to the interacting rules in Appendix A, we have the following microdynamic equations for each particle state:

$$S_{-Xy}(x-l, y, z, t + \Delta t) = S_{-Xy}(x, y, z, t) + \omega_{-Xy}(S^\dagger(x, t)) , \quad (2.24)$$

$$S_{-Xz}(x-l, y, z, t + \Delta t) = S_{-Xz}(x, y, z, t) + \omega_{-Xz}(S^\dagger(x, t)) , \quad (2.25)$$

$$S_{Xy}(x+l, y, z, t + \Delta t) = S_{Xy}(x, y, z, t) + \omega_{Xy}(S^\dagger(x, t)) , \quad (2.26)$$

$$S_{Xz}(x+l, y, z, t + \Delta t) = S_{Xz}(x, y, z, t) + \omega_{Xz}(S^\dagger(x, t)) , \quad (2.27)$$

$$S_{-Yx}(x, y-l, z, t + \Delta t) = S_{-Yx}(x, y, z, t) + \omega_{-Yx}(S^\dagger(x, t)) , \quad (2.28)$$

$$S_{-Yz}(x, y-l, z, t + \Delta t) = S_{-Yz}(x, y, z, t) + \omega_{-Yz}(S^\dagger(x, t)) , \quad (2.29)$$

$$S_{Yx}(x, y+l, z, t + \Delta t) = S_{Yx}(x, y, z, t) + \omega_{Yx}(S^\dagger(x, t)) , \quad (2.30)$$

$$S_{Yz}(x, y+l, z, t + \Delta t) = S_{Yz}(x, y, z, t) + \omega_{Yz}(S^\dagger(x, t)) , \quad (2.31)$$

$$S_{-Zx}(x, y, z-l, t + \Delta t) = S_{-Zx}(x, y, z, t) + \omega_{-Zx}(S^\dagger(x, t)) , \quad (2.32)$$

$$S_{-Zy}(x, y, z-l, t + \Delta t) = S_{-Zy}(x, y, z, t) + \omega_{-Zy}(S^\dagger(x, t)) , \quad (2.33)$$

$$S_{Zy}(x, y, z+l, t + \Delta t) = S_{Zy}(x, y, z, t) + \omega_{Zy}(S^\dagger(x, t)) , \quad (2.34)$$

$$S_{Zx}(x, y, z+l, t + \Delta t) = S_{Zx}(x, y, z, t) + \omega_{Zx}(S^\dagger(x, t)) , \quad (2.35)$$

where  $S^\dagger(x, t)$  has the same meaning as  $n^\dagger(x, t)$  used in the previous subsection. The

twelve operators  $\omega_{Jk}$  ( $J = \pm X, \pm Y, \pm Z$  and  $k = x, y, z$ ) are specified by,

$$\omega_{-Xy} = \overline{S_{-Xy}} [ S_{Zy} S_{-Zy} \overline{S_{Xy}} + S_{Xy} S_{Yx} \overline{S_{-Yx}} ] - S_{-Xy} [ \overline{S_{Zy} S_{-Zy} S_{Xy}} + \overline{S_{Xy} S_{Yx} S_{-Yx}} ], \quad (2.36)$$

$$\omega_{-Xz} = \overline{S_{-Xz}} [ S_{Yz} S_{-Yz} \overline{S_{Xz}} + S_{Xz} S_{Zx} \overline{S_{-Zx}} ] - S_{-Xz} [ \overline{S_{Yz} S_{-Yz} S_{Xz}} + \overline{S_{Xz} S_{Zx} S_{-Zx}} ], \quad (2.37)$$

$$\omega_{Xy} = \overline{S_{Xy}} [ S_{Zy} S_{-Zy} \overline{S_{-Xy}} + S_{-Xy} S_{-Yx} \overline{S_{Yx}} ] - S_{Xy} [ \overline{S_{Zy} S_{-Zy} S_{-Xy}} + \overline{S_{-Xy} S_{-Yx} S_{Yx}} ], \quad (2.38)$$

$$\omega_{Xz} = \overline{S_{Xz}} [ S_{Yz} S_{-Yz} \overline{S_{-Xz}} + S_{-Xz} S_{-Zx} \overline{S_{Zx}} ] - S_{Xz} [ \overline{S_{Yz} S_{-Yz} S_{-Xz}} + \overline{S_{-Xz} S_{-Zx} S_{Zx}} ], \quad (2.39)$$

$$\omega_{-Yx} = \overline{S_{-Yx}} [ S_{Zx} S_{-Zx} \overline{S_{Yx}} + S_{Xy} S_{Yx} \overline{S_{-Xy}} ] - S_{-Yx} [ \overline{S_{Zx} S_{-Zx} S_{Yx}} + \overline{S_{Xy} S_{Yx} S_{-Xy}} ], \quad (2.40)$$

$$\omega_{-Yz} = \overline{S_{-Yz}} [ S_{Xz} S_{-Xz} \overline{S_{Yz}} + S_{Zy} S_{Yz} \overline{S_{-Yz}} ] - S_{-Yz} [ \overline{S_{Xz} S_{-Xz} S_{Yz}} + \overline{S_{Yz} S_{Zy} S_{-Yz}} ], \quad (2.41)$$

$$\omega_{Yx} = \overline{S_{Yx}} [ S_{Zx} S_{-Zx} \overline{S_{-Yx}} + S_{-Xy} S_{-Yx} \overline{S_{Xy}} ] - S_{Yx} [ \overline{S_{Zx} S_{-Zx} S_{-Yx}} + \overline{S_{-Xy} S_{-Yx} S_{Xy}} ], \quad (2.42)$$

$$\omega_{Yz} = \overline{S_{Yz}} [ S_{Xz} S_{-Xz} \overline{S_{-Yz}} + S_{-Zy} S_{-Yz} \overline{S_{Zy}} ] - S_{Yz} [ \overline{S_{Xz} S_{-Xz} S_{-Yz}} + \overline{S_{-Yz} S_{-Zy} S_{Zy}} ], \quad (2.43)$$

$$\omega_{-Zx} = \overline{S_{-Zx}} [ S_{Yx} S_{-Yx} \overline{S_{Zx}} + S_{Xz} S_{Zx} \overline{S_{-Xz}} ] - S_{-Zx} [ \overline{S_{Yx} S_{-Yx} S_{Zx}} + \overline{S_{Xz} S_{Zx} S_{-Xz}} ], \quad (2.44)$$

$$\omega_{-Zy} = \overline{S_{-Zy}} [ S_{Xy} S_{-Xy} \overline{S_{Zy}} + S_{Zy} S_{Yz} \overline{S_{-Yz}} ] - S_{-Zy} [ \overline{S_{Xy} S_{-Xy} S_{Zy}} + \overline{S_{Yz} S_{Zy} S_{-Yz}} ], \quad (2.45)$$

$$\omega_{Zy} = \overline{S_{Zy}} [ S_{Xy} S_{-Xy} \overline{S_{-Zy}} + S_{-Zy} S_{-Yz} \overline{S_{Yz}} ] - S_{Zy} [ \overline{S_{Xy} S_{-Xy} S_{-Zy}} + \overline{S_{Yz} S_{-Zy} S_{Yz}} ], \quad (2.46)$$

$$\omega_{Zx} = \overline{S_{Zx}} [ S_{Yx} S_{-Yx} \overline{S_{-Zx}} + S_{-Xz} S_{-Zx} \overline{S_{Xz}} ] - S_{Zx} [ \overline{S_{Yx} S_{-Yx} S_{-Zx}} + \overline{S_{-Xz} S_{-Zx} S_{Xz}} ]. \quad (2.47)$$

### 2.3.4 Conserved Quantities of 3-d Vector LGA

The conserved quantities in the 3-d vector model correspond to the six components of polarization vector  $\mathbf{e}$  and magnetic vector  $\mathbf{h}$ . The two vectors are conserved at both the microscopic and macroscopic levels. It follows from the equations (2.36) through (2.47) that the conservations of six components can be written as

$$(\omega_{-Yx} + \omega_{Yx} + \omega_{-Zx} + \omega_{Zx}) \hat{x} = 0, \quad (2.48)$$

$$(\omega_{-Xy} + \omega_{Xy} + \omega_{-Zy} + \omega_{Zy}) \hat{y} = 0, \quad (2.49)$$

$$(\omega_{-Xz} + \omega_{Xz} + \omega_{-Yz} + \omega_{Yz}) \hat{z} = 0, \quad (2.50)$$

$$(\omega_{Yz} - \omega_{Yz} + \omega_{Zy} - \omega_{Zy})\hat{x} = 0, \quad (2.51)$$

$$(\omega_{Xz} - \omega_{Xz} - \omega_{Zx} + \omega_{Zx})\hat{y} = 0, \quad (2.52)$$

$$(\omega_{Xy} - \omega_{Xy} + \omega_{Yz} - \omega_{Yz})\hat{z} = 0, \quad (2.53)$$

where the first three equations indicate the conservation of three components of polarization vectors  $\mathbf{e}$ , and the last three denote the conservation of magnetic vector  $\mathbf{h}$  in the  $x$ -,  $y$ - and  $z$ -directions respectively. Their components in a particular cell can be calculated in terms of the bit variables as,

$$u_{x1}^{local} = (S_{-Yx} + S_{Yx} + S_{-Zx} + S_{Zx})\hat{x},$$

$$u_{y1}^{local} = (S_{-Xy} + S_{Xy} + S_{-Zy} + S_{Zy})\hat{y},$$

$$u_{z1}^{local} = (S_{-Xz} + S_{Xz} + S_{-Yz} + S_{Yz})\hat{z},$$

$$u_{x2}^{local} = (S_{Yz} - S_{Yz} + S_{-Zy} - S_{Zy})\hat{x},$$

$$u_{y2}^{local} = (S_{-Xz} - S_{Xz} - S_{-Zx} + S_{Zx})\hat{y},$$

$$u_{z2}^{local} = (S_{Xy} - S_{Xy} + S_{-Yz} - S_{Yz})\hat{z}.$$

## 2.4 Macroscopic Observables

Within a lattice gas, macroscopic physical observables such as density and flow can be determined by an average over an ensemble of possible microscopic particle configurations. In practical cellular automaton simulation experiments, we strive to obtain enough experimental samples. To avoid limitation of averaging only over a few specific microscopic con-

figurations, the samples should be randomly created. Based on the samples, statistical averaging is carried out. The process of numerical experiments designed in such a way is a good approximation to the standard statistical procedure [9].

As described in above sections, various microscopic observables for a particular cell can be defined in terms of the bit variables associated with the cell. For instance, when modelling the two-dimensional *HPP* lattice gas, the microscopic density at a particular cell  $j$  will be defined as the density of the particles in the cell,

$$\rho_{cell}^{j\ k}(x_j, y_j) = \sum_{i=1}^4 n_i^k(x_j, y_j), \quad (2.54)$$

where 4 is the total number of the bit variables of the moving particles,  $(x_j, y_j)$  indicates the coordinates of the cell  $j$ , and  $n_i^k(x_j, y_j)$  is the  $i$ th bit variable. The superscript  $k$  represents the order number of the experimental samples obtained by running  $N_s$  times on *CA* machine (to be introduced in section 2.7). This summation in (2.54) is simply equivalent to counting the particles inside cell  $j$ . For a given sample  $k$ , the sample macroscopic density  $\rho^k$  at a particular spatial location  $(x, y)$  can be determined by averaging the values of  $\rho_{cell}^{j\ k}$  as,

$$\rho^k(x, y) = \frac{1}{N_T} \sum_{R} \sum_{i=1}^4 n_i^k(x_j, y_j), \quad j \in \mathfrak{R}.$$

where  $R$  describes a neighbourhood of cells centered around  $(x, y)$ ,  $(x_j, y_j)$  is the location of a particular cell within the area  $R$ , and  $N_T$  is the total number of bit variables within  $R$ .

The density  $\rho$  can be obtained by averaging a total of  $N_s$  macroscopic samples, that is,

$$\rho(x,y) = \frac{1}{N_s} \sum_{k=1}^{N_s} \rho^k = \frac{1}{N_s N_T} \sum_{k=1}^{N_s} \sum_R \sum_{i=1}^4 n_i^k(x_j, y_j) , \quad (2.55)$$

In Fig.2.13, a circular neighbourhood  $\mathfrak{R}$  is depicted.

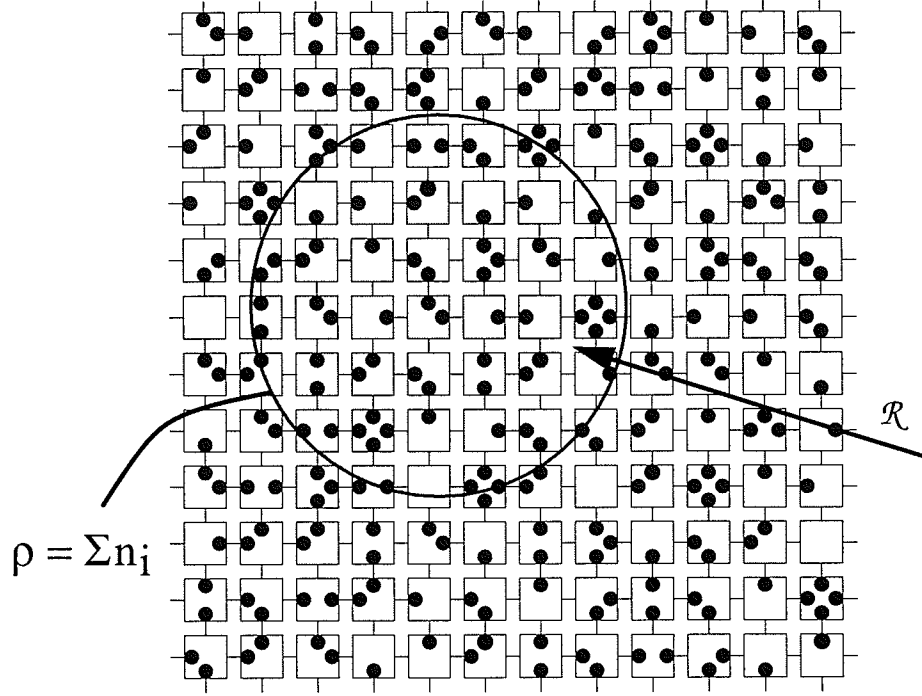
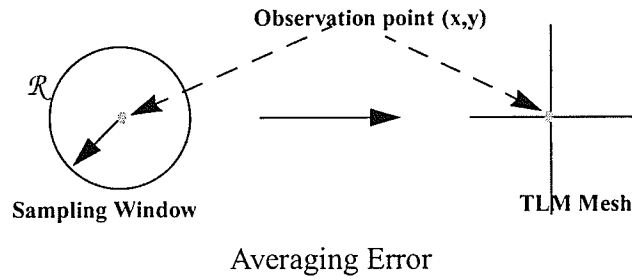


Fig.2.13: Macroscopic quantities as obtained through spatial averaging of microscopic states over a region  $R$ .

The averaging process described above is the method of encoding the observables. The complete microscopic bit information is retained at each timestep in the lattice gas automata. The dynamic range of macroscopic variables is thus proportional to the number of bits of memory[24]. If a sufficiently large window size is used, a continuum approximation is obtained. The dynamic range and accuracy of the observable quantity depends on the numbers of possible states contributing to the quantity and an inherent noise (is proportional to



$-\frac{1}{\sqrt{N_T}}$ ) respectively. Generally, a larger dynamic range and better statistical accuracy can be attained by using a larger sampling window. However, there is a trade-off between dynamic range, statistical accuracy and spatial averaging accuracy, since a larger size window always results in a spatial error range centred around a particular observation points. Although the lattice spacing used in our simulation is ten times finer than that of the transmission-line matrix mesh [40]. The graph below illustrates the spatial error associated with the averaging process.



## 2.5 Review of Lattice Gas Theory

### 2.5.1 Collision Operator

In what follows, we will not, for convenience, use the different notations for the different *LGA* models. The discussion presented below is valid for all above models except those specifically indicated.

The state of a particular cell at a timestep can be fully specified by a collection of the values of its  $n$  bit variables:

$$s = (s_1, \dots, s_n), \quad (2.56)$$

where  $s_i$  represents the value of the  $i$ th bit in the state  $s$ . If the particle  $i$  is present in the state  $s$ , its value  $s_i$  takes the value of one ( $s_i = 1$ ), otherwise  $s_i$  equals to zero ( $s_i = 0$ ). For example, in the *HPP* lattice gas, the pattern of the state  $s=(1,0,1,0)$  indicates that two particles with velocities  $\pm\hat{x}$  are present in the cell.

For a particular cell with  $n$  bits, we can have a total of  $2^n$  different collections, denoted by the set  $S$ . If  $s = (s_1, \dots, s_n) \in S$  as an in-state, then, after updating the bit variables, we have an out-state, expressed by the collection of  $s' = (s'_1, \dots, s'_n) \in S$ . Therefore, in the lattice gas, the transition process from an in-state to an out-state could be specified by  $2^n$  by  $2^n$  Boolean transmission matrix  $a$ . The element  $a(s \rightarrow s')$  characterizes the transition rules from an in-state  $s = \{s_i = 0 \text{ or } 1, i=1, \dots, n\}$  to an out-state  $s' = \{s'_i = 0 \text{ or } 1, i = 1, \dots, n\}$ . In the case of deterministic collisions,  $a(s \rightarrow s')$  is unity if and only if the particles in states collide to yield particles in states  $s'$ . Here the head-on collisions in *HPP* and those collisions in the 3-d vector models are examples of deterministic collisions, In the case of a non-deterministic collision,  $a(s \rightarrow s') = \xi$ , where  $\xi$  is a time and site-dependent random bit variable  $\xi$  with average value of  $\langle \xi \rangle = p$ . The example of non-deterministic collisions can be found in a *FHP* model where there are two possible out-states corresponding to every in-state of a head-on collision event. Thus one can use the random bit  $\xi$  probabilistically to describe the event.

Since each in-state  $s$  gives rise to exactly only one out-state  $s'$ , we have the relation:

$$\sum_{s'} a(s \rightarrow s') = 1 \quad (2.57)$$

This is simply a statement of conservation of probability.

Now we consider the production function[31,33]

$$p(n, s) = \prod_{j=1} n_j^{s_j} (1-n_j)^{(1-s_j)}, \quad (2.58)$$

where the arguments  $(n_1, \dots, n_n) \in S$  represent all possible states of a particular site, and the collection of  $s = (s_1, \dots, s_n) \in S$  describes the pattern of an in-state. Note that if the pattern of  $n_j$ 's matches a given the pattern of input states  $s_j$ 's, the function is equal to one ( $p(n, s) = 1$ ), otherwise  $p(n, s) = 0$ . Thus the function  $p(n, s)$  defines a Kronecker delta function of two bit collections:

$$p(n, s) = \delta(n, s) = \begin{cases} 1 & \text{if } s = n \\ 0 & \text{otherwise} \end{cases} \quad (2.59)$$

Note that the function  $p(n, s)$  defined in (2.58) has the selecting function which can pick up one state from all possible states  $(n_1, \dots, n_n) \in S$  of a particular cell. In addition to this, the Kronecker delta  $p(n, s)$ , like the conventional Kronecker delta functions with continue arguments, has the following two properties[31]:

$$\sum_s p(n, s) = \sum_s \prod_{j=1} n_j^{s_j} (1-n_j)^{(1-s_j)} = 1, \quad (2.60)$$

$$\text{and} \quad \sum_s s_i p(n, s) = \sum_s s_i \prod_{j=1} n_j^{s_j} (1-n_j)^{(1-s_j)} = n_i, \quad (2.61)$$

where the summation  $\sum_s$  denotes  $\sum_{s_1=1}^1 \dots \sum_{s_n=1}^1$ .

With the aid of the above properties, the microdynamic equation can be generally rewritten as

$$n_i(t + \Delta t, \mathbf{x} + \mathbf{c}_i) = \sum_{s, s'} s'_i a(s \rightarrow s') \delta(n, s) = \sum_{s, s'} s'_i a(s \rightarrow s') \left( \prod_{j=1}^{s_j} n_j^{s_j} (1-n_j)^{(1-s_j)} \right) . \quad (2.62)$$

The equation (2.62) has the following physical meaning[31]:

- (1) Before the collision, if the current pattern of  $n_j's$  matches that of  $s_j's$ , then the pattern is chosen by the term  $\delta(n, s)$ .
- (2) Through the collision, the input state describing the pattern of  $n_j's$  is transferred to the out-state with the pattern of  $s_j's$  characterized by the element of  $\langle a(s \rightarrow s') \rangle$ .
- (3) Finally, the value  $n'_i$  at next timestep of the  $i$ th bit of the out-state  $n'$  is determined by the factor  $s'_i$ .

Using the equation (2.61), we can have the microdynamical equation in a form that brings out the lattice collision operator:

$$n_i(t + \Delta t, \mathbf{x} + \mathbf{c}_i) = n_i(t, \mathbf{x}) + \omega_i(n^\dagger(t, \mathbf{x})) , \quad (2.63)$$

and the collision operator:

$$\omega_i(n^\dagger(t, \mathbf{x})) = \sum_{s, s'} (s'_i - s_i) a(s \rightarrow s') \left( \prod_{j=1}^{s_j} n_j^{s_j} (1-n_j)^{(1-s_j)} \right) . \quad (2.64)$$

---

## 2.5.2 Semi-Detailed Balance and Ensemble Average

### 2.5.2.1 Ensemble Average

A macroscopic description of an *LGA* can be obtained as an average over an ensemble of possible microscopic particle configurations. But an actual *LGA* simulation involves the evolution of just a single, specific, microscopic configuration. Nevertheless, many investigations show that suitable space or time average of this specific configuration can yield results which are close to those obtained from averages over the whole ensemble[9]. We denote the averages over this ensemble used in a *LGA* simulation by angular brackets  $\langle \rangle$ , *i.e.*,

$$N_i(\mathbf{x}, t) \equiv \langle n_i(\mathbf{x}, t) \rangle , \quad (2.65)$$

where  $n_i$  is a binary value while the average  $N_i(\mathbf{x}, t)$  of bit  $i$  is a real number and is called the *mean population* of bit  $i$ , taking a value ranging from 0 to 1.

When considering a non-linear function of bits  $n_i$  to be those terms appearing in the collision operators, the average of the function is not in general expressible as a function of the averaged quantities, since the correlations among these bits  $n_i$  must be considered. However, in many applications, we can reduce the complexity of the problem using the Boltzmann Molecular Chaos Assumption. The current lattice gas version of this assumption relies on the streaming (advection) phase of the simulation to effectively decorrelate the different bits at every site. In other words, the colliding particles have never had any prior effect on each other [31,33]. The theoretical analysis [33] shows that this assumption is reasonably valid in three or more dimensional lattice gases. In two dimensions, however, we must con-

sider corrections and employ some type of renormalization [33]. In this research we are most interested in an *LGA* system involving small perturbation to an equilibrium state (uniform background distribution) with low fluid velocity, such that the correction among the particles is small enough to be neglected [31]. Under this condition, for any combination of particles  $n_1 \dots n_b$ , the ensemble average could be

$$\langle n_1 \dots n_b \rangle \approx \langle n_1 \rangle \dots \langle n_b \rangle . \quad (2.66)$$

It would then follow that  $\langle \omega(n^\dagger) \rangle \approx \Omega(\langle n^\dagger \rangle) \approx \Omega(N^\dagger)$ , where  $N^\dagger$  stands for the complete set of mean population at site  $\mathbf{x}$  and time  $t$ .

Thus, by taking the ensemble averages of the microdynamic equations for the lattice gas, the lattice gas Boltzmann equation can be obtained as

$$N_i(t + \Delta t, \mathbf{x} + \mathbf{c}_i) = N_i(t, \mathbf{x}) + \Omega_i(N^\dagger(t, \mathbf{x})) \quad (i = 1 \dots b^m) , \quad (2.67)$$

and the average of the collision operator

$$\Omega_i(N^\dagger(t, \mathbf{x})) = \sum_{s, s'} (s'_i - s_i) A(s \rightarrow s') \left( \prod_{j=1} N_j^{s_j} (1 - N_j)^{(1-s_j)} \right) , \quad (2.68)$$

where  $A(s \rightarrow s')$  is the ensemble average of the element of the matrix element  $a(s \rightarrow s')$ , that is,

$$A(s \rightarrow s') = \langle a(s \rightarrow s') \rangle . \quad (2.69)$$

$A(s \rightarrow s')$  now represents the transition probability from an in-state  $s = \{s_i; i = 1, \dots, n\}$  to an out-state  $s' = \{s'_i; i = 1, \dots, n\}$  in a collision event. Again, note that a Boltzmann equation is in terms of real number variables,  $N_i(\mathbf{x}, t)$ , while a microdynamic equation is in terms of binary variables  $n_i$ .

### 2.5.2.2 Semi-Detailed Balance and Equilibrium Distribution

One of the important criteria used to obtain the equilibrium solution for the Boltzmann equation is the Semi-Detailed Balance. Simply stated, it means that before collision, if all states which lead to a particular out-state have equal probabilities, they stay so after collision [31,33]. Explicitly, it can be written as

$$\sum_s A(s \rightarrow s') = 1 \quad \forall s'. \quad (2.70)$$

Here an important difference between the semi-detailed balance (2.70) and  $\sum_{s'} A(s \rightarrow s') = 1$  should be noted: the latter represents the conservation probability while the former is the condition which is required to obtain the steady state solution of the Boltzmann equation. Also note that semi-detailed balance is a weaker condition than detailed balance. Detailed balance describes the deterministic, one-to-one and reversible collision process, and can be stated as:

*If a lattice gas is said to obey detailed balance, its transition matrix satisfies*

$$A(s \rightarrow s') = A(s' \rightarrow s), \quad \forall s, s' \quad (2.70)$$

Theoretical analyses, for example [16,31,33] have shown that, for kinetic systems of lattice gases which are finite and periodically wrapped around, there are very simple statistical equilibrium solutions in which the Boolean variables at all sites are independent due to their purely local collisions on the lattices. The analytical results presented in [31] will be quoted as the following lemma:

**Lemma:** *if any lattice gas at an equilibrium obeys semi-detailed balance, then the solution to the mean population  $N_i (i = 1 \dots b_m)$  satisfies the set of equations for the  $b_m$  collision operators, i.e.,*

$$\Omega_i(N^\dagger(t, \mathbf{x})) = \sum_{s, s'} (s'_i - s_i) A(s - s') \prod_{j=1} N_j^{s_j} (1 - N_j)^{(1-s_j)} = 0 \quad (i = 1 \dots b_m) \quad , \quad (2.71)$$

*and the solutions  $N_i (i = 1 \dots b_m)$  are given by the Fermi-Dirac distribution*

$$N_i = \frac{1}{1 + \exp(h + \mathbf{q} \cdot \mathbf{c}_i)} \quad (2.72)$$

*where  $h$  is an arbitrary real number and  $\mathbf{q}$  is an arbitrary  $D$ -dimensional vector.*

The important consequence of the lemma is that the mean populations given by (2.72) are independent of time and spatial coordinates. The equilibrium solutions are then universal over the lattices, and are only dependent on the density  $\rho$  and the mass current (momentum density)  $\mathbf{j} = \rho \mathbf{u}$ . The Lagrange multipliers  $h$  and  $\mathbf{q}$  can be calculated in terms of the dependence of the *Fermi-Dirac* distribution on the mass and momentum density.

## 2.6 The CAM-8 Cellular Automata Machine

The computational inefficiency of simulating CA on conventional serial computers (such as a workstation or PC) is a concern. The Information Mechanics Group at the MIT Laboratory for Computer Science has been involved in the development of special purpose computational hardware for the efficient evaluation of CA [24,27]. *CAM-8* is a cellular automata machine newly developed by this group. *CAM-8* is an implementation of a partitioning cellular automata (PCA) in which hardware is organized as 16 separate bit-planes.



---

Each plane stores exactly 1 bit of state information of a particular cell, thus the 16 bits of state of every cell are distributed across the 16 bit-planes. The *CAM-8* machine operates in two alternating stages:

(1) Data-update stage, during which PCA partition the space into individual sites, and each particular site's state is isolated and is not allowed to have any influence on the new state of any other site. At this time, the new state of a particular site is a function merely of its current state. In the most elementary case, the state information of the site is described by 16 bits, and using the values of 16 bits as an index into a look up table, a new 16 bit values of the new state is extracted, and then restored to the original position of the site. This updates the state of all the sites in parallel. The format follows the lattice gas models and corresponds to the collision phase.

(2) Data-transport stage, during which isolation among sites is eliminated, allowing the state information of one site to be exchanged with another. Every site's state is separated into 16 bit-planes, and the contents of any bit-plane can be moved relative to the contents of the other bit-planes by a data-movement facility, kicking [27], which is performed by offsetting memory registers rather than physically moving the bits around. This process realizes the transfer of data to its neighbouring sites, and therefore corresponds to the advection phase of lattice gas models. Fig.2.14 show this basic operation for cells.

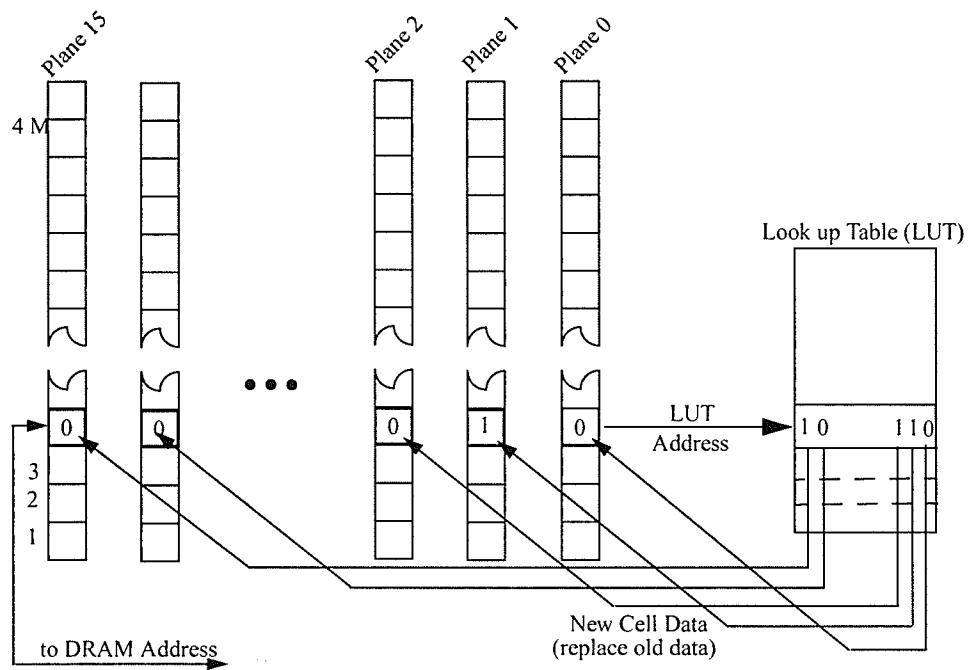


Fig.2.14. Basic operations of *CAM-8* [27].

---

## Chapter 3. Mixture Lattice Gas Automata

### 3.1 Introduction

In this chapter the mixture *HPP LGA* model which is not limited to a concrete configuration of rest particles is presented. Detailed analysis is developed to show how this model can be applied to the simulation of two-dimensional electromagnetic phenomena in inhomogeneous media.

Considering the relative rigour and the exclusion of viscosity in the analysis, we begin the analysis with the more complex *FHP* lattice and limit it to the *Euler* equation derived from the lowest order of the Chapman-Enskog expansions. With the small perturbation assumption, in *Euler* equation the non-linear terms involved with more than the third rank symmetry can be ignored. At this point, there will be no difference between *HPP* and *FHP* models and both of the lattices can lead to a linear wave equation.

An important aspect of this chapter is the development of an algorithm showing how to model the media with different sound speeds, analogous to modelling different dielectric constants in inhomogeneous media of electromagnetics. An *LGA* model without zero-velocity “rest particles” can only yield an uniform sound speed. Change in sound speed of an *LGA* can be achieved by incorporating rest particles at a lattice site with moving particles. We note that the form of macroscopic wave equation is in fact insensitive to microscopic details. It will be seen in the following analysis that there are only a few restrictions, such as conservations of mass and momentum and semi-detail balance, that are imposed when con-

structuring an *LGA* model. A wide range of dielectric constants can be modelled by specifying various interaction models. One can specify that certain regions of the *LGA* are different in the rest particle number and mass, so that energy exchange between the rest and moving particles in the regions are different, and an *LGA* with inhomogeneous sound speeds can be realized.

In the following section, the derivation of the kinetic and hydrodynamical equations of the model is presented in a more detailed way. Section 3 gives some results of the numerical experiments. Two of the experiments are designed to check the validity of the mixture model. A variety of applications of this model for problems of wave interaction with dielectric objects, from a simple heterogeneous dielectric cylinder to complex biological structures, are reported and compared with traditional numerical methods.

### 3.2 Theoretical Analysis for the Mixture Model

The mixture lattice gas models are described in Subsection 2.2.3 and illustrated in Figs.2.4 and 2.7. The dynamic description for the models is given in the Subsection 2.2.4.5. The notations used in the sequence analysis can be referred to those subsections and figures.

#### 3.2.1 Lattice Boltzmann Equation

Consider the *FHP* lattice gas model shown in Fig.2.7(b). The Boltzmann equations for the lattice dynamic system can be written for moving and rest particles respectively as,

$$N_{i,o}(\mathbf{x} + \mathbf{c}_i, t + \Delta t) = N_{i,o}(\mathbf{x}, t) + \Omega_{i,o}[N^\dagger(\mathbf{x}, t)] \quad (i = 1, \dots, b_m), \quad (3.1)$$

and

$$N_{o,k}(\mathbf{x}, t + \Delta t) = N_{o,k}(\mathbf{x}, t) + \Omega_{o,k}[N^{\dagger}(\mathbf{x}, t)] \quad (k = 1, \dots, b_r) . \quad (3.2)$$

Note that the rest particles always reside at some sites, and have zero velocity  $c_i (=0)$ . Again, the symbol  $f(N^{\dagger}(\mathbf{x}, t))$  indicates that dependency of the function  $f$  on the mean populations  $N_{i,k}$  of all bit variables at site  $\mathbf{x}$  and timestep  $t$ .

### 3.2.2 The Equilibrium Distribution

In what follows, we are interested in obtaining the solutions of the physical system around equilibrium (at quasi-equilibrium), since the uniform equilibrium lattice gas can not be used to simulate the wave propagation. However, to study an *LGA* around an equilibrium, we must first consider the solutions at equilibrium. Thereafter the solutions of the system at quasi-equilibrium can be obtained through a Chapman-Enskog expansion [31,41] in terms of mass density and momentum at equilibrium.

Now, if the system is at an equilibrium, according to the Lemma in chapter 2[31], the collision operators for the moving and rest particles satisfy

$$\Omega_{i,o}[N^{\dagger eq}(\mathbf{x}, t)] = \Omega_{k,o}[N^{\dagger eq}(\mathbf{x}, t)] = 0, \quad (3.3)$$

and the equilibrium solutions for the moving and rest particles, respectively, are expressed as:

$$N_{i,o}^{eq} = \frac{1}{1 + \exp(h + \mathbf{q} \cdot \mathbf{c}_i)}, \quad (3.4)$$

---

and 
$$N_{o,k}^{eq} = \frac{1}{1 + \exp(h)} \quad , \quad (3.5)$$

where the subscript *eq* stresses that the mean populations are evaluated at equilibrium. The Lagrange multipliers *h* and *q* can be calculated in terms of the relations of the conserved macroscopic physical quantities with the mean populations at equilibrium.

In the system, the two conserved macroscopic quantities, density  $\rho$  and momentum  $\rho \mathbf{u}$ , are related to the local mean population  $N_{i,k}$  of particles with mass  $m_k$ , velocity  $c_i$  and mixture ratio  $p_k$  by

$$\rho = \sum_{\substack{i=1 \\ (k=0)}}^{b_m} N_{i,o}^{eq} + \sum_{\substack{k=1 \\ (i=0)}}^{b_r} m_k N_{o,k}^{eq} p_k \quad , \quad (3.6)$$

and 
$$\rho \mathbf{u} = \sum_{\substack{i=1 \\ (k=0)}}^{b_m} N_{i,o}^{eq} c_i \quad , \quad (3.7)$$

where  $\rho$  and  $\mathbf{u}$  are mass density and fluid flow velocity per cell, respectively. Note that the distinction between the mixture ratio  $p_k$  and the random bit probability of  $p'_k$  discussed in chapter 2.  $p_k$  represents that the percentage of sites in a particular region is filled with rest particles  $m_k$ , while  $p'_k$  is related with the local collision rules and represents the probability of the creation or annihilation of the rest particle  $m_k$  in each collision event.

To calculate the equilibrium distributions, we consider the equilibrium with low flow speed  $u = |\mathbf{u}| \ll c$  ( $c$  the speed of moving particles), such that the microscopic collisions can approximately maintain a local equilibrium [31]. In a CA numerical experiment, the equilibrium is easy to realized by operating the *LGA* near a local equilibrium state[32,33]. With

consideration of the symmetry of the density and velocity of the lattice[31], the  $h$  and  $q$  functions can be formally expanded as the following series of velocity  $u$

$$h(\rho, u) = h_0 + h_2 u^2 + O(u^4) , \quad (3.8)$$

$$q(\rho, u) = q_1 u + O(u^3) . \quad (3.9)$$

Note that the  $h$  is an even function and  $q$  is an odd function due to the symmetry of the LGA. When  $u = 0$ , the average density for all particles with mass  $m_k$  is the same, and denoted by  $d_k$ . If taking the mass of the lightest particles (moving particles) as unit, and denoting its density by  $d_0 = d$ , we have the following expression for the moving particles

$$N_{i,0}^{eq}(h_0) = d = \frac{1}{1 + \exp(h_0)} , \quad (3.10)$$

and for rest particle

$$N_{0,k}^{eq}(h_0) = d_k = \frac{1}{1 + \exp(m_k h_0)} . \quad (3.11)$$

Thus, the density of rest particle  $d_k$  can be related to the moving particle  $d$  at  $u=0$  through the relation:

$$d_k = \frac{d^{m_k}}{d^{m_k} + (1 - d)^{m_k}} . \quad (3.12)$$

Now, to determine the coefficients of  $h_0$ ,  $h_2$  and  $q_1$  in the equations (3.8) and (3.9), we can calculate the equilibrium distribution functions perturbationally in powers of  $u$ . Consider the Fermi-Dirac type function:

$$f(x+x_0) = \frac{1}{1 + \exp(x+x_0)} . \quad (3.13)$$

If the function is expanded around  $x_0$  and  $x \ll x_0$ , then

$$f(x_0+x) = f(x_0) + f'(x_0)x + \frac{1}{2}f''(x_0)x^2 + \dots , \quad (3.14)$$

where  $f'(x_0) = -f(x_0)(1-f(x_0))$  and  $f''(x_0) = f(x_0)(1-f(x_0))(1-2f(x_0))$  .

Using the above formulas, the expansion of the equilibrium distribution function (3.4) for moving particles can be written as

$$N_{i,0}^{eq} = N_{i,0}(h_0) + N'_{i,0}(h_0)(q_1(\mathbf{u} \cdot \mathbf{c}_1) + h_2 u^2) + \frac{1}{2}N''_{i,0}(h_0)q_1^2(\mathbf{u} \cdot \mathbf{c}_1)^2 + O(u^3), \quad (3.15)$$

where

$$N_{i,0}^{eq}(h_0) = \frac{1}{1 + \exp(h_0)} = d ,$$

$$\begin{aligned} N'_{i,0}(h_0) &= -N_{i,0}^{eq}(h_0)(1 - N_{i,0}^{eq}(h_0)) \\ &= -d(1-d) , \end{aligned}$$

$$\begin{aligned} N''_{i,0}(h_0) &= N_{i,0}^{eq}(h_0)(1 - N_{i,0}^{eq}(h_0))(1 - 2N_{i,0}^{eq}(h_0)) \\ &= d(1-d)(1-2d) . \end{aligned}$$

The expansion of the equilibrium distribution function for moving particles can thus be found up to the second order  $O(u^2)$  as:

$$N_{i,0}^{eq} = d[1 - (1-d)(q_1(\mathbf{u} \cdot \mathbf{c}_1) + h_2 u^2) + \frac{(1-d)(1-2d)}{2}q_1^2(\mathbf{u} \cdot \mathbf{c}_1)^2] + O(u^3) . \quad (3.16)$$

A similar expansion can be obtained for a rest particle with mass  $m_k$  by letting  $\mathbf{c}_k = \mathbf{0}$ ,



that is,

$$N_{0,k}^{eq} = d_k[1 - (1 - d_k)h_2 u^2 m_k] + O(u^3) . \quad (3.17)$$

The two unknowns  $q_1$  and  $h_2$  in (3.16) and (3.17) can be determined through the relationships of the density  $\rho$  and momentum  $\rho u$  to the distribution functions(3.16). It follows from (3.5) and (3.7) that

$$\rho = \sum_{\substack{i=1 \\ (k=0)}}^{b_m} m_0 N_{i,0}^{eq} + \sum_{\substack{k=1 \\ (i=0)}}^{b_r} m_k p_k N_{0,k}^{eq} = d b_m + \sum_{k=1}^{b_r} m_k p_k d_k, \quad (3.18)$$

and

$$\rho u_\alpha = \sum_{\substack{i=1 \\ (k=0)}}^{b_m} m_0 N_{i,0}^{eq} c_{i,\alpha} + \sum_{\substack{k=1 \\ (i=0)}}^{b_r} m_k p_k N_{0,k}^{eq} c_{0,\alpha} = \sum_{i=1}^{b_m} N_{i,0}^{eq} c_{i,\alpha}, \quad (3.19)$$

where  $c_{0,\alpha} = 0$  for the rest particles has been used in (3.19). The Greek index  $\alpha$  represents the spatial components of velocity of the particles. For the case of two dimensional lattice  $\alpha \in (x, y)$ , but in general  $\alpha$  is valid in the  $N$ -dimensional case. Since  $d$  and  $d_m$  represent the mean population of the moving and rest particles per site, the first and second terms in (3.18), respectively, can be identified as the density of the moving and rest particles, that is,

$$\rho_m = b_m d \quad \text{and} \quad \rho_r = \sum_{k=1}^{b_r} m_k p_k d_k, \quad \text{thus,} \quad \rho = \rho_m + \rho_r. \quad (3.20)$$

Substituting the expansion expressions of (3.16) and (3.17) in (3.18) and (3.19), the two unknowns  $q_1$  and  $h_2$  can be found as:

$$q_1 = -\frac{2\rho}{(1-d)\rho_m c^2}, \quad (3.21)$$

$$h_2 = \frac{(1-2d)c_s^2}{2} q_1^2. \quad (3.22)$$

where  $c_s$  is defined below as. It will be shown in Subsection 3.2.5 that the parameter  $c_s$  represents the sound speed of the lattice gas.

$$c_s = \sqrt{\frac{d(1-d)b_m c^2}{2[d(1-d)b_m + \sum_{k=1}^{b_r} m_k^2 p_k d_k (1-d_k)]}}. \quad (3.23)$$

When formulating the above expressions, the following specific properties related to the symmetry of the tensors have been used. Generally, for the modelling of fluid dynamic problems, it is a basic requirement that all tensor formed from outer products of the lattice vectors be isotropic through all of four ranks, and so yield the standard hydrodynamic equations and correct viscosity coefficient for *LGAs* [16,31,33]. For the *HPP* lattice gas model, however, the tensors formed from outer products only satisfy the first *three* isotropic requirements. Fortunately, it will be seen in subsequent discussion that, for the problem of modelling wave propagation (*i.e.* not requiring a correct viscosity), we do not need to involve those terms obtained from the evaluation of the fourth rank tensor. Therefore, the simple *HPP* model is valid for our applications of linear wave propagation. Mathematically, the tensor products to the fourth order rank for the present model with  $b_m$  moving particles can be expressed as

$$\sum_{i=1}^{b_m} c_{i\alpha} = 0, \quad (3.24)$$

$$\sum_{i=1}^{b_m} c_{i\alpha} c_{i\beta} = \frac{b_m c^2}{2} \delta_{\alpha\beta}, \quad (3.25)$$

$$\sum_{i=1}^{b_m} c_{i\alpha} c_{i\beta} c_{i\delta} = 0, \quad (3.26)$$

and

$$\sum_{i=1}^{b_m} c_{i\alpha} c_{i\beta} c_{i\delta} c_{i\gamma} = \frac{b_m c^4}{8} (\delta_{\alpha\beta} \delta_{\delta\gamma} + \delta_{\alpha\delta} \delta_{\beta\gamma} + \delta_{\alpha\gamma} \delta_{\beta\delta}), \quad (3.27)$$

where equations (3.24) to (3.27) are the first, second, third and fourth order vector outer product, respectively. The summation on the repeated Greek indices is implied.

Using the above relations of (3.24) to (3.27), the expansion for mean populations at an equilibrium state can be obtained for moving and rest particles up to the second order of  $\mathbf{u}$ . For moving particles, using (3.16), (3.21) and (3.22),

$$N_{i,o}^{eq} = d \left\{ 1 + \frac{2\rho}{c^2 \rho_m} \mathbf{c}_i \cdot \mathbf{u} + G(\rho) \left[ Q_{i\gamma\delta} + \left( \frac{c^2}{2} - c_s^2 \right) \delta_{\gamma\delta} \right] u_\gamma u_\delta \right\}, \quad (3.28)$$

where  $i=1$  to  $b_m$ ,  $Q_{i\gamma\delta} = c_{i\gamma} c_{i\delta} - \frac{c^2}{2} \delta_{\gamma\delta}$  and function  $G(\rho)$

$$G(\rho) = \frac{2\rho^2(1-2d)}{c^4 \rho_m^2(1-d)}.$$

For rest particles, using (3.17), (3.21) and (3.22),

$$N_{o,k}^{eq} = d_k \left[ 1 - G(\rho) \frac{(1-d_k)}{(1-d)} u^2 m_k c_s^2 \right], \quad (3.29)$$

where  $k=1$  to  $b_k$

### 3.2.3 Chapman-Enskog Expansion and Conservation Laws

In the above subsections, the mean equilibrium population with low speed has been obtained. In the subsequent derivation of lattice gas hydrodynamical equations we are interested in an *LGA* system at a local equilibrium with density and momentum slowly changing in space and time. From the conservations of mass and momentum, the macrodynamic equations can be derived by using Chapman-Enskog expansion and multi-scale technique[31,41]. This analytical process is almost the same method as that used in real fluid dynamics. The Chapman-Enskog expansion is a perturbation solution to Boltzmann equations (3.1) and (3.2) near an equilibrium state. Let the solution be expanded as a series in powers of  $\epsilon$  (very small number  $\epsilon \rightarrow 0$ ) [33]:

$$N_{i,k} = N_{i,k}^{(0)} + N_{i,k}^{(1)} + N_{i,k}^{(2)} + O(\epsilon^3) , \quad (3.30)$$

where  $N_{i,k}^{(0)} = N_{i,k}^{eq}$  is the mean population distribution at equilibrium. The multi-scale technique used here is called wave ordering since the ordering is appropriate for wave propagation[31]. The multi-scale technique can be introduced by assuming that the gradients of the  $N_{i,k}^{(n)}$  and the differential with respect to time  $\partial t$  are very small. Thus the postulation could be written for the first order derivative as

$$\nabla \sim \partial t = O(\epsilon),$$

and for the  $n$ th order derivative as

$$\nabla^{(n)} = O(\epsilon^n) ,$$

such that  $N_{i,k}^{(n)} = \nabla^{(n)} = O(\epsilon^n)$ .

In what follows, we insert the expansion (3.30) in the Boltzmann equations (3.1) and (3.2), and use the above multi-scale technique. By collecting the terms at order  $O(\epsilon)$ , the first order equations for the moving particles  $N_{j,o}^{(1)}$  and rest particles  $N_{o,l}^{(1)}$  can be respectively obtained as,

$$\partial_t N_{i,o}^{(o)} + c_{i\beta} \partial_\beta N_{i,o}^{(o)} = \sum_{j=1}^{b_m} \Lambda_{i,j}^m N_{j,o}^{(1)} + \sum_{k=1}^{b_r} \Lambda_{i,k}^m N_{o,k}^{(1)}, \quad (3.31)$$

and

$$\partial_t N_{o,k}^{(o)} = \sum_{l=1}^{b_r} \Lambda_{k,l}^r N_{o,l}^{(1)} + \sum_{j=1}^{b_m} \Lambda_{k,j}^r N_{j,o}^{(1)}, \quad (3.32)$$

where  $\Lambda_{i,j}^m = \left( \frac{\partial \Omega_{i,o}}{\partial N_{j,o}} \right) \Big|_{N^+ = N^{+eq}}$ ,  $\Lambda_{i,k}^m = \left( \frac{\partial \Omega_{i,o}}{\partial N_{o,k}} \right) \Big|_{N^+ = N^{+eq}}$ ,

$$\Lambda_{k,l}^r = \left( \frac{\partial \Omega_{o,k}}{\partial N_{o,l}} \right) \Big|_{N^+ = N^{+eq}} \text{ and } \Lambda_{k,j}^r = \left( \frac{\partial \Omega_{o,k}}{\partial N_{j,o}} \right) \Big|_{N^+ = N^{+eq}}.$$

### 3.2.3.1 Mass Conservation

Now the conservation of mass and the series expansions obtained in the above subsection could be used to derive a partial differential equation which describes the macroscopic density of mass for the lattice. In order to do this, taking the summation of equations (3.1) and (3.2) over the indices  $i$  and  $k$  respectively, and adding the resultant equations, we get,

$$\begin{aligned}
& \sum_{i=1}^{b_m} N_{i,o}(\mathbf{x} + \mathbf{c}_i, t + \Delta t) + \sum_{k=1}^{b_r} N_{o,k}(\mathbf{x}, t + \Delta t) = \\
& \sum_{i=1}^{b_m} N_{i,o}(\mathbf{x}, t) + \sum_{k=1}^{b_r} N_{o,k}(\mathbf{x}, t) + \sum_{i=1}^{b_m} \Omega_{i,o} [N^\dagger(\mathbf{x}, t)] + \sum_{k=1}^{b_r} \Omega_{o,k} [N^\dagger(\mathbf{x}, t)] .
\end{aligned} \tag{3.33}$$

Note that in (3.33) the terms on the left hand side and the first two terms on the right hand side represent the mass density at time  $t + \Delta t$  and  $t$  respectively. Since the mass conservation is independent of spatial position and time, *i.e.*

$$\rho = \sum_{i=1}^{b_m} N_{i,o}(\mathbf{x} + \mathbf{c}_i, t + \Delta t) + \sum_{k=1}^{b_r} N_{o,k}(\mathbf{x}, t + \Delta t) = \sum_{i=1}^{b_m} N_{i,o}(\mathbf{x}, t) + \sum_{k=1}^{b_r} N_{o,k}(\mathbf{x}, t) , \tag{3.34}$$

this leads to

$$\sum_{i=1}^{b_m} \Omega_{i,o} [N^\dagger(\mathbf{x}, t)] + \sum_{k=1}^{b_r} \Omega_{o,k} [N^\dagger(\mathbf{x}, t)] = 0. \tag{3.35}$$

Inserting the perturbation expansion of (3.30) in the equation (3.35) and expanding the resultant expression at the equilibrium state  $N_{i,k}^{eq}$ , we have

$$\begin{aligned}
& \sum_{i=1}^{b_m} \Omega_{i,o} (N^{eq\dagger}) + \sum_{k=1}^{b_r} \Omega_{o,k} (N^{eq\dagger}) + \sum_{j=1}^{b_r} \sum_{i=1}^{b_m} \Lambda_{i,j}^m N_{j,o}^{(1)} + \sum_{k=1}^{b_r} \sum_{i=1}^{b_m} \Lambda_{i,k}^m N_{o,k}^{(1)} + \\
& + \sum_{l=1}^{b_r} \sum_{k=1}^{b_r} \Lambda_{k,j}^r N_{o,k}^{(1)} + \sum_{k=1}^{b_r} \sum_{i=1}^{b_m} \Lambda_{k,j}^r N_{j,o}^{(1)} = 0.
\end{aligned} \tag{3.36}$$

Since, at equilibrium state  $\sum_{i=1}^{b_m} \Omega_{i,o}(N^{eq\dagger}) = \sum_{k=1}^{b_r} \Omega_{o,k}(N^{eq\dagger}) = 0$ , such that

$$\sum_{j=1}^{b_m} \sum_{i=1}^{b_m} \Lambda_{i,j}^m N_{j,o}^{(1)} + \sum_{k=1}^{b_r} \sum_{i=1}^{b_m} \Lambda_{i,k}^m N_{o,k}^{(1)} + \sum_{l=1}^{b_r} \sum_{k=1}^{b_r} \Lambda_{k,j}^r N_{o,k}^{(1)} + \sum_{k=1}^{b_r} \sum_{i=1}^{b_m} \Lambda_{k,j}^r N_{j,o}^{(1)} = 0. \quad (3.37)$$

Similarly, if we multiply the equation (3.1) with  $c_{i\alpha}$ , and take the summation over the moving particle index  $i$ , then

$$\sum_{i=1}^{b_m} c_{i\alpha} N_{i,o}(\mathbf{x} + \mathbf{c}_i, t + \Delta t) = \sum_{i=1}^{b_m} c_{i\alpha} N_{i,o}(\mathbf{x}, t) + \sum_{i=1}^{b_m} c_{i\alpha} \Omega_{i,o}[N^\dagger(\mathbf{x}, t)]. \quad (3.38)$$

It follows from the conservation of momentum (the first and second terms in (3.38) are equal) that we have

$$\sum_{i=1}^{b_m} c_{i\alpha} \Omega_{i,o}[N^\dagger(\mathbf{x}, t)] = 0. \quad (3.39)$$

Substituting the perturbation expansion given in (3.30) into (3.39), and expanding it, we get

$$\sum_{i=1}^{b_m} c_{i\alpha} \Omega_{i,o}(N^{\dagger eq}) + \sum_{j=1}^{b_m} \sum_{i=1}^{b_m} c_{i\alpha} \Lambda_{i,j}^m N_{j,o}^{(1)} + \sum_{l=1}^{b_r} \sum_{i=1}^{b_m} c_{i\alpha} \Lambda_{i,l}^m N_{o,l}^{(1)} = 0. \quad (3.40)$$

The first term  $\sum_{i=1}^{b_m} c_{i\alpha} \Omega_{i,o}(N^{\dagger eq}) = 0$  due to the conservation of momentum at an equilibrium

state. Thus we have

$$\sum_{j=1}^{b_m} \sum_{i=1}^{b_m} c_{i\alpha} \Lambda_{i,j}^m N_{j,o}^{(1)} + \sum_{l=1}^{b_r} \sum_{i=1}^{b_m} c_{i\alpha} \Lambda_{i,l}^m N_{o,l}^{(1)} = 0. \quad (3.41)$$

Now, by taking the summation of equation(3.31) over index  $i$  and equation (3.32) over index  $k$ , and then adding the two resultant equations, we obtain

$$\begin{aligned} \partial_t \left( \sum_{i=1}^{b_m} N_{i,o}^{eq} + \sum_{k=1}^{b_r} N_{o,k}^{eq} \right) + \partial_\beta \left( \sum_{i=1}^{b_m} c_{i\beta} N_{i,o}^{eq} \right) = \sum_{i=1}^{b_m} \sum_{j=1}^{b_m} \Lambda_{i,j}^m N_{j,o}^{(1)} + \\ \sum_{i=1}^{b_m} \sum_{k=1}^{b_r} \Lambda_{i,k}^m N_{o,k}^{(1)} + \sum_{k=1}^{b_r} \sum_{l=1}^{b_r} \Lambda_{k,l}^r N_{o,l}^{(1)} + \sum_{k=1}^{b_r} \sum_{j=1}^{b_m} \Lambda_{k,j}^r N_{j,o}^{(1)} . \end{aligned} \quad (3.42)$$

It then follows from (3.37) and the definition of mass and momentum per cell, which is given as

$$\rho = \sum_{i=1}^{b_m} N_{i,o}^{eq} + \sum_{k=1}^{b_r} N_{o,k}^{eq} \text{ and } \rho u_\beta = \sum_{i=1}^{b_m} c_{i\beta} N_{i,o}^{eq} , \quad (3.43)$$

thus we end up with the following equation:

$$\partial_t \rho + \nabla \cdot (\rho \mathbf{u}) = 0 . \quad (3.44)$$

This is the macroscopic equation for conservation of mass.

### 3.2.3.2 Momentum Conservation (*Euler Equation*)

Similarly, it follows from the conservation of momentum and the series expansion(3.30) that the macroscopic behaviour of the flow momentum (*Euler equation*) can be derived. To do this, we multiply the equation(3.31) with  $c_{i\alpha}$ , and take summation over index  $i$ , such that

$$\sum_{i=1}^{b_m} c_{i\alpha} \partial_t N_{i,o}^{(o)} + \partial_\beta \sum_{i=1}^{b_m} c_{i\alpha} c_{i\beta} N_{i,o}^{(o)} = \sum_{i=1}^{b_m} \sum_{j=1}^{b_m} c_{i\alpha} \Lambda_{i,j}^m N_{j,o}^{(1)} + \sum_{i=1}^{b_m} \sum_{k=1}^{b_r} c_{i\alpha} \Lambda_{i,k}^m N_{o,k}^{(1)} . \quad (3.45)$$



By using the equation(3.41), the above equation can be written as

$$\sum_{i=1}^{b_m} c_{i\alpha} \partial_t N_{i,o}^{(o)} + \partial_\beta \sum_{i=1}^{b_m} c_{i\alpha} c_{i\beta} N_{i,o}^{(o)} = 0, \quad (3.46)$$

where  $N_{i,k}^{(o)} = N_{i,k}^{eq}$ . Substituting the expression for  $N_{i,o}^{(o)}$  given in (3.28) in the above equation and using the relations of the tensor products to the fourth order rank described in expressions (3.24) to (3.27), the macrodynamic equation for momentum (*Euler equation*) up to the second order can be obtained as:

$$\partial_t(\rho u_\alpha) + \partial_\beta(\rho g(\rho) u_\alpha u_\beta) = -\partial_\alpha P(\rho, u^2), \quad (3.47)$$

or in vector form,

$$\partial_t(\rho \mathbf{u}) + \nabla \cdot (\rho g(\rho) \mathbf{u} \mathbf{u}) = -\nabla P(\rho, u^2), \quad (3.48)$$

where the pressure

$$P(\rho, u^2) = \frac{\rho_m c^2}{2} - \rho g(\rho) \frac{c_s^2}{c^2} \left( 2 - \frac{1}{2} \frac{c^2}{c_s^2} \left( 1 + \frac{1}{2} \right) \right) u^2, \quad (3.49)$$

and

$$g(\rho) = \frac{1}{2} \frac{\rho}{\rho_m} \frac{1-2d}{1-d}. \quad (3.50)$$

It should be noted that the simple *HPP* model does not satisfy the fourth rank tensor product relation given in (3.27) which has been used in the above derivation. But, by carefully inspecting the proceeding analysis, only the first two rank isotropic properties given in (3.24) and (3.25) have been used in the evaluation of the first term of the expression(3.49) for pressure. In the next subsection, it will be shown that, under the regime of undamped sound waves, the simple *HPP* model is valid for the modelling of the linear wave propagation.

### 3.2.4 Undamped Sound Wave Propagation

Consider a case in which a small perturbation  $(\rho', \mathbf{u}')$  is superimposed onto an equilibrium state with density  $\rho_o$  and zero velocity  $\mathbf{u}_o = \mathbf{0}$ , explicitly

$$\rho \approx \rho_o + \rho' \text{ and } \mathbf{u} \approx \mathbf{u}',$$

where  $\rho_o$  is the uniform background density, and  $\rho'$  and  $\mathbf{u}'$  are weak density and flow perturbation respectively. For this case, at order  $O(\epsilon)$  the conservation of mass equation (3.44) can be rewritten as

$$\partial_t \rho' + \rho_o \nabla \cdot \mathbf{u}' = 0, \quad (3.51)$$

and the *Euler* equation for the conservation of momentum (3.38) as

$$\partial_t \mathbf{u}' + \frac{c_s^2}{\rho_o} \nabla \rho' = 0, \quad (3.52)$$

where the sound speed  $c_s$  can be found from (3.49) as follows

$$c_s^2 = \left( \frac{\partial P}{\partial \rho} \right) \Big|_{u=0} = \frac{c^2}{2} \left( \frac{\partial \rho_m}{\partial \rho} \right) \Big|_{u=0}. \quad (3.53)$$

If equations (3.51) and (3.52) are combined to eliminate  $\mathbf{u}'$ , then the linear wave equation in terms of  $\rho'$  could be obtained as

$$\partial_t^2 \rho' - c_s^2 \nabla^2 \rho' = 0 \quad (3.54)$$

Here, since the regime of undamped sound wave involves only tensor calculations up to the second order, at this point, there is no difference between the simple *HPP* and *FHP* models. Thus the simple *HPP* is valid for modelling linear wave propagation. For the subsequent

discussion we need only to focus on the *HPP* model.

We can now make an analogy between the above two-dimensional wave equation (3.54) and two-dimensional *TM* or *TE* electromagnetic fields. For *TM<sub>z</sub>* case, the macroscopic perturbation density,  $\rho'$ , can be equated to the electric field  $E_z$ , and the x- and y- components of the perturbation flow velocity,  $\mathbf{u}' = (u'_x, u'_y)$ , can be equated to magnetic field components,  $H_y$  and  $H_x$ , respectively. Similarly, for the case of *TE<sub>z</sub>*,  $\rho'$  can be equated to the magnetic field  $H_z$ , and  $\mathbf{u}' = (u'_x, u'_y)$  can then be equated to electric field components  $E_y$  and  $E_x$  respectively.

### 3.2.5 Sound Speed and Dielectric Constant

For our present mixture *HPP* model, the mass density is  $\rho = \rho_m + \rho_r$ , where

$$\rho_m = b_m d, \quad \rho_r = \sum_{k=1}^{b_r} m_k p_k d_k, \quad (3.55)$$

and

$$d_k = \frac{d^{m_k}}{d^{m_k} + (1-d)^{m_k}},$$

where  $d$  and  $d_k$  were previously defined as the equilibrium density of moving and rest particles per cell, respectively, and  $p_k$  as the existing probability (mixture ratio) of the rest particle of mass  $m_k$ .

From the definition of the sound speed (3.53), we have

$$\frac{\partial \rho_m}{\partial \rho} = \frac{1}{\left(\frac{\partial \rho}{\partial \rho_m}\right)}.$$

It follows from the above expressions (3.12) and (3.55) and  $\rho = \rho_m + \rho_r$  that we get

$$\left(\frac{\partial \rho}{\partial \rho_m}\right) = 1 + \frac{1}{b_m} \left(\frac{\partial \rho_r}{\partial d}\right) = 1 + \frac{1}{b_m} \sum_{k=1}^{b_r} m_k p_k \left(\frac{\partial d_k}{\partial d}\right).$$

Using the expression (3.12) the partial differential  $\left(\frac{\partial d_k}{\partial d}\right)$  can be obtained as

$$\left(\frac{\partial d_k}{\partial d}\right) = \frac{m_k d_k (1 - d_k)}{d(1 - d)},$$

whence

$$\left(\frac{\partial \rho_m}{\partial \rho}\right) = \frac{b_m d(1 - d)}{b_m d(1 - d) + \sum_{k=1}^{b_r} m_k^2 p_k d_k (1 - d_k)}.$$

Consequently the square of the sound speed  $c_s$  can be found as,

$$c_s^2 = \frac{c^2 b_m d(1 - d)}{2 \left[ b_m d(1 - d) + \sum_{k=1}^{b_r} m_k^2 p_k d_k (1 - d_k) \right]}. \quad (3.56)$$

This is a general formula of sound speed for the mixture *LGA*.

The sound speed  $c_s$  on a lattice without rest particles (plain *LGA*) is obtained by letting

$m_k = 0$  ( $k=1 \dots b_r$ ), that is

$$c_s \equiv c_o = \frac{c}{\sqrt{2}}, \quad (3.57)$$

where  $c_o$  is defined as the sound speed on a plain *LGA*, analogous to the light speed in vac-

uum, and  $c$  is the speed of moving particle. The dielectric constant  $\epsilon_r$ , corresponding to the sound speed  $c_s$  (3.56) of the mixture model, can then be found as:

$$\epsilon_r = \left( \frac{c_o}{c_s} \right)^2$$

$$\epsilon_r = \frac{\left[ b_m d(1-d) + \sum_{k=1}^{b_r} m_k^2 p_k d_k(1-d_k) \right]}{b_m d(1-d)}, \quad (3.58)$$

for the *HPP* mixture model,  $b_m = 4$  i.e. 4 moving particles per cell, then

$$\epsilon_r = \frac{\left[ 4d(1-d) + \sum_{k=1}^{b_r} m_k^2 p_k d_k(1-d_k) \right]}{4d(1-d)}. \quad (3.59)$$

Here several special cases commonly used in *LGA* simulation are concerned below.

**Case1:** The background density is 50%( $d=0.5$ ). It follows from the expression of

(3.12) that  $d_k = 1/2$  and this simplifies equation(3.59) to:

$$\epsilon_r = 1 + \frac{1}{4} \sum_{k=1}^{b_r} m_k^2 p_k. \quad (3.60)$$

Note that regions with an arbitrary desired  $\epsilon_r$  value can be created by probabilistically assigning cells with different rest particles  $m_k$  based on the mixture ratio  $p_k$ . The Fig.3.1 shows some  $\epsilon_r$  values for various mixture ratios.

**Case2:** The background density is 50%( $d=0.5$ ), and in some regions all cells are assigned with rest particle(s)  $m_k$  i.e.  $p_k = 1$ . This further simplifies equation(3.59) to:

$$\epsilon_r = 1 + \frac{1}{4} \sum_{k=1}^{b_r} m_k^2. \quad (3.61)$$

For example, if a desired  $\epsilon_r = 5$  is to be modelled in a region, using the above formula, this can be realized by assigning a rest particle with  $m_k = 4$  per cell. Again, if  $\epsilon_r = 21$ , two rest particles with  $m_k = 4$  and  $m_k = 8$  are required with each cell.

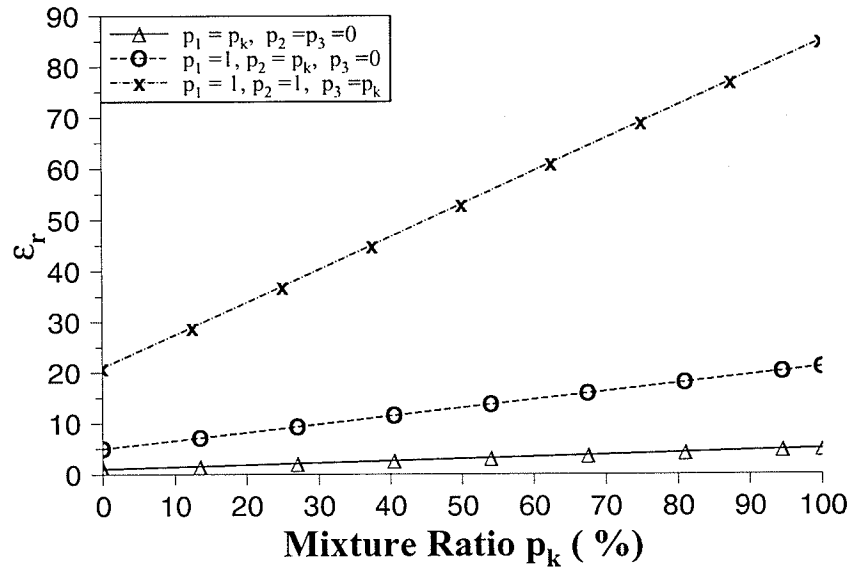


Fig. 3.1 Theoretical results for dielectric constants  $\epsilon_r$  versus the combinations of rest particle mixture ratios.

Based on the above discussion, it has been noted that a mixture *HPP LGA* has the ability to control the sound speed (dielectric constant) in a very flexible way. The general formula

mula for the sound speed enables a wide range of dielectric constant to be modelled by specifying various interaction models.

### 3.3 Numerical Simulation and Results

In this section, to validate the mixture *HPP* model, we design two simple numerical experiments with different collision models. The two group of collision rules describe the models given in the Tables 3.1 and 3.2, each with the cases of (A), (B), (C) and (D). Case (A) defines the collision rule of the sites without rest particle, case (B) with one rest particle of  $m_k = 2$ , case (C) with one rest particle of  $m_k = 4$  and case (D) with two rest particles of  $m_k = 2$  and  $m_k = 4$ . In those tables a transformation of velocity states of site occurs for two particle head-on collisions, the creation of moving particles from rest particles and the annihilation of moving particles after the interaction among them. For the mixture *HPP* models there are a total of  $2^6 = 64$  states per site, the rules describing the change of particle states after collision are listed below, and all other states not listed are streamed (*i.e.*, without the change of particle states after one step evolution).

Note that there is a difference between the two collision models. In collision model 1 (Tables 3.1(a), 3.1(b), 3.1(c) and 3.1(d)), for each incoming state there are two possible outgoing states, each with an equal probability of  $1/2$ . However, in collision model 2 (Tables 3.2(a), 3.2(b), 3.2(c) and 3.2(d)) there are three possible outgoing states, corresponding to each incoming moving particle state. The first two possible outgoing states are the same as those outgoing states described in model 1, but each with the probability of  $1/3$ . In the third possible outgoing state, also with the probability of  $1/3$ , the moving particles are allowed to keep their original states. For example, in Table 3.1(b) if two incoming mov-

---

ing particles exist in opposing velocity states (head-on), with an equal probability of  $1/2$ , the collision results in either transferring moving particles in the opposing velocity states vertical to the incoming particle pair, or creating one rest particle with mass  $m_k = 2$  where initially there is no mass 2 rest particle. Alternatively, if a mass 2 rest particle already exists at a site without other moving particles, two moving particles are created in pair either in the vertical or horizontal direction, each with a probability of  $1/2$ . But, Table 3.2(b) defines three possible outcoming states, in which the first two possible outcoming states are the same as those outcoming states illustrated in Table 3.1(b), but each with the probability of  $1/3$ . In the third possible outcoming state, also with the probability of  $1/3$ , the two incoming moving particles will just stream through the cell.

In the numerical simulations for the collision models described in the above tables, a two-dimension lattice with size  $1024 \times 256$  cells has been employed. Reflecting (perfect magnetic conductor in the  $TM_z$  case) boundary conditions[25] are applied to both  $x$  and  $y$  axes. Different uniform background densities  $d$  ranging from  $0.1$  to  $0.9$  are applied to the lattice. This mixture  $LGA$  can be constructed by probabilistically assigning cells a rest particle with 2 mass units based on the mixture ratio of  $30\%(p_1)$  and assigning cells a rest particle with 4 mass units based on the ratio of  $40\%(p_2)$ .

A  $TM_{20}$  field at cutoff frequency is used as an exciting source. The source with the maximum initial perturbation of 15% above the background is superimposed on the top of the background density. With the source, we can study both equilibrium and quasi-equilibrium behaviours of the system. The equilibrium behaviour can be obtained by taking time average of the macroscopic quantities. An observation window is chosen with the size of



---

59x59 cells, and is located at  $x=94l$  and  $y=128l$ .

The simulations were evolved for 15,000 time steps. As an example with  $d = 0.5$ , the standing wave responses at the observation window for the moving and rest particles are recorded and shown in Fig.3.2. The experimental results at equilibrium for the rest particle density were obtained by counting their numbers at the observation window, and taking the time average of the numbers. For example, in the case of  $d = 0.5$  shown in Fig.3.2, the two numbers were 745( $m_k = 2$ ) and 534( $m_k = 4$ ), thus the equilibrium density for rest particles was  $(745 \times 2 + 534 \times 4) / (59 \times 59) = 1.042$ . The experimental results for the density of rest particles at equilibrium, as well as the analytic values calculated using (3.12) are shown in Fig.3.3.

Collision Model 1: case A\*








$A(s, s')$		Outcoming States $s'$			
					
Incoming States $s$		0	1/2	1/2	0
		1/2	0	1/2	0
		0	0	0	1

Table 3.1(a): Collision rule for the sites of incoming states without rest particles

Collision Model 2: case A \*


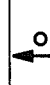
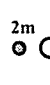


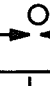





$A(s, s')$		Outcoming States $s'$			
					
Incoming States $s$		1/3	1/3	1/3	0
		1/3	1/3	1/3	0
		0	0	0	1

Table 3.2(a): Collision rule for the sites of incoming states without rest particles

- \* Symbols used in the tables: a)   $\Rightarrow$  no rest particle(  $m_k = 2$  )  
b)   $\Rightarrow$  no rest particle(  $m_k = 4$  )  
c)   $\Rightarrow$  with rest particle(  $m_k = 2$  )  
d)   $\Rightarrow$  with rest particle(  $m_k = 4$  )

Collision Model 1: case B\*



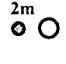



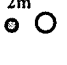
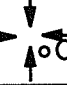
$A(s, s')$		Outcoming States $s'$			
					
Incoming States $s$		0	1/2	1/2	0
		1/2	0	1/2	0
		1/2	1/2	0	0
		0	0	0	1

Table 3.1(b): Collision rule for the sites of incoming states with a rest particle of  $m_k = 2$

Collision Model 2: case B \*


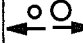
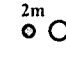



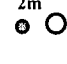

$A(s, s')$		Outcoming States $s'$			
					
Incoming States $s$		1/3	1/3	1/3	0
		1/3	1/3	1/3	0
		1/3	1/3	1/3	0
		0	0	0	1

Table 3.2(b): Collision rule for the sites of incoming states with a rest particle of  $m_k = 2$

Collision Model 1: case C \*

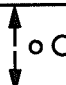
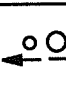
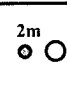
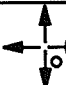
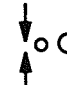


$A(s, s')$		Outcoming States $s'$			
					
Incoming States $s$		0	1/2	1/2	0
		1/2	0	1/2	0
		0	0	0	1

Table 3.1(c): Collision rule for the sites of incoming states with a rest particle of  $m_k = 4$

Collision Model 2: case C\*


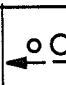
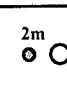
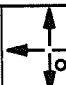
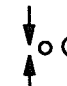
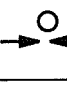

$A(s, s')$		Outcoming States $s'$			
					
Incoming States $s$		1/3	1/3	1/3	0
		1/3	1/3	1/3	0
		0	0	0	1

Table 3.1(c): Collision rule for the sites of incoming states with a rest particle of  $m_k = 4$

Collision Model 1: case D \*


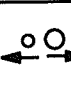
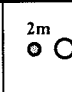
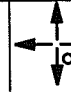
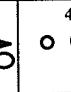
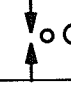
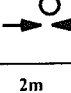

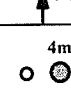
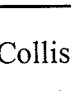
$A(s, s')$		Outcoming States $s'$				
						
Incoming States $s$		0	1/2	1/2	0	0
		1/2	0	1/2	0	0
		1/2	1/2	0	0	0
		0	0	0	0	1
		0	0	0	1	0

Table 3.1(d): Collision rule for the sites of incoming states with two rest particles of  $m_k = 2$  and  $m_k = 4$

Collision Model 2: case D \*

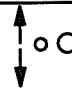
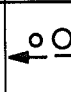
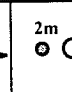
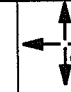

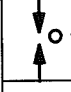
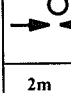

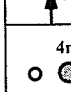
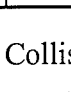
$A(s, s')$		Outcoming States $s'$				
						
Incoming States $s$		1/3	1/3	1/3	0	0
		1/3	1/3	1/3	0	0
		1/3	1/3	1/3	0	0
		0	0	0	0	1
		0	0	0	1	0

Table 3.2(d): Collision rule for the sites of incoming states with two rest particles of  $m_k = 2$  and  $m_k = 4$

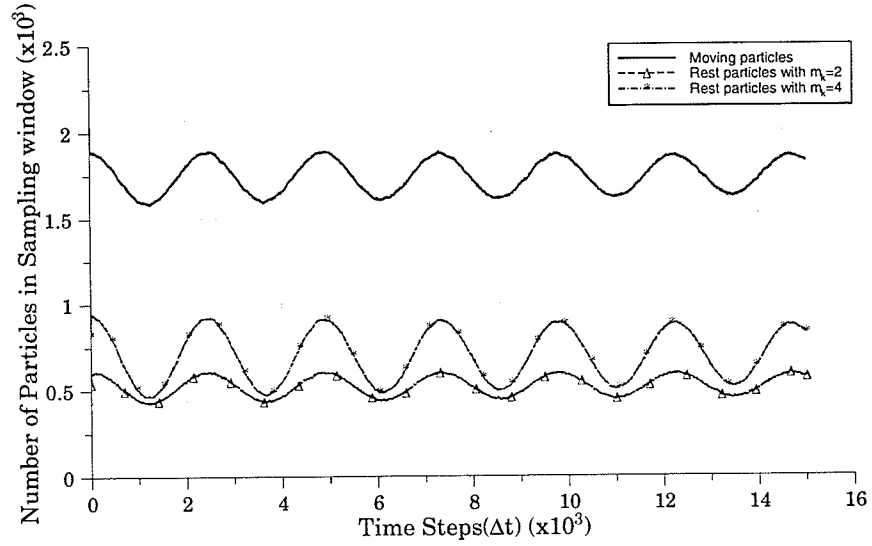


Fig.3.2: Time domain waveforms for model 1. Note that the number of moving particles has been divided by 4.

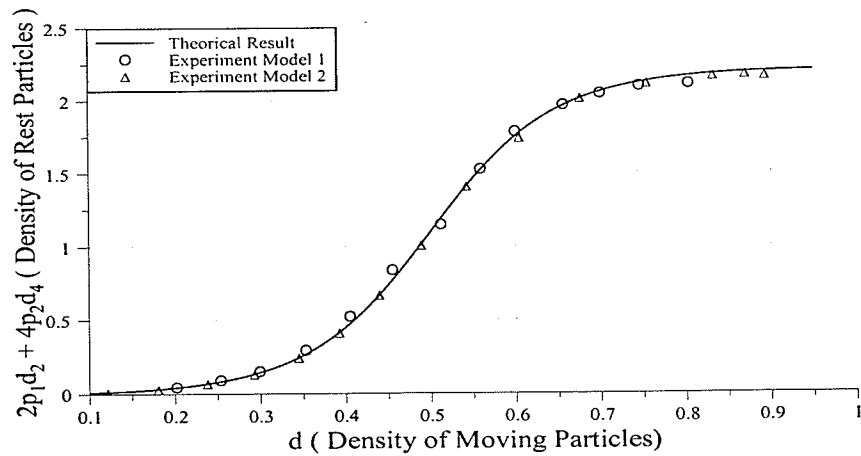


Fig.3.3: Equilibrium for the models with two rest particles described in Tables 3.1 and 3.2. Theoretical results calculated using (3.12) are compared with the experimental results.

Next we examine the propagation speed of the mixture models. The experimental values obtained from the two local collision models are given in Fig.3.4. The theoretical results by using (3.55) are also given for comparison. The propagation speed was calculated by measuring the resonant frequency in the  $TM_{20}$  cavity, an example of which was shown in Fig 3.2.

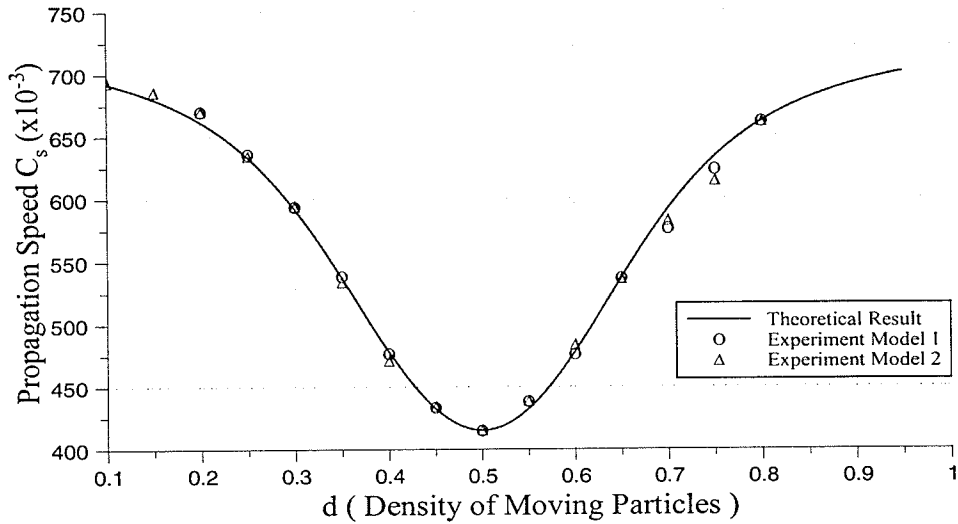


Fig.3.4: Propagation speed for the two mixture models described in Tables 2.1 and 2.2.

The above results indicate a very good agreement between the two local collision models and the analytical ones. We confirmed that the mixture *HPP LGA* model can be applied to modelling the linear wave equation in inhomogeneous media, and that macroscopic quantities (such as density, mass flow, density of rest particles and sound speed) do not depend on the details of the microscopic difference.

A variety of applications of the mixture *HPP LGA* models to two-dimensional electromagnetic problems in inhomogeneous media have been investigated[36,37,42]. The applications demonstrate that by concretely constructing different local appropriate collision

---

models, an *LGA* algorithm is capable of simulating electromagnetic wave propagation and scattering in inhomogeneous dielectric structures with a large range of dielectric constant. Some examples are presented below.

Among the examples, we examined a plane wave propagating through dielectric solid cylinders and cylindrical shells with different dielectric constants  $\epsilon_r$ . Figs.3.5 and 3.6 show the snapshots of a gaussian plane wave propagating through a dielectric solid cylinder with  $\epsilon_r = 5$  (radius  $a = 20l$ ) and a cylindrical shell with  $\epsilon_r = 21$  (inner radius  $a=80l$  and outer radius  $b=100l$ ), respectively[42]. The time-domain electric field intensity inside a dielectric cylinder and shell with  $\epsilon_r = 5$  and  $\epsilon_r = 21$  are given in Figs. 3.7 and 3.8. The cylinder or shell was embedded in a lattice of size  $2048l \times 4096l$  and the circular sampling window is chosen at the center of each geometry. The radius of the window was a function of its location. The radius inside the solid cylinder was  $25l$  for  $\epsilon_r = 5$  and  $15l$  for  $\epsilon_r = 21$ , respectively. The window at the center of cylinder shell had a radius of  $50l$ . The dielectric constants  $\epsilon_r = 5$  can be created using a single rest particle model of  $m_1 = 4$ , and  $\epsilon_r = 21$  created using two rest particle model of  $m_1 = 4$  and  $m_2 = 8$ . The construction of the two models can be referred to the formula of (3.61) and the related discussion in Section 2.25. The results obtained using a *TLM* [8,35] numerical approach are also given for comparison.

To assess the difference of the mixture model with respect to *TLM* based on the above results, the knowledge of the error sources for the two techniques should be considered. The damping effect and spatial averaging error (described in Subsection2.4) are two main errors in the lattice gas model. The damping effect is the dispersion associated with viscosity in a fluid model, and can not correctly predicted with the linear lattice gas model. In the simula-



tions, the small perturbations (plane wave pulse) were imposed on an equilibrium state, so that the damping effects can be neglected as described in Subsection 3.2.4. The spatial averaging error and a 10:1 lattice gas cell to *TLM* cell discretization resulted in the field sampling locations not matched up exactly, and did cause the difference between the two approaches. However, a comparison can be made between the results shown in Figs.3.7(A and B) (solid cylinders) or in Figs.3.8(A and B) (cylinder shells), even the simulations with the same plane wave pulse and numerical schemes. The case of  $\epsilon_r = 21$  gave a poor agreement between the two methods on each geometry. Conversely, the case of  $\epsilon_r = 5$  gave a good agreement between the two methods on each geometry. This indicates the major differences are due to the stair-stepping errors present in the *TLM* discretization. A more detailed discussion of the errors can be found in [36].

Next as an example of wave interaction with a complex biological structure as simulated by D. Cule[36]. The scattering field from a human body cross-section model is shown. In this simulation, only the dielectric constant of a tissue has been considered. Unfortunately, the conductivity of the tissue has not been involved since the current fluid dynamics based mixture *LGA* model can not describe the dissipative property related to a lossy media in electromagnetics. In this body cross-section model more than eight tissues with different dielectric constants ranging from 6 to 62 were constructed using a 3.4mm resolution grid of electrical parameter values[36], as shown in Fig.3.9 and Table 3.3. Also included in this Table are the details of the mixture ratios  $p_k$  of rest particles related to the different mixture models for the modelling of dielectric constants. Note that the combination of the mixture ratio  $p_k$ s given in Table 3.3 for the modelling of the human body cross-section is just one of

---

many possible combinations. As discussed in Section 2.2.5, a desired arbitrary dielectric constant value  $\epsilon_r$  can be created by non-uniquely constructing the mixture models with different rest particles  $m_k$  and mixture ratio  $p_k$ . This can be found in Fig.3.1 and the formula (3.59). The image of the instantaneous field intensity for harmonic plane wave incident on the human torso model at 975 MHz is simulated and given in Fig.3.10[36].

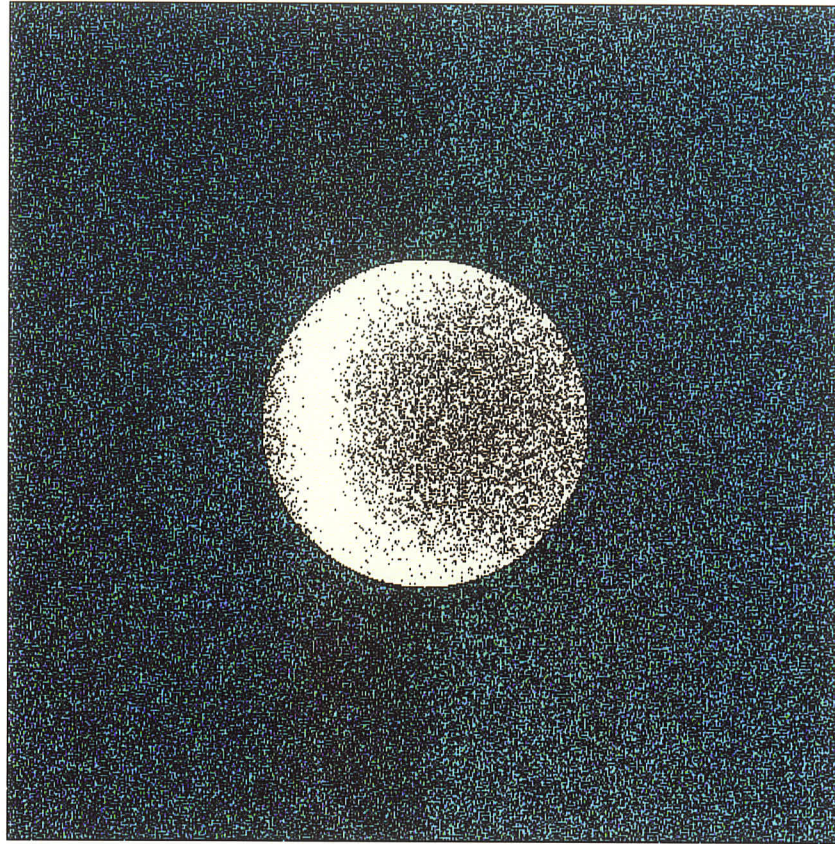


Fig.3.5: Snapshot of gaussian plane wave propagating through a dielectric solid cylinder with  $\epsilon_r = 5$  (radius  $R = 20l$ )[42].



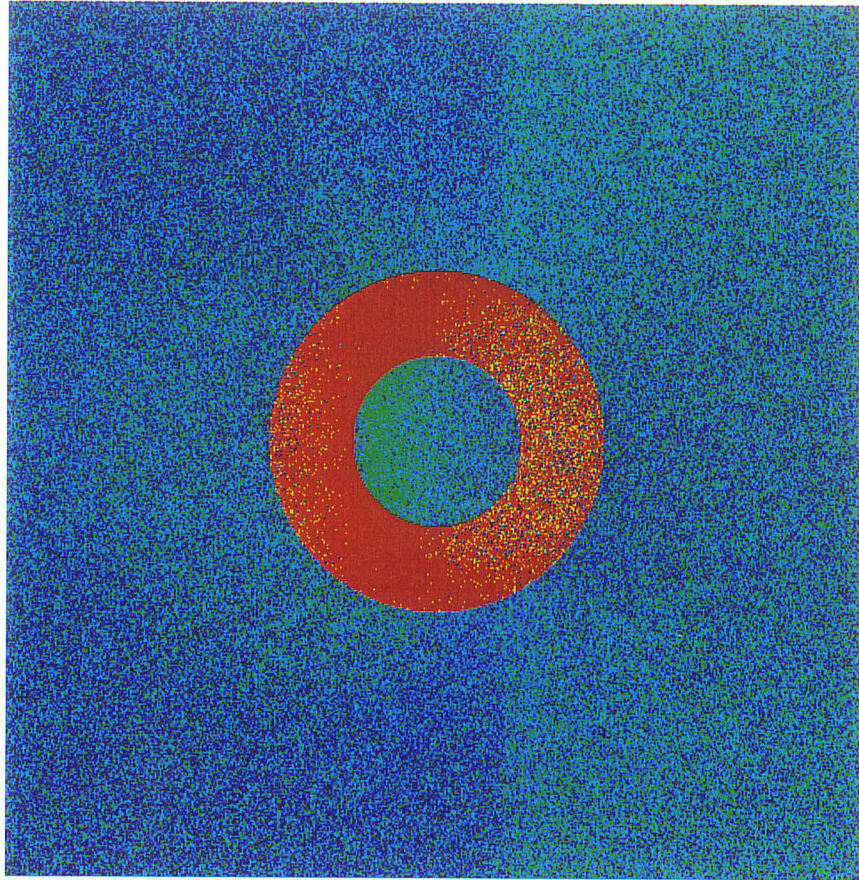


Fig.3.6: Snapshot of gaussian plane wave propagating through a dielectric solid cylindrical shell with  $\epsilon_r = 21$  (inner radius  $a=80 \text{ l}$  and outer radius  $b=100 \text{ l}$ )[42].

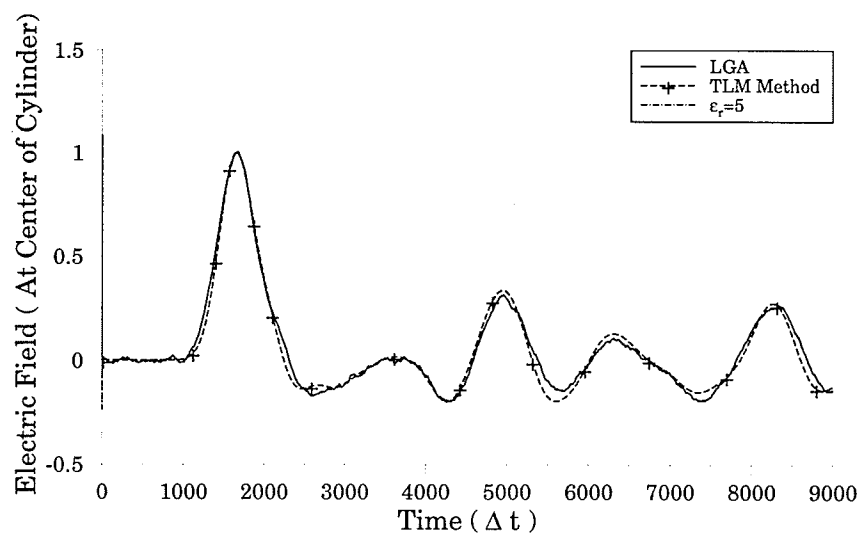


Fig. 3.7(A)

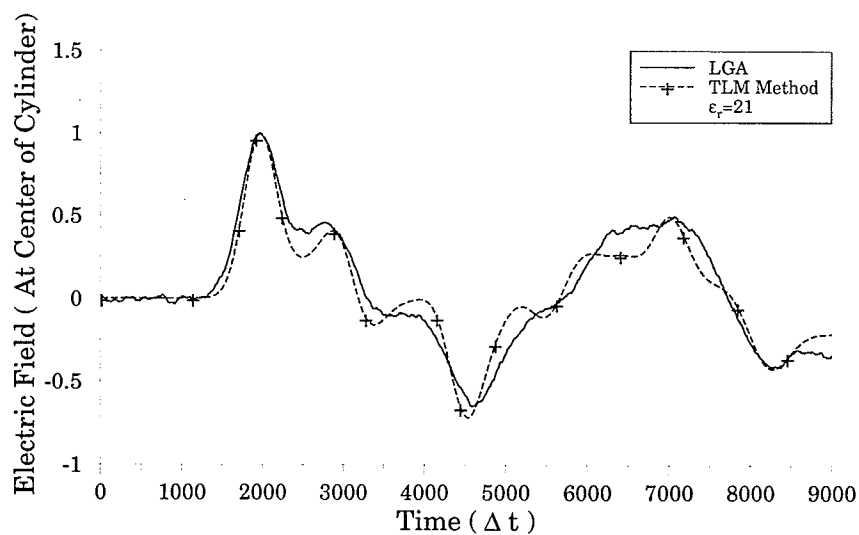


Fig. 3.7(B)

Fig. 3.7: Time-domain electric field intensity inside the dielectric cylinder with a):  $\epsilon_r = 5$  and b):  $\epsilon_r = 21$ . Comparison of the results obtained using TLM method is provided for an observation location a central region of cylinder.

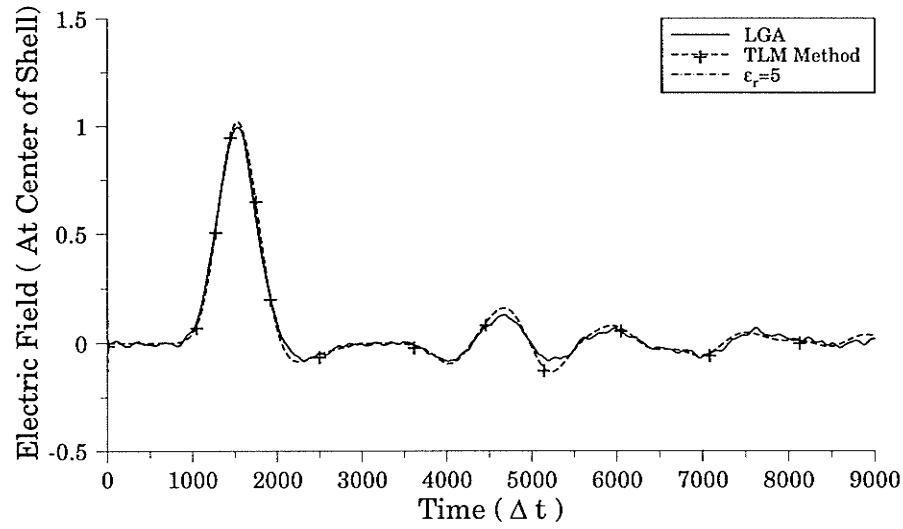


Fig. 3.8(A)

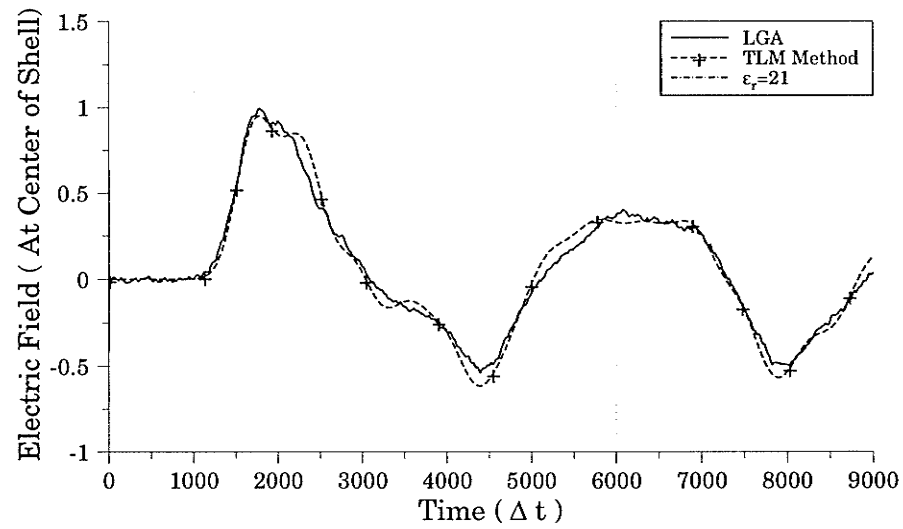


Fig. 3.8(B)

Fig. 3.8: Time-domain electric field intensity inside a dielectric cylindrical shell with a):  $\epsilon_r = 5$  and b):  $\epsilon_r = 21$ . Comparison of the results obtained using TLM method is provided for an observation location a central region of shell.

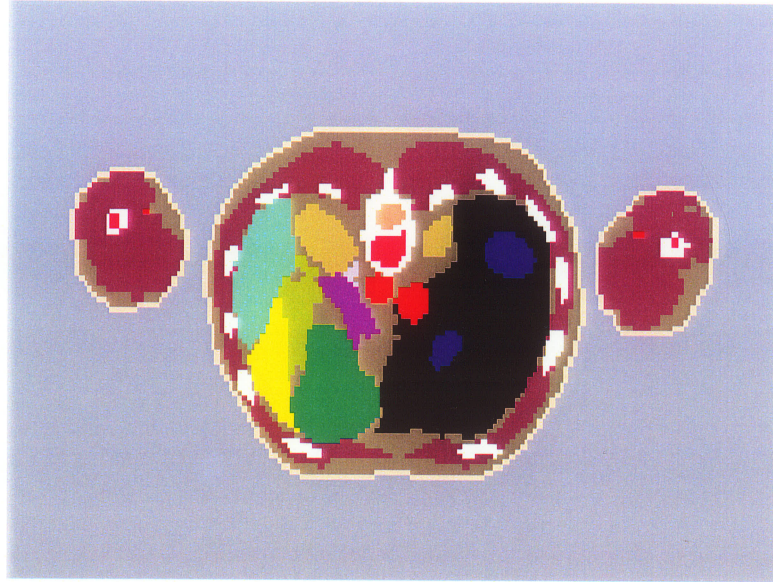


Fig. 3.9: Cross section of human torso model for a 3.4 mm resolution lattice used in the *LGA* simulation by D. Cule[36]. Permittivity values for eight different tissue range from  $\epsilon_r = 6$  for fat to  $\epsilon_r = 62$  for blood, the details given in Table 3.3.



Table 3.3: Body cross-section model[36]

Material	$\epsilon_r$	Mixture		
		$p_1(m_1 = 4)$	$p_2(m_2 = 8)$	$p_3(m_3 = 16)$
Skin	35.0	1.000	1.000	0.2188
Spinal Cord	49.0	1.000	1.000	0.4375
Spine	8.0	1.000	0.1875	0.000
Ribs	8.0	1.000	0.1875	0.000
Long Bones	8.0	1.000	0.1875	0.000
Skeletal Muscle	58.0	1.000	1.000	0.5781
Liver	48.0	1.000	1.000	0.4219
Kidney	43.0	1.000	1.000	0.3488
Stomach	43.0	1.000	1.000	0.3488
Small Bowel	43.0	1.000	1.000	0.3488
Colon	43.0	1.000	1.000	0.3488
Pancreas	43.0	1.000	1.000	0.3488
Fat	6.0	1.000	0.0625	0.000
Blood Pool	62.0	1.000	1.000	0.854
Bone Marrow	62.0	1.000	1.000	0.854
Spleen	62.0	1.000	1.000	0.854



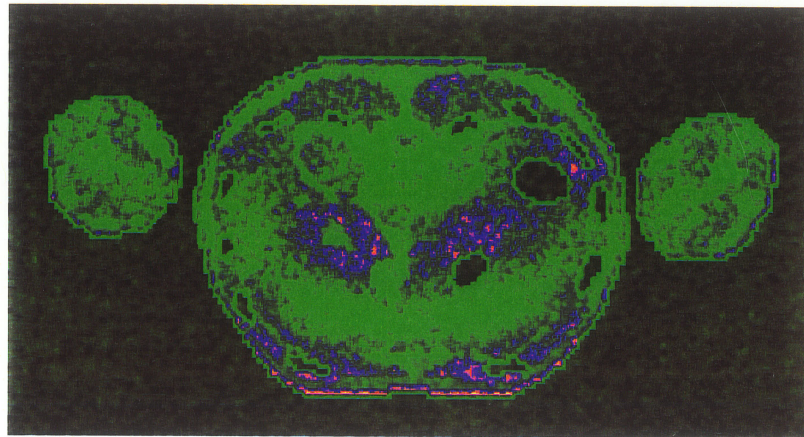


Fig. 3.10: Image of the instantaneous field intensity for harmonic plane wave incidence on the cross section of the human torso model at 975MHz[36].

---

## Chapter 4

# Three-Dimensional Vector Lattice Gas Automata

### 4.1: Introduction

In this chapter, we show how the three-dimensional vector *LGA* (*3-d vector LGA*) model described in Section 2.3 can be used to model vector electromagnetic fields in three dimensions. Because polarization has been introduced in the model as an important inherent property, the mathematical analysis used here is somewhat different from that used in two-dimensional scalar wave models, where the Euler equations under the regime of the undamped wave have analogy with the two-dimensional Maxwell's equations of *TE* or *TM* types. For three-dimensional problems, it seems that one is not able to find direct analogy between the three hydrodynamical equations and Maxwell's equations. As discussed in chapter 2, the present *3-d vector LGA* model is still based on the interaction of Fermi-type particles. Each particle is endowed with the inherent physical quantities: a propagating vector  $\mathbf{k}$ , polarization  $\mathbf{e}$  as well as magnetic vector  $\mathbf{h}$ . The collision rules conserve the mass, polarization vector  $\mathbf{e}$  and magnetic vector  $\mathbf{h}$ , but do not conserve propagating vector  $\mathbf{k}$ . The analysis begins with setting up the Boltzmann equations of the *3-d vector LGA*. The perturbation solution to the Boltzmann equations is developed using the Chapman-Enskog expansion, and appropriate mathematical methods. The solution characterizes how small perturbation of the mean population of particles vary with time and space. We show how

in the macroscopic limit the three-dimensional Maxwell's equations can be derived from the *LGA* model.

In the following sections, the Boltzmann equations for the *3-d vector LGA* are presented in section 4.2. Based on the equations, a group of perturbation equations at the first order  $O(\epsilon)$  can be obtained. Section 4.3 shows how the Maxwell's equations could be derived from the perturbation equations. Some numerical simulation results conducted on *CA* machines are presented in section 4.4. As well, comparison is made to the results obtained using the *TLM* method.

#### 4.2 Macro dynamics and Solution for 3-d vector *LGA*

By taking the ensemble average of the microdynamical equations of (2.24) through (2.35) the Boltzmann equations of *3-d vector LGA* can be obtained as:

$$N_{-x,y}(x-l, y, z, t + \Delta t) = N_{-x,y}(x, y, z, t) + \Omega_{-x,y}(N^{\dagger}(x, t)), \quad (4.1)$$

$$N_{-x,z}(x-l, y, z, t + \Delta t) = N_{-x,z}(x, y, z, t) + \Omega_{-x,z}(N^{\dagger}(x, t)), \quad (4.2)$$

$$N_{x,y}(x+l, y, z, t + \Delta t) = N_{x,y}(x, y, z, t) + \Omega_{x,y}(N^{\dagger}(x, t)), \quad (4.3)$$

$$N_{x,z}(x+l, y, z, t + \Delta t) = N_{x,z}(x, y, z, t) + \Omega_{x,z}(N^{\dagger}(x, t)), \quad (4.4)$$

$$N_{-y,x}(x, y-l, z, t + \Delta t) = N_{-y,x}(x, y, z, t) + \Omega_{-y,x}(N^{\dagger}(x, t)), \quad (4.5)$$

$$N_{-y,z}(x, y-l, z, t + \Delta t) = N_{-y,z}(x, y, z, t) + \Omega_{-y,z}(N^{\dagger}(x, t)), \quad (4.6)$$

$$N_{y,x}(x, y+l, z, t + \Delta t) = N_{y,x}(x, y, z, t) + \Omega_{y,x}(N^{\dagger}(x, t)), \quad (4.7)$$

$$N_{y,z}(x, y+l, z, t + \Delta t) = N_{y,z}(x, y, z, t) + \Omega_{y,z}(N^{\dagger}(x, t)), \quad (4.8)$$

$$N_{-zx}(x, y, z-l, t + \Delta t) = N_{-zx}(x, y, z, t) + N_{-zx}(N^\dagger(x, t)), \quad (4.9)$$

$$N_{-zy}(x, y, z-l, t + \Delta t) = N_{-zy}(x, y, z, t) + \Omega_{-zy}(N^\dagger(x, t)), \quad (4.10)$$

$$N_{zy}(x, y, z+l, t + \Delta t) = N_{zy}(x, y, z, t) + \Omega_{zy}(N^\dagger(x, t)), \quad (4.11)$$

$$N_{zx}(x, y, z+l, t + \Delta t) = N_{zx}(x, y, z, t) + \Omega_{zx}(N^\dagger(x, t)), \quad (4.12)$$

where the symbol  $N^\dagger$  has the same meaning as used in the previous chapters. The

$\Omega_{ji}(N^\dagger)$ ; ( $J \in \pm X, \pm Y, \pm Z$  and  $i \in x, y, z$ ), represents the ensemble average of the collision operators given in the expressions of (2.36) through (2.47), and can be explicitly written as

$$\Omega_{-xy} = \overline{N_{-xy}} [N_{zy}N_{-zy}\overline{N_{xy}} + N_{yx}N_{yx}\overline{N_{-yx}}] - N_{-xy} [\overline{N_{zy}N_{-zy}N_{xy}} + \overline{N_{yx}N_{yx}N_{-yx}}], \quad (4.13)$$

$$\Omega_{-xz} = \overline{N_{-xz}} [N_{yz}N_{-yz}\overline{N_{xz}} + N_{zx}N_{zx}\overline{N_{-zx}}] - N_{-xz} [\overline{N_{yz}N_{-yz}N_{xz}} + \overline{N_{zx}N_{zx}N_{-zx}}], \quad (4.14)$$

$$\Omega_{xy} = \overline{N_{xy}} [N_{zy}N_{-zy}\overline{N_{-xy}} + N_{-yx}N_{-yx}\overline{N_{yx}}] - N_{xy} [\overline{N_{zy}N_{-zy}N_{-xy}} + \overline{N_{-yx}N_{-yx}N_{yx}}], \quad (4.15)$$

$$\Omega_{xz} = \overline{N_{xz}} [N_{yz}N_{-yz}\overline{N_{-xz}} + N_{-zx}N_{-zx}\overline{N_{zx}}] - N_{xz} [\overline{N_{yz}N_{-yz}N_{-xz}} + \overline{N_{-zx}N_{-zx}N_{zx}}], \quad (4.16)$$

$$\Omega_{-yx} = \overline{N_{-yx}} [N_{zx}N_{-zx}\overline{N_{yx}} + N_{xy}N_{xy}\overline{N_{-xy}}] - N_{-yx} [\overline{N_{zx}N_{-zx}N_{yx}} + \overline{N_{xy}N_{xy}N_{-xy}}], \quad (4.17)$$

$$\Omega_{-yz} = \overline{N_{-yz}} [N_{xz}N_{-xz}\overline{N_{yz}} + N_{zy}N_{zy}\overline{N_{-zy}}] - N_{-yz} [\overline{N_{xz}N_{-xz}N_{yz}} + \overline{N_{zy}N_{zy}N_{-zy}}], \quad (4.18)$$

$$\Omega_{Yx} = \overline{N_{Yx}} [N_{Zx}N_{-Zx}\overline{N_{-Yx}} + N_{-Xy}N_{-Yx}\overline{N_{Xy}}] - N_{Yx} [\overline{N_{Zx}N_{-Zx}N_{-Yx}} + \overline{N_{-Xy}N_{-Yx}N_{Xy}}], \quad (4.19)$$

$$\Omega_{Yz} = \overline{N_{Yz}} [N_{Xz}N_{-Xz}\overline{N_{-Yz}} + N_{-Zy}N_{-Yz}\overline{N_{Zy}}] - N_{Yz} [\overline{N_{Xz}N_{-Xz}N_{-Yz}} + \overline{N_{-Zy}N_{-Yz}N_{Zy}}], \quad (4.20)$$

$$\Omega_{-Zx} = \overline{N_{-Zx}} [N_{Yx}N_{-Yx}\overline{N_{Zx}} + N_{Xz}N_{Zx}\overline{N_{-Xz}}] - N_{-Zx} [\overline{N_{Yx}N_{-Yx}N_{Zx}} + \overline{N_{Xz}N_{Zx}N_{-Xz}}], \quad (4.21)$$

$$\Omega_{-Zy} = \overline{N_{-Zy}} [N_{Xy}N_{-Xy}\overline{N_{Zy}} + N_{Zy}N_{Yz}\overline{N_{-Yz}}] - N_{-Zy} [\overline{N_{Xy}N_{-Xy}N_{Zy}} + \overline{N_{Yz}N_{Zy}N_{-Yz}}], \quad (4.22)$$

$$\Omega_{Zy} = \overline{N_{Zy}} [N_{Xy}N_{-Xy}\overline{N_{-Zy}} + N_{-Zy}N_{-Yz}\overline{N_{Yz}}] - N_{Zy} [\overline{N_{Xy}N_{-Xy}N_{-Zy}} + \overline{N_{Yz}N_{-Zy}N_{Yz}}], \quad (4.23)$$

$$\Omega_{Zx} = \overline{N_{Zx}} [N_{Yx}N_{-Yx}\overline{N_{-Zx}} + N_{-Xz}N_{-Zx}\overline{N_{Xz}}] - N_{Zx} [\overline{N_{Yx}N_{-Yx}N_{-Zx}} + \overline{N_{-Xz}N_{-Zx}N_{Xz}}]. \quad (4.24)$$

where  $\Omega_{\pm J i} = \langle \omega_{\pm J i} \rangle$ ,  $N_{\pm J i} = \langle S_{\pm J i} \rangle$  and  $\overline{N_{\pm J i}} = 1 - N_{\pm J i} = \langle \bar{S}_{\pm J i} \rangle$ , and  $N_{J i}$  represents the mean population of the particle polarized in  $i$ -direction and travelling along the  $J$ -direction. Here  $\omega_{\pm J i}$  and  $S_{\pm J i}$  were defined previously in Subsections 2.3.2 and 2.3.3.

For convenience, we prefer to write the above equations in a compact form, that is,

$$N_{\pm J i}(x + c_J, t + \Delta t) = N_{\pm J i}(x, t) + \Omega_{\pm J i}(N^\dagger(x, t)), \quad (4.25)$$

and

$$\begin{aligned} \Omega_{\pm J i} = & \overline{N_{\pm J i}} [N_{\pm K i}N_{\mp K i}\overline{N_{\mp J i}} + N_{\mp J i}N_{\mp I j}\overline{N_{\pm I j}}] - \\ & - N_{\pm J i} [\overline{N_{\pm K i}N_{\mp K i}N_{\mp J i}} + \overline{N_{\mp J i}N_{\mp I j}N_{\pm I j}}], \end{aligned} \quad (4.26)$$

where the vector  $c_J$  is defined as

$$c_J = \begin{cases} \pm l \hat{e}_x & J = \pm X \\ \pm l \hat{e}_y & J = \pm Y, \\ \pm l \hat{e}_z & J = \pm Z \end{cases} \quad (4.27)$$

where  $l$  is the lattice spacing and  $\pm \hat{e}_i$  ( $i = x, y$  and  $z$ ) are the unit direction vectors. The notation used here means that the indices  $i$  and  $j$  take the value of the circular set of  $\{x, y, z\}$  with  $j=i+1$ , that is, if  $i = x, j = y$ ;  $i = y, j = z$  and  $i = z, j = x$ . The capital indices  $I, J$  and  $K$  are defined as:  $I \equiv \text{cap}(i)$ ,  $J \equiv \text{cap}(i+1)$  and  $K \equiv \text{cap}(i+2)$ , where the symbol  $\text{cap}()$  means “to take the capital letter of the argument”, i.e.,  $\text{cap}(y) = Y$ .

It is important to note that every collision event defined in the 3-*d* vector *LGA* model is one-to-one and reversible. The collision rules are illustrated in Appendix A as a reference. Thus the *LGA* obeys detailed balance, a stronger condition than the semi-detailed balance. Applying the lemma of chapter 2, the equilibrium mean population  $N_{\pm J i}^{eq}$  of the particles could be specified as Fermi-Dirac distribution

$$N_{\pm J i}^{eq} = \frac{1}{1 + \exp(g_o + (\mathbf{h}_i \cdot \mathbf{q}_1) + (\mathbf{e}_i \cdot \mathbf{q}_2))} \quad (4.28)$$

where there are three Lagrange multipliers  $g_o$ ,  $\mathbf{q}_1$  and  $\mathbf{q}_2$ .

For subsequent discussion, we denote  $\mathbf{u}_1$  and  $\mathbf{u}_2$  to be the macroscopic conserved quantities which correspond to the microscopic conserved quantities  $\mathbf{e}$  and  $\mathbf{h}$ , respectively. With consideration of the symmetry of the lattice[31],  $\mathbf{q}_1$  and  $\mathbf{q}_2$  could be formally expanded as a series in odd powers of the conserved vectors of  $\mathbf{u}_1$  and  $\mathbf{u}_2$ . Now, if the lat-

tice is assumed to be at an equilibrium and with  $|u_1| \ll |e|$  and  $|u_2| \ll |h|$ , then the equilibrium mean population  $N_{\pm J i}^{eq}$  of the particles could be expressed as a series in powers of  $u_1$  and  $u_2$  as

$$N_{\pm J i}^{eq} = f(g_o) + O(u_1) + O(u_2) + \dots \quad (4.29)$$

where  $f(g_o) = \frac{1}{1 + \exp(g_o)}$  is evaluated at  $|u_1| = 0$  and  $|u_2| = 0$ , and is set to be the background density of particles.

Next, if we consider the lattice gas at near-equilibrium, the mean population  $N_{\pm J i}$  are close to the equilibrium values of  $N_{\pm J i}^{eq}$  and can be expanded in a perturbation series in powers of  $\epsilon$  (very small  $\epsilon \rightarrow 0$ ) about the equilibrium as

$$N_{\pm J i} = N_{\pm J i}^{eq} + \epsilon N_{\pm J i}^{(1)} + O(\epsilon^2), \quad (4.30)$$

For this assumption, it is required that a large lattice size  $L$  be at least  $O(\epsilon^{-1})$ , such that the change of macroscopic quantities (density of particles and the vectors of  $u_1$  and  $u_2$ ) on the lattice is sufficiently regular [31]. Now substituting the expression (4.30) for  $N_{\pm J i}$  in the Boltzmann equation (4.25) and expanding the operators (4.26) in a perturbation series in powers of  $\epsilon$ , we get

$$\begin{aligned} & N_{\pm J i}^{eq}(x + c_J, t + \Delta t) + \epsilon N_{\pm J i}^{(1)}(x + c_J, t + \Delta t) + O(\epsilon^2) = N_{\pm J i}^{eq}(x, t) + \\ & + \epsilon N_{\pm J i}^{(1)}(x, t) + \Omega_{\pm J i}[N^{eq}(x, t)] + \epsilon \sum'_{K, m} N_{\pm K m}^{(1)} \left( \frac{\partial \Omega_{\pm J i}}{\partial N_{\pm K m}} \right) \Big|_{N^{\dagger} = N^{eq}} + O(\epsilon^2), \end{aligned} \quad (4.31)$$

where the prime over the symbol of summation indicates that  $\sum'_{K,m}$  is over the values of  $m = y$  and  $m = z$  when  $K = \pm X$ ; over the values of  $m = x$  and  $z$  when  $K = \pm Y$ ; and over the values of  $m = x$  and  $y$  when  $K = \pm Z$ . Recall that at equilibrium the mean population distribution is spatially uniform and independent of  $t$ , such that

$$N_{\pm J i}^{eq}(\mathbf{x} + \mathbf{c}_J, t + \Delta t) = N_{\pm J i}^{eq}(\mathbf{x}, t) \approx f(g_o)$$

and 
$$\Omega_{\pm J i}[N^{eq\dagger}(\mathbf{x}, t)] = 0.$$

Using the above expressions and (4.31), the first order equations for  $N_{\pm J i}^{(1)}$  can be found as

$$N_{\pm J i}^{(1)}(\mathbf{x} + \mathbf{c}_J, t + \Delta t) = N_{\pm J i}^{(1)}(\mathbf{x}, t) + \sum_{K, t} N_{\pm K t}^{(1)} \left( \frac{\partial \Omega_{\pm J i}}{\partial N_{\pm K t}} \right) \bigg|_{N^{\dagger} = N^{eq}}. \quad (4.32)$$

We can rewrite the equation (4.32) in a compact matrix form:



$$\begin{bmatrix}
N_{-x,y}^{(1)}(x-l, y, z, t + \Delta t) \\
N_{-x,z}^{(1)}(x-l, y, z, t + \Delta t) \\
N_{x,y}^{(1)}(x+l, y, z, t + \Delta t) \\
N_{x,z}^{(1)}(x+l, y, z, t + \Delta t) \\
N_{-y,x}^{(1)}(x, y-l, z, t + \Delta t) \\
N_{-y,z}^{(1)}(x, y-l, z, t + \Delta t) \\
N_{y,x}^{(1)}(x, y+l, z, t + \Delta t) \\
N_{y,z}^{(1)}(x, y+l, z, t + \Delta t) \\
N_{-z,x}^{(1)}(x, y, z-l, t + \Delta t) \\
N_{-z,y}^{(1)}(x, y, z-l, t + \Delta t) \\
N_{z,y}^{(1)}(x, y, z+l, t + \Delta t) \\
N_{z,x}^{(1)}(x, y, z+l, t + \Delta t)
\end{bmatrix} = (I + T_D) \begin{bmatrix}
N_{-x,y}^{(1)}(x, y, z, t) \\
N_{-x,z}^{(1)}(x, y, z, t) \\
N_{x,y}^{(1)}(x, y, z, t) \\
N_{x,z}^{(1)}(x, y, z, t) \\
N_{-y,x}^{(1)}(x, y, z, t) \\
N_{-y,z}^{(1)}(x, y, z, t) \\
N_{y,x}^{(1)}(x, y, z, t) \\
N_{y,z}^{(1)}(x, y, z, t) \\
N_{-z,x}^{(1)}(x, y, z, t) \\
N_{-z,y}^{(1)}(x, y, z, t) \\
N_{z,y}^{(1)}(x, y, z, t) \\
N_{z,x}^{(1)}(x, y, z, t)
\end{bmatrix} \quad (4.33)$$

where the matrix  $I$  is a  $12 \times 12$  unit matrix, corresponding to the “streaming” process of the evolution of the lattice gas while the matrix  $T_D$  is derived from the differential of collision operators  $\Omega_{\pm J, i}$  with respect to  $N_{\pm K, m}$ , thus describing the “the interaction” among parti-

cles. The elements of  $(T_D)_{\pm K, m}^{\pm J, i} = \left( \frac{\partial \Omega_{\pm J, i}}{\partial N_{\pm K, m}} \right) \Big|_{N^{\dagger} = N^{eq}}$  can be calculated by the expressions

of (4.13) through (4.24), and can be written below (the more details about the calculation is given in Appendix B).

$$T_D = f(g_0)(1 - f(g_0))T_I, \quad (4.34)$$

where the collision matrix  $T_I$  is

$$T_I = \begin{bmatrix} -2 & 0 & 0 & 0 & -1 & 0 & 1 & 0 & 0 & 1 & 1 & 0 \\ 0 & -2 & 0 & 0 & 0 & 1 & 0 & 1 & -1 & 0 & 0 & 1 \\ 0 & 0 & -2 & 0 & 1 & 0 & -1 & 0 & 0 & 1 & 1 & 0 \\ 0 & 0 & 0 & -2 & 0 & 1 & 0 & 1 & 1 & 0 & 0 & -1 \\ -1 & 0 & 1 & 0 & -2 & 0 & 0 & 0 & 1 & 0 & 0 & 1 \\ 0 & 1 & 0 & 1 & 0 & -2 & 0 & 0 & 0 & -1 & 1 & 0 \\ 1 & 0 & -1 & 0 & 0 & 0 & -2 & 0 & 1 & 0 & 0 & 1 \\ 0 & 1 & 0 & 1 & 0 & 0 & 0 & -2 & 0 & 1 & -1 & 0 \\ 0 & -1 & 0 & 1 & 1 & 0 & 1 & 0 & -2 & 0 & 0 & 0 \\ 1 & 0 & 1 & 0 & 0 & -1 & 0 & 1 & 0 & -2 & 0 & 0 \\ 1 & 0 & 1 & 0 & 0 & 1 & 0 & -1 & 0 & 0 & -2 & 0 \\ 0 & 1 & 0 & -1 & 1 & 0 & 1 & 0 & 0 & 0 & 0 & -2 \end{bmatrix}. \quad (4.35)$$

For convenience in the following discussion, we define a scattering matrix  $T_s \equiv I + T_D = I + f(1 - f)T_I$ . Note that if the lattice is almost fully filled, or almost vacant (*i.e.*  $f \approx 1$  or  $0$ ), the effective mean free path [41] of particles on the lattice is extremely long such that the streaming event is most dominate in the evolution of the lattice gas. In this case  $T_s \approx I$  and  $T_D \approx 0$ , and the interactions among particles rarely happen as it should be in the real world of fluid dynamics. For the almost half filled lattice ( $f \approx 0.5$ ), the scattering matrix will be

$$T_s|_{f=0.5} \equiv T_{\frac{1}{2}} = I + \frac{1}{4}T_I = \frac{1}{4} \begin{bmatrix} 2 & 0 & 0 & 0 & -1 & 0 & 1 & 0 & 0 & 1 & 1 & 0 \\ 0 & 2 & 0 & 0 & 0 & 1 & 0 & 1 & -1 & 0 & 0 & 1 \\ 0 & 0 & 2 & 0 & 1 & 0 & -1 & 0 & 0 & 1 & 1 & 0 \\ 0 & 0 & 0 & 2 & 0 & 1 & 0 & 1 & 1 & 0 & 0 & -1 \\ -1 & 0 & 1 & 0 & 2 & 0 & 0 & 0 & 1 & 0 & 0 & 1 \\ 0 & 1 & 0 & 1 & 0 & 2 & 0 & 0 & 0 & -1 & 1 & 0 \\ 1 & 0 & -1 & 0 & 0 & 0 & 2 & 0 & 1 & 0 & 0 & 1 \\ 0 & 1 & 0 & 1 & 0 & 0 & 0 & 2 & 0 & 1 & -1 & 0 \\ 0 & -1 & 0 & 1 & 1 & 0 & 1 & 0 & 2 & 0 & 0 & 0 \\ 1 & 0 & 1 & 0 & 0 & -1 & 0 & 1 & 0 & 2 & 0 & 0 \\ 1 & 0 & 1 & 0 & 0 & 1 & 0 & -1 & 0 & 0 & 2 & 0 \\ 0 & 1 & 0 & -1 & 1 & 0 & 1 & 0 & 0 & 0 & 0 & 2 \end{bmatrix}. \quad (4.36)$$

### 4.3 Macroscopic Property and Conserved Quantity

To understand the macroscopic behaviour of the 3-*d* vector *LGA*, we proceed by exploring the equation(4.33).

Using the definition of the matrix  $T_s$  (4.34) we rewrite the equation of (4.33) as

$$N_{\pm J_i}^{(1)}(\mathbf{x} + \mathbf{c}_J, t + \Delta t) = T_s N_{\pm J_i}^{(1)}(\mathbf{x}, t), \quad (4.37)$$

and the scattering matrix  $T_s$  as:

$$T_s \equiv I + f(1-f)T_I = \left(I + \frac{1}{4}T_I\right) + \left[f(1-f) - \frac{1}{4}\right]T_I = T_{\frac{1}{2}} + \gamma T_I, \quad (4.38)$$

where  $\gamma = f(1-f) - \frac{1}{4}$ .

Note that the 12x12 matrix  $T_s$  is singular due to only six conserved quantities being

enforced in the collision events. To understand the collision, rewrite the collision matrix

$T_I$  as

$$T_I = 4(T_{1/2} - I),$$

In reference to the generalized inverse of the linear transformations [43], the  $T_I$  could be constructed as the product of a  $12 \times 6$  matrix and its generalized  $6 \times 12$  inverse matrix  $A^+$  [43], that is

$$T_{1/2} = AA^+, \quad (4.39)$$

where the number 6 is related to the six conserved vector components. This will be seen later. It can be found that the rank two singular matrix  $T_I$  has two eigenvalues, 0 and 4, each with six eigenvectors. The six eigenvectors associated with eigenvalue 0:

$$\begin{aligned} & [0, 0, 0, -2, 1, 1, 1, 1, 0, 0, 0, -2]^T, & [0, 0, 0, 0, -1, 0, -1, 0, 1, 0, 0, 1]^T, \\ & [1, 0, 0, -1, 1, 1, 0, 0, 0, 0, -1, -1]^T, & [0, 0, 1, -1, 0, 1, 1, 0, 0, 0, -1, -1]^T, \\ & [0, 1, 0, -1, 1, 0, 1, 0, 0, 0, 0, -2]^T, & [0, 0, 0, -2, 1, 2, 1, 1, 0, 0, 1, -2]^T, \end{aligned}$$

and the other six eigenvectors with eigenvalue 4:

$$\begin{aligned} & [0, 0, 0, 0, 1, 0, 1, 0, 1, 0, 0, 1]^T, & [-1, 0, 1, 0, 1, 0, -1, 0, 0, 0, 0, 1]^T, \\ & [-2, 0, 0, 0, 1, -1, -1, 1, 0, 0, -2, 0]^T, & [2, 0, 0, 0, -1, 0, 1, 0, 0, 1, 1, 0]^T, \\ & [1, 0, 0, 1, -1, 1, 0, 0, 0, 0, 1, -1]^T, & [1, 1, 0, 0, 0, 1, 1, 0, 0, 0, 1, 1]^T. \end{aligned}$$

Also,  $T_I$  has a 6-dimensional null space whose basis can be formed by the six independent vectors:

$$\begin{aligned} & [1, -2, -1, 0, 2, 1, 0, 1, -2, 0, 0, 0]^T, & [0, -1, -1, 0, 1, 1, 0, 0, -1, 1, 0, 0]^T, \\ & [-1, 0, 1, 0, -1, 0, 1, 0, 0, 0, 0, 0]^T, & [-1, 0, 1, 0, -2, 0, 0, 0, 1, 0, 0, 1]^T, \\ & [-1, 1, 0, 0, -1, -1, 0, 0, 1, 0, 1, 0]^T, & [1, -1, -1, 2, 0, 0, 0, -2, 0, 0, 0]^T. \end{aligned} \quad (4.40)$$

Where  $T$  denotes the transpose of a matrix.

In what follows, the matrix  $A$  could define as a linear transformation  $A$  from a vector

space  $\mathcal{U}$  with dimension 6 to another vector space  $\mathcal{N}^{(1)}$  with dimension 12, and its inverse  $A^+$  as the inverse transformation. In the vector space of  $\mathcal{U}$ , each element  $[u_{1x}, u_{1y}, u_{1z}, u_{2x}, u_{2y}, u_{2z}]^T$  is the six components of macroscopic conserved vector of  $\mathbf{u}_1$  and  $\mathbf{u}_2$ , which are related to two local microscopic conserved vectors  $\{e, h\}$ , as indicated before. On the other hand, the space  $\mathcal{N}^{(1)}$  is defined as a population vector space. In this space, any vector  $N^{(1)}$  has twelve components which correspond to the mean populations of twelve particle states, *i.e.*,  $\forall N_{\pm J i}^{(1)} \in \mathcal{N}^{(1)}$  ( $J = X, i=y, z$ ;  $J = Y, i=z, x$  and  $J = Z, i=x, y$ ).

Explicitly, these two transformations could be expressed as:

$$A: (\mathcal{U} \rightarrow \mathcal{N}^{(1)}) \quad \text{and} \quad A^+: (\mathcal{N}^{(1)} \rightarrow \mathcal{U}), \quad (4.41)$$

or in matrix form, for  $\forall N^{(1)} \in \mathcal{N}^{(1)}$  and  $\forall \mathbf{u} \in \mathcal{U}$ , that is,

$$N^{(1)} = A\mathbf{u} \quad \text{or} \quad \mathbf{u} = A^+ N^{(1)}. \quad (4.42)$$

Note that a Moore-Penrose generalized inverse [43] has the properties:

$$1): \quad AA^+A = A, \quad (4.43)$$

$$2): \quad A^+AA^+ = A^+, \quad (4.44)$$

$$3): \quad (AA^+)^H = AA^+, \quad (4.45)$$

$$4): \quad (A^+A)^H = A^+A, \quad (4.46)$$

where the superscript  $H$  denotes the operation of taking the conjugate transpose of a matrix.

Now, by using the above properties, we can show that the vector space  $\mathcal{U}$  is a con-

served vector space with respect to the scattering matrix  $T_s$ . To do this, at a particular site on the lattice, let  $(u)^{(t)} \in \mathcal{U}$  be an arbitrary vector before one updating (or collision) and  $(u)^{(t+\Delta t)} \in \mathcal{U}$  be the vector after the updating, such that

$$(u)^{(t)} = A^+ N^{(1)}(t) = A^+ A A^+ N^{(1)}(t) ,$$

where the property 2) (4.43) has been applied. Note that  $T_I$  is singular matrix with a dimension six null-space with the basis vectors given in (4.40). This allows us to choose another constraint for  $A^+$ , that is,  $A^+ T_I = 0$ , then

$$(u)^{(t)} = A^+ (A A^+ + \gamma T_I) N^{(1)}(t)$$

where  $\gamma$  could be an arbitrary real number, *i.e.*,  $\forall \gamma \in \mathcal{R}$ . In the present case,

$\gamma = f(1-f) - 1/4$ , such that we get

$$T_s = A A^+ + \gamma T_I \quad \text{and} \quad (u)^{(t)} = A^+ T_s N^{(1)}(t) .$$

It follows from  $T_s N^{(1)}(t) = N^{(1)}(t + \Delta t)$  and  $A^+ N^{(1)}(t + \Delta t) = (u)^{(t+\Delta t)}$  that, we end with

$$(u)^{(t)} = (u)^{(t+\Delta t)} = u . \quad (4.47)$$

Thus,  $u$  is a conserved vector with respect to transformation  $T_s$ , but  $N^{(1)}(t) \neq$

$N^{(1)}(t + \Delta t)$  due to  $A A^+ \neq I$ .

A straightforward solution to the equation  $A A^+ = T_{1/2}$  for the matrices  $A$  and  $A^+$ , which satisfies the constraint:  $A^+ T_I = 0$  and the properties given in expressions of (4.43) through (4.46), is very difficult. Nevertheless, referring to [43], one special solution for the matrix  $A$  which meets all conditions and the constraint, could be found as

$$A = \frac{1}{2} \times \begin{bmatrix} 0 & 1 & 0 & 0 & 0 & -\kappa \\ 0 & 0 & 1 & 0 & \kappa & 0 \\ 0 & 1 & 0 & 0 & 0 & \kappa \\ 0 & 0 & 1 & 0 & -\kappa & 0 \\ 1 & 0 & 0 & 0 & 0 & \kappa \\ 0 & 0 & 1 & -\kappa & 0 & 0 \\ 1 & 0 & 0 & 0 & 0 & -\kappa \\ 0 & 0 & 1 & \kappa & 0 & 0 \\ 1 & 0 & 0 & 0 & -\kappa & 0 \\ 0 & 1 & 0 & \kappa & 0 & 0 \\ 0 & 1 & 0 & -\kappa & 0 & 0 \\ 1 & 0 & 0 & 0 & \kappa & 0 \end{bmatrix}, \quad (4.48)$$

and its inverse matrix  $A^+$  as

$$A^+ = (A^T A)^{-1} A^T = \frac{1}{2} \begin{bmatrix} 0 & 0 & 0 & 0 & 1 & 0 & 1 & 0 & 1 & 0 & 0 & 1 \\ 1 & 0 & 1 & 0 & 0 & 0 & 0 & 0 & 0 & 1 & 1 & 0 \\ 0 & 1 & 0 & 1 & 0 & 1 & 0 & 1 & 0 & 0 & 0 & 0 \\ 0 & 0 & 0 & 0 & 0 & -\frac{1}{\kappa} & 0 & \frac{1}{\kappa} & 0 & \frac{1}{\kappa} & -\frac{1}{\kappa} & 0 \\ 0 & \frac{1}{\kappa} & 0 & -\frac{1}{\kappa} & 0 & 0 & 0 & 0 & -\frac{1}{\kappa} & 0 & 0 & \frac{1}{\kappa} \\ -\frac{1}{\kappa} & 0 & \frac{1}{\kappa} & 0 & \frac{1}{\kappa} & 0 & -\frac{1}{\kappa} & 0 & 0 & 0 & 0 & 0 \end{bmatrix}, \quad (4.49)$$

where  $\kappa$  is a parameter to be determined later. It can be verified that  $AA^+ = T_{1/2}$  and

$$A^+ T_I = 0.$$

#### 4.4 3-d Vector LGA and Maxwell's Equation

Based on the above discussion, it has been shown that for each updating of the LGA, the macroscopic quantity  $\mathbf{u}$  is conserved. Now, it is desired to get the equations, describing the variation of the conserved vector quantity  $\mathbf{u}$  with time and space. Thereafter Maxwell's

differential curl equations in conservation law form will be derived from the equations.

Recall that the small perturbation components of  $N_{\pm J i}^{(1)}$  ( $J = X, i=y, z$ ;  $J = Y, i=x, z$  and  $J = Z, i=x, y$ ) describe the particles polarized in  $i$ -direction and independently traveling along  $\pm J$  in the lattice. As discussed earlier, if the perturbation component is small enough, at spatial sites, the continuity of mean population  $N_{\pm J i}^{(1)}$  (particle density per cell) would be satisfied by assuming only the first order corrections among particles. Thus, the following continuity equations for the mean population  $N_{\pm J i}^{(1)}$  could be written as:

For the components  $N_{\pm X i}^{(1)} \in \mathcal{N}^{(1)}$  ( $i=y$  and  $z$ ), we have

$$\begin{cases} \partial_t N_{-X y}^{(1)} - c_x \partial_x N_{-X y}^{(1)} = 0 \\ \partial_t N_{-X z}^{(1)} - c_x \partial_x N_{-X z}^{(1)} = 0 \\ \partial_t N_{X y}^{(1)} + c_x \partial_x N_{X y}^{(1)} = 0 \\ \partial_t N_{X z}^{(1)} + c_x \partial_x N_{X z}^{(1)} = 0 \end{cases}, \quad (4.50)$$

or, in the matrix form:

$$\partial_t \begin{bmatrix} N_{-X y}^{(1)} \\ N_{-X z}^{(1)} \\ N_{X y}^{(1)} \\ N_{X z}^{(1)} \end{bmatrix} + \begin{bmatrix} -c_x & 0 & 0 & 0 \\ 0 & -c_x & 0 & 0 \\ 0 & 0 & c_x & 0 \\ 0 & 0 & 0 & c_x \end{bmatrix} \partial_x \begin{bmatrix} N_{-X y}^{(1)} \\ N_{-X z}^{(1)} \\ N_{X y}^{(1)} \\ N_{X z}^{(1)} \end{bmatrix} = 0. \quad (4.51)$$

Similarly, for the components  $N_{\pm Y i}^{(1)}$  ( $i=x$  and  $z$ ) and  $N_{\pm Z i}^{(1)}$  ( $i=x$  and  $y$ ), we have



$$\partial_t \begin{bmatrix} N_{-Yx}^{(1)} \\ N_{-Yz}^{(1)} \\ N_{Yx}^{(1)} \\ N_{Yz}^{(1)} \end{bmatrix} + \begin{bmatrix} -c_y & 0 & 0 & 0 \\ 0 & -c_y & 0 & 0 \\ 0 & 0 & c_y & 0 \\ 0 & 0 & 0 & c_y \end{bmatrix} \partial_y \begin{bmatrix} N_{-Yx}^{(1)} \\ N_{-Yz}^{(1)} \\ N_{Yx}^{(1)} \\ N_{Yz}^{(1)} \end{bmatrix} = 0, \quad (4.52)$$

and

$$\partial_t \begin{bmatrix} N_{-Zx}^{(1)} \\ N_{-Zy}^{(1)} \\ N_{Zx}^{(1)} \\ N_{Zy}^{(1)} \end{bmatrix} + \begin{bmatrix} -c_z & 0 & 0 & 0 \\ 0 & -c_z & 0 & 0 \\ 0 & 0 & c_z & 0 \\ 0 & 0 & 0 & c_z \end{bmatrix} \partial_z \begin{bmatrix} N_{-Zx}^{(1)} \\ N_{-Zy}^{(1)} \\ N_{Zx}^{(1)} \\ N_{Zy}^{(1)} \end{bmatrix} = 0, \quad (4.53)$$

where  $c_x$ ,  $c_y$  and  $c_z$  denote the propagating speed of the particle travelling along x-, y- and z-directions, respectively. The lattice under consideration is homogeneous, thus symmetric. This leads to  $c_x = c_y = c_z = c$ .

Again, under Boltzmann assumption the wave vector space  $\mathcal{N}^{(1)}$  could be decomposed into three wave subspaces  $\mathcal{N}_{\pm x}^{(1)}$ ,  $\mathcal{N}_{\pm y}^{(1)}$  and  $\mathcal{N}_{\pm z}^{(1)}$  respectively, each corresponding to the wave spaces travelling along  $\pm\hat{x}$ -,  $\pm\hat{y}$ - and  $\pm\hat{z}$ - directions and each with dimension 4, *i.e.*,

$$\mathcal{N}^{(1)} = \mathcal{N}_{\pm x}^{(1)} \oplus \mathcal{N}_{\pm y}^{(1)} \oplus \mathcal{N}_{\pm z}^{(1)}, \quad (4.54)$$

where for example,  $\{ N_{\pm x}^{(1)} \in \mathcal{N}_{\pm x}^{(1)}$ , with components  $( N_{-xy}^{(1)}, N_{-xz}^{(1)}, N_{xy}^{(1)}, N_{xz}^{(1)} ) \}$ .

Correspondingly, with reference to the above subspaces, the conserved vector space  $\mathcal{U}$  could be decomposed into the three subspaces  $\mathcal{U}_x$ ,  $\mathcal{U}_y$  and  $\mathcal{U}_z$ , *i.e.*,  $\mathcal{U} = \mathcal{U}_x \oplus \mathcal{U}_y \oplus \mathcal{U}_z$

$\mathcal{U}_Z$ , each with dimension 4 and containing the conserved vectors associated with one of the three wave subspaces. For instance, for any conserved vector  $\mathbf{u}_X \in \mathcal{U}_X$ , the components of  $\mathbf{u}_X$  could be related to the mean population  $N_{\pm X}^{(1)} \in \mathcal{N}_{\pm X}^{(1)}$  of particles travelling in  $\pm \hat{x}$ -directions, that is,

$$\mathbf{u}_X \equiv \begin{bmatrix} u_{y1} \\ u_{z1} \\ u_{y2} \\ u_{z2} \end{bmatrix}, \quad (4.55)$$

Similarly, for  $\forall \mathbf{u}_Y \in \mathcal{U}_Y$  and  $\forall \mathbf{u}_Z \in \mathcal{U}_Z$ ,

$$\mathbf{u}_Y \equiv \begin{bmatrix} u_{x1} \\ u_{z1} \\ u_{x2} \\ u_{z2} \end{bmatrix} \quad \text{and} \quad \mathbf{u}_Z \equiv \begin{bmatrix} u_{x1} \\ u_{y1} \\ u_{x2} \\ u_{y2} \end{bmatrix}. \quad (4.56)$$

Referring to the transformation  $A$  between the wave function space  $\mathcal{N}^{(1)}$  and the conserved vector space  $\mathcal{U}$  (see (4.41)), the mapping between the subspaces  $\mathcal{N}_{\pm X}^{(1)} \in \mathcal{N}_{\pm X}^{(1)}$  and  $\mathcal{U}_X \in \mathcal{U}$  could be set up by the transformation  $A_X$ , the mapping between subspaces  $\mathcal{N}_{\pm Y}^{(1)} \in \mathcal{N}^{(1)}$  and  $\mathcal{U}_Y \in \mathcal{U}$  by the transformation  $A_Y$ , and the mapping between subspaces  $\mathcal{N}_{\pm Z}^{(1)} \in \mathcal{N}^{(1)}$  and  $\mathcal{U}_Z \in \mathcal{U}$  by the transformation  $A_Z$ . That is, for the particle travelling in the  $x$ -direction,

$$A_X: \mathcal{N}_{\pm X}^{(1)} \rightarrow \mathcal{U}_X \quad \text{and} \quad A_X^{-1}: \mathcal{U}_X \rightarrow \mathcal{N}_{\pm X}^{(1)}. \quad (4.57)$$

The transformation  $A_X$  could be written in a matrix form. The matrix  $A_X$  corresponds to the composition which associates with the particles travelling in  $\pm \hat{x}$  directions in matrix

A. For  $\forall \mathbf{u}_X \in \mathcal{U}$  and  $\forall N_X^{(1)} \in \mathcal{N}_{\pm X}^{(1)}$ , we have

$$\underbrace{\begin{bmatrix} N_{-Xy}^{(1)} \\ N_{-Xz}^{(1)} \\ N_{Xy}^{(1)} \\ N_{Xz}^{(1)} \end{bmatrix}}_{N_{\pm X}^{(1)}} = \underbrace{\frac{1}{2} \begin{bmatrix} 1 & 0 & 0 & -\kappa \\ 0 & 1 & \kappa & 0 \\ 1 & 0 & 0 & \kappa \\ 0 & 1 & -\kappa & 0 \end{bmatrix}}_{A_X} \underbrace{\begin{bmatrix} u_{1y} \\ u_{1z} \\ u_{2y} \\ u_{2z} \end{bmatrix}}_{\mathbf{u}_{\pm X}}, \quad (4.58)$$

or its inverse form  $A_X^{-1}$

$$\underbrace{\begin{bmatrix} u_{1y} \\ u_{1z} \\ u_{2y} \\ u_{2z} \end{bmatrix}}_{\mathbf{u}_{\pm X}} = \underbrace{\begin{bmatrix} 1 & 0 & 1 & 0 \\ 0 & 1 & 0 & 1 \\ 0 & \frac{1}{\kappa} & 0 & -\frac{1}{\kappa} \\ -\frac{1}{\kappa} & 0 & \frac{1}{\kappa} & 0 \end{bmatrix}}_{A_X^{-1}} \underbrace{\begin{bmatrix} N_{-Xy}^{(1)} \\ N_{-Xz}^{(1)} \\ N_{Xy}^{(1)} \\ N_{Xz}^{(1)} \end{bmatrix}}_{N_{\pm X}^{(1)}}. \quad (4.59)$$

Similarly, for the particles travelling in  $y$ - and  $z$ - directions, we get

$$A_Y: \mathcal{N}_{\pm Y}^{(1)} \rightarrow \mathcal{U}_Y \quad \text{and} \quad A_Y^{-1}: \mathcal{U}_Y \rightarrow \mathcal{N}_{\pm Y}^{(1)}, \quad (4.60)$$

$$\text{and} \quad A_Z: \mathcal{N}_{\pm Z}^{(1)} \rightarrow \mathcal{U}_Z \quad \text{and} \quad A_Z^{-1}: \mathcal{U}_Z \rightarrow \mathcal{N}_{\pm Z}^{(1)}. \quad (4.61)$$

Or, in the matrix form, for  $\forall \mathbf{u}_y \in \mathcal{U}_Y$  and  $\forall N_y^{(1)} \in \mathcal{N}_{\pm y}^{(1)}$ ;  $\forall \mathbf{u}_z \in \mathcal{U}$  and

$\forall N_{\pm z}^{(1)} \in \mathcal{N}_{\pm z}^{(1)}$ , the transformations  $A_Y$  and  $A_Z$  could be written as

$$\underbrace{\begin{bmatrix} N_{-Yx}^{(1)} \\ N_{-Yz}^{(1)} \\ N_{Yx}^{(1)} \\ N_{Yz}^{(1)} \end{bmatrix}}_{N_{\pm Y}^{(1)}} = \underbrace{\frac{1}{2} \begin{bmatrix} 1 & 0 & 0 & \kappa \\ 0 & 1 & -\kappa & 0 \\ 1 & 0 & 0 & -\kappa \\ 0 & 1 & \kappa & 0 \end{bmatrix}}_{A_Y} \underbrace{\begin{bmatrix} u_{1x} \\ u_{1z} \\ u_{2x} \\ u_{2z} \end{bmatrix}}_{u_{\pm Y}}, \quad (4.62)$$

and

$$\underbrace{\begin{bmatrix} N_{-Zx}^{(1)} \\ N_{-Zy}^{(1)} \\ N_{Zy}^{(1)} \\ N_{Zx}^{(1)} \end{bmatrix}}_{N_{\pm Z}^{(1)}} = \underbrace{\frac{1}{2} \begin{bmatrix} 1 & 0 & 0 & -\kappa \\ 0 & 1 & \kappa & 0 \\ 1 & 0 & -\kappa & 0 \\ 0 & 1 & 0 & \kappa \end{bmatrix}}_{A_Z} \underbrace{\begin{bmatrix} u_{1x} \\ u_{1y} \\ u_{2x} \\ u_{2y} \end{bmatrix}}_{u_{\pm Z}} \quad (4.63)$$

Or, their inverse forms  $A_Y^{-1}$  and  $A_Z^{-1}$

$$\underbrace{\begin{bmatrix} u_{1x} \\ u_{1z} \\ u_{2x} \\ u_{2z} \end{bmatrix}}_{u_{\pm Y}} = \underbrace{\begin{bmatrix} 1 & 0 & 1 & 0 \\ 0 & 1 & 0 & 1 \\ 0 & -\frac{1}{\kappa} & 0 & \frac{1}{\kappa} \\ \frac{1}{\kappa} & 0 & -\frac{1}{\kappa} & 0 \end{bmatrix}}_{A_Y^{-1}} \underbrace{\begin{bmatrix} N_{-Yx}^{(1)} \\ N_{-Yz}^{(1)} \\ N_{Yx}^{(1)} \\ N_{Yz}^{(1)} \end{bmatrix}}_{N_{\pm Y}^{(1)}}. \quad (4.64)$$

and

$$\underbrace{\begin{bmatrix} u_{1x} \\ u_{1y} \\ u_{2x} \\ u_{2y} \end{bmatrix}}_{u_{\pm Z}} = \underbrace{\begin{bmatrix} 1 & 0 & 0 & 1 \\ 0 & 1 & 0 & 0 \\ 0 & \frac{1}{\kappa} & -\frac{1}{\kappa} & 0 \\ -\frac{1}{\kappa} & 0 & 0 & \frac{1}{\kappa} \end{bmatrix}}_{A_Z^{-1}} \underbrace{\begin{bmatrix} N_{-Zx}^{(1)} \\ N_{-Zy}^{(1)} \\ N_{Zy}^{(1)} \\ N_{Zx}^{(1)} \end{bmatrix}}_{N_{\pm Z}^{(1)}}. \quad (4.65)$$

Now, using the expression  $N_{\pm X}^{(1)} = A_X u_X$  in the equation (4.51), we have

$$\partial_t \begin{bmatrix} u_{1y} \\ u_{1z} \\ u_{2y} \\ u_{2z} \end{bmatrix} + A_X^{-1} \begin{bmatrix} -c & 0 & 0 & 0 \\ 0 & -c & 0 & 0 \\ 0 & 0 & c & 0 \\ 0 & 0 & 0 & c \end{bmatrix} A_X \partial_x \begin{bmatrix} u_{1y} \\ u_{1z} \\ u_{2y} \\ u_{2z} \end{bmatrix} = 0, \quad (4.66)$$

where the matrix

$$\begin{aligned} A_X^{-1} \begin{bmatrix} -c & 0 & 0 & 0 \\ 0 & -c & 0 & 0 \\ 0 & 0 & c & 0 \\ 0 & 0 & 0 & c \end{bmatrix} A_X &= \frac{1}{2} \begin{bmatrix} 1 & 0 & 0 & -\kappa \\ 0 & 1 & \kappa & 0 \\ 1 & 0 & 0 & \kappa \\ 0 & 1 & -\kappa & 0 \end{bmatrix} \begin{bmatrix} -c & 0 & 0 & 0 \\ 0 & -c & 0 & 0 \\ 0 & 0 & c & 0 \\ 0 & 0 & 0 & c \end{bmatrix} \begin{bmatrix} 1 & 0 & 1 & 0 \\ 0 & 1 & 0 & 1 \\ 0 & \frac{1}{\kappa} & 0 & -\frac{1}{\kappa} \\ -\frac{1}{\kappa} & 0 & \frac{1}{\kappa} & 0 \end{bmatrix} \\ &= c \begin{bmatrix} 0 & 0 & 0 & \kappa \\ 0 & 0 & -\kappa & 0 \\ 0 & -1/\kappa & 0 & 0 \\ 1/\kappa & 0 & 0 & 0 \end{bmatrix} \end{aligned}$$

Thus we have

$$\partial_t \begin{bmatrix} u_{1y} \\ u_{1z} \\ u_{2y} \\ u_{2z} \end{bmatrix} + c \begin{bmatrix} 0 & 0 & 0 & \kappa \\ 0 & 0 & -\kappa & 0 \\ 0 & -1/\kappa & 0 & 0 \\ 1/\kappa & 0 & 0 & 0 \end{bmatrix} \partial_x \begin{bmatrix} u_{1y} \\ u_{1z} \\ u_{2y} \\ u_{2z} \end{bmatrix} = 0. \quad (4.67)$$

Similarly, using the  $N_{\pm Y}^{(1)} = A_Y u_Y$  and  $N_{\pm Z}^{(1)} = A_Z u_Z$ , respectively, in the wave equations (4.51) and (4.52), we get

$$\partial_t \begin{bmatrix} u_{1x} \\ u_{1z} \\ u_{2x} \\ u_{2z} \end{bmatrix} + c \begin{bmatrix} 0 & 0 & 0 & -\kappa \\ 0 & 0 & \kappa & 0 \\ 0 & 1/\kappa & 0 & 0 \\ -1/\kappa & 0 & 0 & 0 \end{bmatrix} \partial_y \begin{bmatrix} u_{1x} \\ u_{1z} \\ u_{2x} \\ u_{2z} \end{bmatrix} = 0, \quad (4.68)$$

and

$$\partial_t \begin{bmatrix} u_{1x} \\ u_{1y} \\ u_{2x} \\ u_{2y} \end{bmatrix} + c \begin{bmatrix} 0 & 0 & 0 & \kappa \\ 0 & 0 & -\kappa & 0 \\ 0 & -1/\kappa & 0 & 0 \\ 1/\kappa & 0 & 0 & 0 \end{bmatrix} \partial_z \begin{bmatrix} u_{1x} \\ u_{1y} \\ u_{2x} \\ u_{2y} \end{bmatrix} = 0. \quad (4.69)$$

Now it can be shown that the equations (4.67), (4.68) and (4.69) are equivalent to the Maxwell's curl equations. To do this, we will consider the Maxwell's curl equations written as system of hyperbolic conservation laws on a discrete numerical space-time grid (lattice) [35]. The Maxwell's equations in terms of continuous variables can be written as the following three systems of equations:

$$\partial_t \begin{bmatrix} E_y \\ E_z \\ H_y \\ H_z \end{bmatrix} + \begin{bmatrix} 0 & 0 & 0 & 1/\mu \\ 0 & 0 & -1/\mu & 0 \\ 0 & -1/\epsilon & 0 & 0 \\ 1/\epsilon & 0 & 0 & 0 \end{bmatrix} \partial_x \begin{bmatrix} E_y \\ E_z \\ H_y \\ H_z \end{bmatrix} = 0, \quad (4.70)$$

$$\partial_t \begin{bmatrix} E_x \\ E_z \\ H_x \\ H_z \end{bmatrix} + \begin{bmatrix} 0 & 0 & 0 & -1/\mu \\ 0 & 0 & 1/\mu & 0 \\ 0 & 1/\epsilon & 0 & 0 \\ -1/\epsilon & 0 & 0 & 0 \end{bmatrix} \partial_y \begin{bmatrix} E_x \\ E_z \\ H_x \\ H_z \end{bmatrix} = 0, \quad (4.71)$$

and

$$\partial_t \begin{bmatrix} E_x \\ E_y \\ H_x \\ H_y \end{bmatrix} + \begin{bmatrix} 0 & 0 & 0 & 1/\mu \\ 0 & 0 & -1/\mu & 0 \\ 0 & -1/\epsilon & 0 & 0 \\ 1/\epsilon & 0 & 0 & 0 \end{bmatrix} \partial_z \begin{bmatrix} E_x \\ E_y \\ H_x \\ H_y \end{bmatrix} = 0. \quad (4.72)$$

To proceed, for a fine space-time discretization we can assume that, in each cell, the wave propagation along the  $x$ -direction involves no variation with respect to the  $y$ - and  $z$ -directions, the wave propagation along the  $y$ -direction involves no variation with respect to the  $x$ - and  $z$ -directions and the wave propagation along the  $z$ -direction involves no variation with respect to the  $x$ - and  $y$ -directions, and equations(4.70) through(4.72) still hold true[35].

Note that the macroscopic behaviour described by the equations (4.67) though (4.69) are equivalent to Maxwell's differential curl equations(4.70) to (4.72) in conservation law form. Thus we conclude that the *3-d vector* lattice gas model can be utilized to simulate the three -dimensional vector electromagnetic fields. The analogy between the macroscopic conserved quantities  $(u_1, u_2)$  can be recognized, and yields the following equivalence and relationships between the parameters,

$$\begin{bmatrix} u_{1x} \\ u_{1y} \\ u_{1z} \\ u_{2x} \\ u_{2y} \\ u_{2z} \end{bmatrix} \leftrightarrow \begin{bmatrix} E_x \\ E_y \\ E_z \\ H_x \\ H_y \\ H_z \end{bmatrix}, \quad (4.73)$$

and

$$c\kappa \leftrightarrow 1/\mu; c/\kappa \leftrightarrow 1/\epsilon,$$

$$\Rightarrow \quad (\text{lattice wave speed}) \ c^2 \leftrightarrow \frac{1}{\epsilon\mu},$$

$$\Rightarrow \quad (\text{the parameter}) \ \kappa \leftrightarrow \sqrt{\frac{\mu}{\epsilon}}.$$

#### 4.4 Results of Numerical Experiments

In this section, primary results for experiments conducted on *CAM-8* using the 3-*d* vector *LGA* model are provided. The experiments are designed to examine the collision rules of the model, boundary conditions and dispersion property, as well as the related implement technique on *CAM-8*. These results demonstrate the wave propagating, and are compared with those results obtained from *TLM* simulation for the same problems.

The first experiment examines the collision rules of the model and dispersion property. The geometry of the structure is illustrated in Fig.4.1. Within a cavity of  $0 < x < 256l$ ,  $0 < y < 64l$  and  $0 < z < 64l$ , a Gaussian-pulsed plane wave was excited at the center of cavity ( $x=128l$ ,  $y=32l$  and  $z=32l$ ). The wrapped around boundary conditions are applied to the six walls of the cavity simulating periodic boundaries. A uniform background density of  $f=0.5$  ( $\alpha=0.25$ ) (all possible states are randomly filled) is applied to the lattice. The plane wave (perturbation components) is superimposed based on the Gaussian distribution  $p_o \exp((x-x_o)^2/\tau^2)$  (centred on the plane  $x_o=128l$  with the pulse of  $\tau=32l$ ) of particles on top of the background distribution, at  $t=0$ . Where,  $p_o=0.25$  so 25% of the unoccupied states above the background level on the plan of  $x=128l$ . All perturbation component particles, at  $t=0$ , are assumed to be in the states  $S_{\pm X, z}$  (polarized in  $z$ -



direction and travelling along  $\pm \hat{x}$  directions). A cubic sampling window with the size of  $20l \times 20l \times 20l$  is located at the coordinates  $(128l, 32l, 32l)$ , and used to measure the macroscopic field  $E_z$ . To reduce the statistical noise, a total of 15 random samples based on the method given in Section 2.4 are obtained, taking the averaging value. The transient electric field components in both propagation directions  $\pm \hat{x}$  are presented in Fig.4.2. Also in this figure, the results obtained from a *TLM* simulation of the same problem are shown for comparison. Overall, the results indicate a good agreement between the 3-*d vector LGA* and *TLM* methods, but the results of the *LGA* appear to have lower peak values than those obtained from *TLM* method. This may indicate that at the peak-time points, a larger fluctuation of particle density led to the transient and slight state deviation from the quasi-equilibrium state (An *LGA* working state). Thus, extra non-linear dispersive effects were introduced, and reduced the amplitude of field.

To examine the decay due to the damping effects associated with the dispersion in the model, a series of simulations were carried out with the different values of background density  $f$  (or the parameter  $\alpha = f(1-f)$ ). The results of the simulations show that fast decay exhibits as values  $\alpha$  deviates from 0.25. For example, the results for the case of  $f=0.7$  ( $\alpha=0.21$ ) are provided in Fig. 4.3. This could mean that the equilibrium state with background  $f=0.5$  ( $\alpha=0.25$ ) is an optimal state for the vector model. On the other hand, the current vector model based on the first order solution of Boltzmann equations could not be accurate enough to gives the correct decay. If this is the case, a higher order solution should be developed.

The next numerical experiment examines the perfect magnetic conducting boundaries

and dispersion property of the model. A cavity was excited with  $TM_{111}$  mode, as illustrated in Fig.4.4. The geometrical size of the cavity is  $64l \times 64l \times 64l$ . Perfect magnetic conducting boundary conditions are applied to all of six walls. At  $t=0$ , a uniform background density of  $f=0.5$  is applied to the lattice. The lattice is then excited by superimposing the  $TM_{111}$  wave on the top of the exciting background. Again, at initial time  $t = 0$ , all perturbation component particles are assumed to be in the states  $S_{\pm X, z}$ . The source with the maximum initial perturbation of 15% above the background. Three observation windows are located along the line of ( $x=16l$  and  $z=32l$ ) at  $y= 16l, 32l$  and  $48l$ , each window with the size of  $8l \times 8l \times 8l$ . Notice that at initial time of  $t=0$ , with respect to the known  $TM_{111}$  wave the first observation location( $16l, 16l, 32l$ ) and the third location ( $16l, 48l, 32l$ ) are mirror-symmetric with respect to the plane of  $y=32$ . When a simulation proceeding, the interactions between the initialized particles (propagating in a special direction) and background particles (propagating in an arbitrary direction) occurs. At any time snapshot, the responses obtained respectively from the first and third locations should have the same amplitude, but with a 180 degree phase difference. Also at the second location ( $16l, 48l, 32l$ ), the expected response  $E_z$  should be almost zero (very slightly fluctuating around an equilibrium state) through a whole running process. With this special geometric configuration and the known excitation, we examine the collision rules and the numerical scheme more detail and effectively.

The experiment was randomly conducted thirty times, involving each of the simulation 1000  $\Delta t$  time steps. The averaging results for the electric field  $E_z$  at each observation location is provided in Fig.4.5. The responses obtained respectively from the points

(16l,16l,32l) and (16l,48l,32l) exhibit an actual mirror-symmetry with respect to the plane of  $y=32$ , as expected they should be. Also, noted in Fig.4.5, the expected zero-response at the second location (16l,48l,32l) can be noticed. The results obtained from a *TLM* simulation of the same problem are shown for comparison, which indicates a good agreement between the 3-*d vector LGA* and *TLM* methods.

The  $TM_{111}$  mode and plane wave examples already shown above are a limited set of results. They indicate that the 3-*d vector LGA* model operates as proposed and predicated by theory. The spurious solutions do not appear in the results. These results do not prove linearity, however, and convincingly prove a unique solution in all cases.

To further validate the 3-*d vector LGA*, more numerical experiments should be considered. For instance, the linearity and convergence of the solution could be examined by exciting a given structure with some arbitrary excitation, and observing the response of source superimposed modes. Another experiment proposed here is a pulsed plane wave propagating within a sufficient large size of lattice. In this experiment, several observation locations are specified along the direction of the pulsed plane wave propagating. The responses obtained from the locations can provide the information of the propagating speed, and the shape of waveform obtained from each location can be used to analyse the dispersion properties. However, the numerical experiments require a more powerful cellular automata machine in order for these experiments to be conducted.

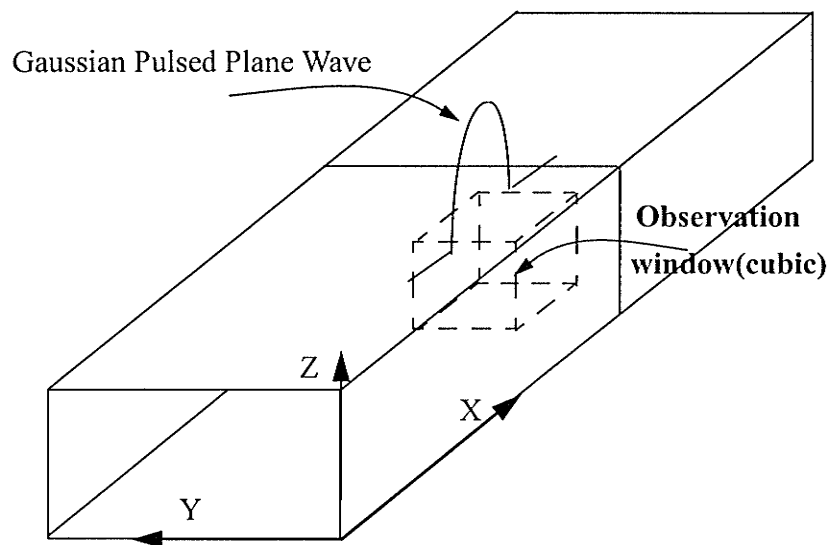


Fig.4.1: Gaussian pulsed plane wave propagating in a cavity with wrapped around boundaries.

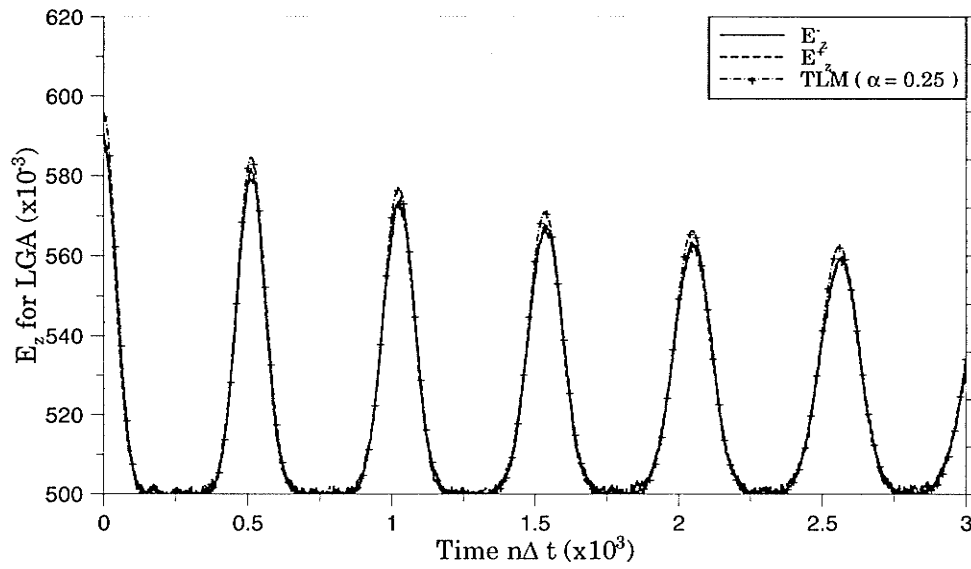


Fig.4.2: Transient electric field intensity  $\alpha = 0.25$  ( $f = 0.5$ ). Comparison is made to the results obtained by using the TLM approach

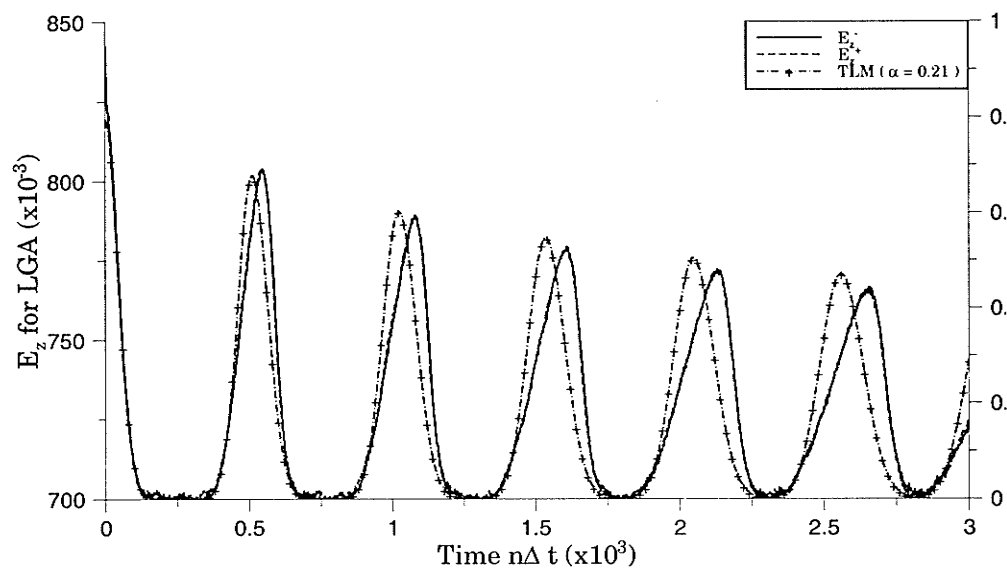


Fig.4.3: Transient electric field intensity for  $\alpha = 0.21$  ( $f = 0.7$ ). Comparison is made to the results obtained by using the TLM approach.

### PMC Boundary Conditions for Six Walls

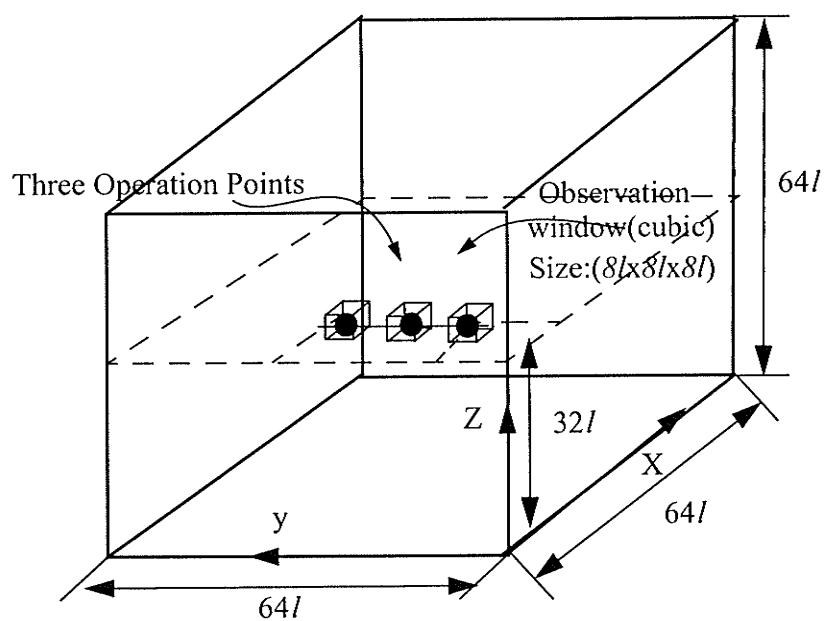


Fig.4.4  $TM_{111}$  Mode wave propagating in a cubic cavity

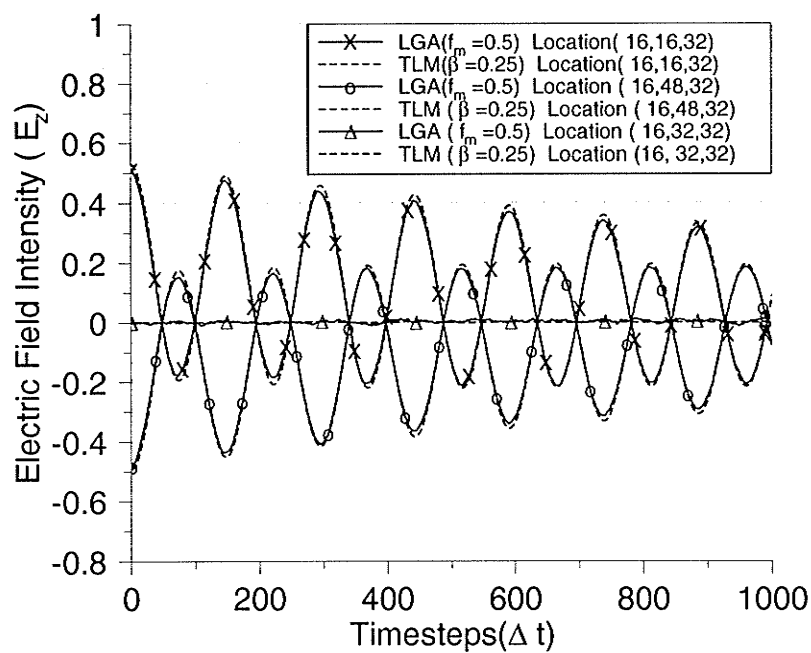


Fig.4.5 Time-Domain electric field intensity in a cavity excited by  $TM_{111}$  mode.



---

## Chapter 5 Summary and Proposed Future Works

In this research, the potential of lattice gas automata as a mathematical tool for the computational electromagnetics has been considered. Lattice gas automata may offer some advantages for the computational electromagnetics. One of these advantages is that only a few or even a single bit(s) per variable per site are needed to describe the very simple microdynamic states in an *LGA*. This enables complex geometric structures to be meshed with finer grid structures, and with less computational memory requirement. In addition to this, they are intrinsically parallel models of computation. This makes them particularly suited to implementation in a parallel processing computing architecture. Furthermore, the computation of the rules of *LGA* at each cell requires only a simple processor performing logical operation, rather than the more complex floating processor required in a general purpose computer conducting computations according to common numerical technique. For the present, it is impossible to provide a rigorous evaluation of the new technique as compared to the other time-domain differential equation based methods such as *FDTD* and *TLM* since the issue is hardware-related, and many of theoretic analyses of the algorithms remain to be explored. The issues such as computational complexity, accuracy and stability are briefly discussed here with comparison of the *LGA* method to the *TLM*.

### 5.1 Preliminary Benchmarks

#### 1): Stability

Dispersive errors exist in all time-domain differential equation based numerical

schemes. A stability criterion usually characterizes the discrete approximations (spatial and temporal discretization) to the various differential equation formulations so that the appropriate wave behaviour can emerge. *TLM* does not have a stability criterion, but does have the same dispersion characteristics as *FDTD* algorithm when the spatial and temporal discretization of *TLM* are selected to satisfy a relation given in [25]. For a *TLM* scheme, the scheme does not dissipate the energy from a propagating wave, but does disperse a part of its energy. Thus, the time-domain waveform changes shape as the wave propagates. The dispersive energy can not be tracked, and is exhausted. When the scheme is enforced to reverse from a given states, the original waveform can approximately be recovered only if the dispersive effect within the scheme is enough small. Therefore a *TLM* scheme is conditionally reversible.

The *HPP*- type and 3-*d LGA* models on the other hand are exactly reversible, and unconditionally stable. Fundamentally, the collision rules defined in the two models satisfy the detailed balance (the one-by-one mapping between input and output particle states). Due to the non-linear dispersion in *LGA*, a part of the observable wave propagating energy is dispersed into the background and stored there on the lattices. When the models are enforced to run in a backward process, the dispersed energy will be sequentially tracked and recovered, and so will be the waveforms, and finally the initial states of lattices will emerge as they were at very beginning.

## 2): Errors and Accuracy

Two main errors, dispersion and averaging error, affect the accuracy of the lattice gas automata for the modelling linear wave behaviour. The dispersion usually results in a fast wave damping behaviour. For linear wave behaviour to be supported by an *LGA*, the *LGA*

---

must work at an quasi-equilibrium state. A larger fluctuation causes the deviation from the quasi-equilibrium state, and undesired non-linear behaviour is introduced. The non-linear behaviour appears to be the dispersion associated with the viscosity in a fluid model, distinct from the numerical dispersion errors inherent with difference equation approximations. The dispersion can not be correctly predicted by the linear *LGA* models considered. As discussed in Subsection 2.4, the *LGA* requires statistical convergence- averaging over a large number of particles and a lattice of sufficient size. This usually leads to a trade-off between the dynamic range, statistical error and spatial averaging error. The problem can be partially solved by taking multiple random samples averaging (equivalent to ensemble averaging) at expense of the increasing of computing time. Thus, how to quantitatively describe the small perturbation in order to reduce the dispersion while maintaining an *LGA* working at appropriate states, and how to obtain a sufficient computational dynamic range without the excessive increase in the computing cost and averaging error, are two important topics for further consideration.

### 3): Computational Complexity

The computational complexity involved in the binary operation of an *LGA* cell (16 bit per cell) is considerably less than that of a *TLM* unit cell which involves floating-point operations[24]. However, in accordance with experimental observations[36], a ten to thirty times finer lattice spacing than that of the equivalent *TLM* mesh is often required to model observables in the simulations considered in this research. Consequently, the total number of cell updates in *LGA* massively increases by at least a factor of  $10^3$  of the two-dimensional *TLM* case and by at least a factor of  $10^4$  of the three-dimensional *TLM* case. The

memory hardware per cell also increases by factors of  $10^2$  and  $10^3$  for each case, respectively. To compound the problem, *LGA* simulation as used in this thesis, often requires ensemble average (as described in Section 2.4). Even with the pessimistic comparisons, since the unit lattice cell acts only two very simply operations, look up table and kicking as described in Section 2.6, the use of special-purpose computational hardware may still yield a computational advantage[24,27].

#### 4): Computational Cost

The *CAM-8* machine (developed in the early of 1990s) is currently available and well suited to the simulation of lattice gas algorithms owing the nature of its architecture as presented in Section 2.6. When making a comparison of computational cost between an *LGA* and *TLM* simulation, N. Simons *et al.*[24] indicated: “*There are two issues related to benchmarking the lattice gas automata approach. The first involves comparing the cost of simulating cellular automata on a traditional general-purpose computer as compared to using CAM-8. The second aspect involves comparing the computational cost of simulating lattice gas automata on CAM-8 to traditional method on general-purpose computers*”. For example, their analysis shows that the computing times required for the two-dimensional lattice gas simulations on *CAM-8* is in the order of 10s of seconds. It is almost the same order as that of the *TLM* method to simulate the same applications on a traditional general-purpose computer (SPARCstation 10). The required computing times, however, for an *LGA* program on a traditional general-purpose computer is in the order of hours. This indicates the enormous benefit in using *CAM-8* for simulating *LGA* in order to be competitive with the traditional numerical approaches. For the simulation of the three-dimensional vector *LGA*, only one initial data is provided and the geometric structures are as

---

shown in Fig.4.1. In this simple simulation, a periodic (wrapped around) boundary condition is specified. Less than 16 bits per cell are required, therefore the complex sub-cell assembling technique[27] is not necessary for this case. For this problem, it took 20 minutes for the *CAM-8* to complete the analysis. The *TLM* simulation program took about 40 minutes on SPARC station 10. For more complex three dimensional structures, the sufficient size of the lattice is required in the massively increasing cell numbers by a factor of  $10^3$  with respect to *TLM* mesh, employing the sub-cell assembling technique. This procedure will stretch the current *CAM-8* resources and it is time-consuming too. To effectively simulate three-dimensional problems, a more powerful cellular automata machine is essential.

## 5.2 Main Contributions

This research mainly focuses on the development of lattice gas automata models in computational electromagnetics and on the mathematical analyses to validate these models. These analyses have been made by considering fundamental microdynamical models, formulating the appropriate equations with Chapman - Enskog method, and verifying the models by conducting simulations on the *CAM-8* machine. The main contributions of this research are:

- Formulated rules and a theory for *2-D HPP* lattice gas mixtures. We have identified the fact that the macroscopic wave behaviour emerging from an *LGA* hydrodynamic system is not sensitive to microscopic interaction details, and is only

limited by the semi-detailed balance and the conservation law.

- Performed the mathematical analysis and numerical experiments to show the validity of the simple *HPP* mixture model in the modelling of the scale wave propagation. Obtained a general formula for the sound speed which enables a wide range of dielectric constants to be modelled by specifying various interaction models in an *LGA*.
- Constructed one possible three-dimensional vector *LGA* model that is capable of simulating three-dimensional electromagnetic phenomena in homogeneous media.
- Performed the mathematical analysis to show how the developed 3-*d* vector *LGA* model can be used to solve the requisite three-dimensional Maxwell's equations. Formulated the Boltzmann equations based on the Chapman-Enskog expansion and the associated mathematics.
- Implemented the 3-*d* vector *LGA* model on the CAM-8 machine, and conducted numerical simulations for some simple electromagnetic wave propagation problems.

### 5.3 Discussion and Proposed Future Works

Lattice gas automata as a new computational electromagnetics technique has been considered. However, current success in this area is preliminary. There are a number of

---

theoretical and computer simulating problems to be explored. Several topics which are promising candidates for further *LGA* research are indicated below:

- We have only performed simple numerical experiments to validate the vector 3-*d* model. We can extend the applications to other vector time-domain electromagnetic field problems, such as waveguide, finned cavity, scattering and radiation problems. However, the general approach to the analysis of the above problems using the model will be essentially the same as that employed with the time-domain differential equation based methods such as *FDTD* and *TLM*. The entire spatial domain of the problems requires discretization, and thus absorbing boundary conditions will be required for open region problems. As well, for the application of lattice gas automata to the modelling of radiation problems, an algorithm for the modelling of excitation is required. Also, problems resulting from limitations on the maximum number of bits per cell in the current CA machine have to be solved.
- We can explore modification of the current 3-*d LGA* vector model or developed a new *LGA* model which has the ability to model the inhomogeneous media in three-dimensions. In the first case, we may incorporate a new transfer event before each current collision event occurs. The new transfer event will allow the moving particles to exchange energy with the background on a lattice. By specifying regions of the lattice to have different mechanisms of energy exchange, a lattice with an inhomogeneous dielectric constant may be modelled.

As an alternative to the 3- $d$  vector lattice described in this document, one of the new trial models capable of modelling inhomogeneous media is the model developed by G.Bridges and N.Simons [28]. In their model, the basic constituent cell is the same cubic cell as used in *FDTD* method[44]. Each cubic cell is decomposed into six sub-cells based on the three coordinate planes. On each sub-cell the simple two-dimensional *HPP* model may be used to specify the collision rules. This then allows us to easily incorporate rest particles with the lattice framework, and to model the different dielectric as discussed in chapters 2 and 3.

- The problem of reducing statistical noise and dissipation effects exhibited in *LGA* simulations has been noticed. As discussed in section 2.4, statistical averaging over a group of cells (say,  $N$  cells) is necessary to obtain macroscopic field quantities. Thus, according to statistical theory, the statistical noise associated with the situation of  $n$  bits per cell of an *LGA* model averaging over blocks of  $N$  cells is of order  $\sim 1/\sqrt{nN}$ . To reduce the noise to a reasonable amount and yield a reasonable dynamic range for macroscopic variables, a higher density of mesh is required than when using a numerical method based on differential equations. Experimental simulations with various field problems indicate that the increased density is on the order of  $\sim 10$ - $30$  per dimension for an *LGA* technique with respect to *TLM* or finite-difference time-domain mesh [40]. To solve the two problems without a massively increasing in the mesh density, a multi-bit variable *LGA* (*ILGA*) model may be an approach to be considered. In an *IGLA* model, more than one bit per lattice direction (per particle state) will be allowed



---

to exist, in contrast with one bit per direction in a common *LGA*. A mathematical analysis has been presented by B.M. Boghosian *et.al* [39] for the *ILGA* models in fluids. Their analysis shows that the *ILGA* models indeed allow for a reduction both in dispersion and statistical noise to some extent. It can be expected that a similar model [45] will serve our purposes in electromagnetics applications. However, the difference between the model presented in [45] and the Boghosian *ILGA* model [39] still needs to be explored.

## References

- [1] E.K. Miller, "A Selective Survey of Computational Electromagnetics" *IEEE Trans. on Antenna and Propagation*, vol. 36, no.9, pp. 1281-1305, September 1988.
- [2] J.A. Stratton, "Electromagnetic Theory", McGraw-Hill Book Company, 1941.
- [3] R.F. Harrington, "Field Computational by Moment Methods", Macmillan, 1969.
- [4] M.N.O. Sadiku, "Numerical Techniques in Electromagnetics", CRC press, 1992.
- [5] G.J. Burk and E.K. Miller, "Modelling Antennas Near to and Penetrating a Lossy Interface" *IEEE Trans. on Antenna and Propagation*, vol. 35, no.10, pp. 1160-1173, October 1987.
- [6] O.C. Zienkiewicz, "Finite Elements in Time Domain", Chapter 13 in State-of the Art Surveys on Finite Element Technology, Ed: A.K. Noor and W.D.Pilkey, 1983.
- [7] L.Lapidus and G.F.Pinder, "Numerical Solution for Partial Differential Equations in Science and Engineering", John Wiley and Sons, 1982.
- [8] W.J.R.Hofer, "The Transmission-Line Matrix (TLM) Method", in *Numerical Techniques for Microwave and Millimeter Wave Passive Structure*, Ed: T.Itoh(ed.), New York, John Wiley,1989.
- [9] S. Wolfram, "Cellular Automaton Supercomputer" *originally published in High-Speed Computer: Scientific Applications and Algorithm Design*,

ed., B. Wilhelmson Robert, University of Illinois Press, 1988.

- [10] S. Wolfram, "Preface to a Special Issue on Cellular Automata", *Phys.D*, vol.10, pp. vii-xii, 1984.
- [11] T. Toffoli, "Cellular Automats as an Alternative to (Rather Than an Approximation of) Partial Differential Equations in Modelling Physics", *Phys.D*, vol.10, pp. 117-127, 1984.
- [12] N. Margolus, "Physics-like Models of Computation", *Phys.D*, vol.10, pp. 81-95, 1984.
- [13] B.M. Boghosian and W. Taylor, "A Quantum Lattice-Gas Model for the Many-Particles Schrodinger Equation in d Dimensions", *International Journal of Modern Physics*, Aug. 1997.
- [14] I. Bialynicki-Birula, "Weyl, Dirac and Maxwell Equations on a Lattice as Unitary Cellular Automata", *Phys. Rev. D*, vol.49 No.12, pp.6920-6926, 1994.
- [15] U. Frisch, B. Hasslacher and Y. Pomeau, "Lattice Gas Automata for the Navier-Stokes Equation", *Phys.Rev. Lett*, vol.56, pp.1505, 1986.
- [16] S. Wolfram, "Cellular Automata Fluids I: Basic Theory", *Journal of Statistical Physics* vol.45, pp. 471-526, 1986.
- [17] H.D. Chen and W.H. Matthaeus, "Cellular Automaton Formulation of Passive Scalar Dynamics", *Physics Fluids* 30, pp. 1235-1237, 1987.
- [18] C. Burges and S. Zaleski, "Buoyant Mixtures of Cellular Automaton Gases", *Complex Syst.* vol.1, pp. 31-50. 1987.
- [19] D.d'Humieres, P. Lallemand and T. Shimonura, "An Experiment Study of Lattice Gas Hydrodynamics" (Los Alamos National Laboratory), Technical Report

LAUR-85-4051, 1985.

- [20] D.H.Rothman, "Cellular-Automaton Fluids: A Model for Flow in Porous Media", *Geophysics* vol.53, pp. 509-518, 1988.
- [21] J.M. Bornholdt and K.D. Tatalias, "the Application of the Lattice Gas Techniques to Electromagnetic Problems", *IEEE Trans., Magnetics*, vol. 25, pp. 2916-2928, July, 1989.
- [22] E. Thiele, "Parallel Implementation of Cellular Systems for Numerical Modeling", *International Journal Numerical Modelling*, vol.5, pp.203-218, 1992.
- [23] N.R.Simons, G. Bridges, B.Podaima and A.Sebak, "Cellular Automata as Environment for Simulating Electromagnetic Phenomena", *IEEE Microwave and Guided Wave letters*, vol.4, pp.247-249, 1994.
- [24] N.R.Simons, M.Cuhaci, N.Adnani and G. Bridges, "On the Potential Use of Cellular Automata Machines for Electromagnetic Field Solutions", *International Journal Numerical Modelling*, vol.8, pp.301-312, 1995.
- [25] N.R.Simons, Chapter 7 of N.R.Simons' PhD Dissertation, University of Manitoba, 1995.
- [26] J.Hardy, O.de Pazzis and Y.Pomeau, "Molecular Dynamics of a Classical Lattice Gas: Transport Properties and Time Correction Functions", *Phys. Rev.A*, vol.13, pp.1449-1961, 1976.
- [27] N.Margolus, "CAM-8: a Computer Architecture Based on Cellular Automata", *Pattern Formation and Lattice Gas Automata*, American Mathematics Society (Field Institute Series), Providence RI, 1995.

- [28] G. Bridges, N.R. Simons, D. Cule, M. Zhang and M. Cuhaci, "Application of the Lattice Gas Automata Technique to modelling Wave Interaction with Biological Media", *Proceedings of the IEEE 10th International Conference Antennas and Propagation*, vol.2, pp.2.286-2.289, April, 1997.
- [29] N. Adnani, M. Zhang, D. Cule, N.R. Simons, G. Bridges and M. Cuhaci, "Proceedings of Symposium on Antenna Technology and Applied Electromagnetics, (Montreal, Canada), WA2, pp.203-209, Aug. 1996.
- [30] N.R. Simons and G. Bridges, "Cellular Automata and Computational Electromagnetics", *Private Communication*, 1996.
- [31] U. Frisch, D. d'Humieres, B. Hasslacher, P. Lallemand, Y. Pomeau and J.P. Rivert, "Lattice Hydrodynamics in two and three dimensions", *Complex Syst.* vol.1, pp. 649-707, 1987.
- [32] D. Rothman and S. Zaleski, "Lattice-Gas models for Phase Separation: Interface, Phase Transitions and Multiphase Flow", *Rev. of Modern Phys.*, vol.66, No.4, pp. 1417-1479, 1994.
- [33] B.M. Boghosian and W. Taylor, "Corrections and Renormalization in Lattice Gases", *Phys. Rev.E*, vol.52, pp.510-554, 1995.
- [34] D. d'Humieres and P. Lallemand, "Numerical Simulations of Hydrodynamics with Lattice Gas Automata in Two Dimensions", *Complex Syst.* vol.1, pp. 599-632, 1987.
- [35] J. Lovetri and N.R. Simons, "A Class of Symmetrical Condensed Node TLM Methods Derived Directly from Maxwell's Equation", *IEEE Trans. Microwave Theory and Techniques*, vol.41, pp. 1419-1428, 1993.

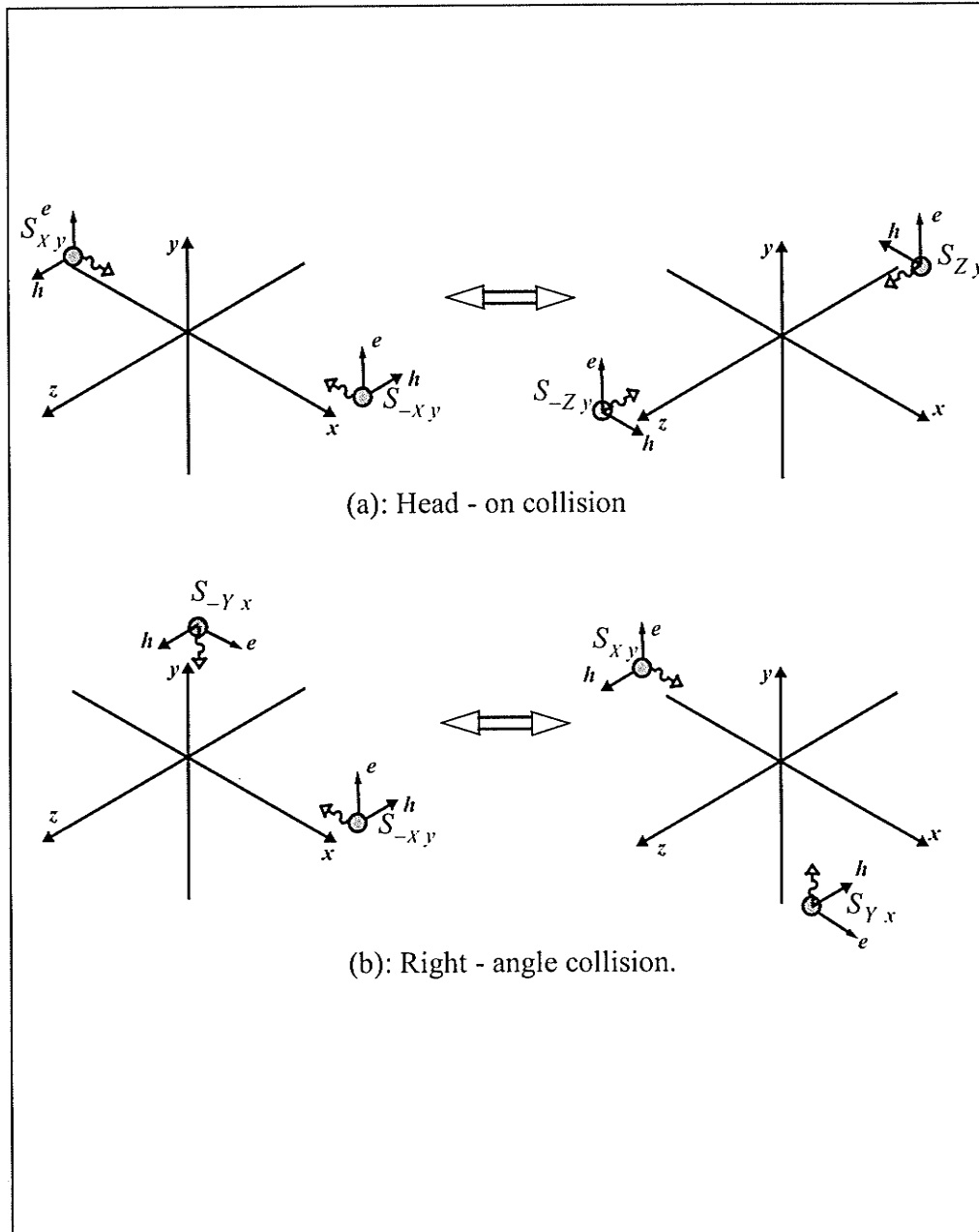
- [36] D. Cule, *HPP Lattice-Gas Automata for Computational Electromagnetics*, Msc thesis, University of Manitoba, 1998.
- [37] N. Adnani, *Cellular Automata for the Two Dimensional Scalar Wave Equation*, Msc thesis, University of Manitoba, May, 1996.
- [38] M.A.Smith, "Cellular Automata Methods in Mathematical Physics", PhD dissertation, pp.15-75, MIT, USA, 1994.
- [39] B.M.Boghossian, J. Yepez, F.J. Alexander and N.H. Margolus, "Integer Lattice Gases", *Phys. Rev.E*, vol.55, pp.4137-4147, 1997.
- [40] D.Cule, N.R.Simons, G. Bridges J. LoVetri and M.Cuhaci, "Investigation of Geometrically Small Features with the Numerical Solutions to Electromagnetic Field Problems". *Proceedings of Symposium on Antenna Technology and Applied Electromagnetics*, (Montreal, Canada), WA2, pp.223-226, Aug. 1996.
- [41] S.Chapman and T. Cowling, "The Mathematical Theory of Non-Uniform Gases", 3rd.ed., Cambridge University, Cambridge, England, 1970.
- [42] M. Zhang, D. Cule, L. Shafai, G. Bridges and N. Simons Computational Electromagnetic Field in Inhomogeneous Media, Proc. Of symposium on Antenna Technology and Applied Electromagnetics, (Ottawa, Canada), pp.527-533, Aug., 1998.
- [43] S.Campell and C.D. Mayer, "Generalized Inverse of Linear Transformations", Dover pub., Inc., New York, 1991.
- [44] A.R. Mitchell and D.F.Griffiths, "Finite Difference Method in Partial differential Equations", Wiley, New York, 1980.

- [45] G. Bridges and N.R.Simons, "Multi-Bit Lattice Gas Automata for Computational Electromagnetics", *Proceedings of USNC/URSI Radio Science Meeting* (Montreal, Canada), B124.5, July, 1997.

# APPENDIX A

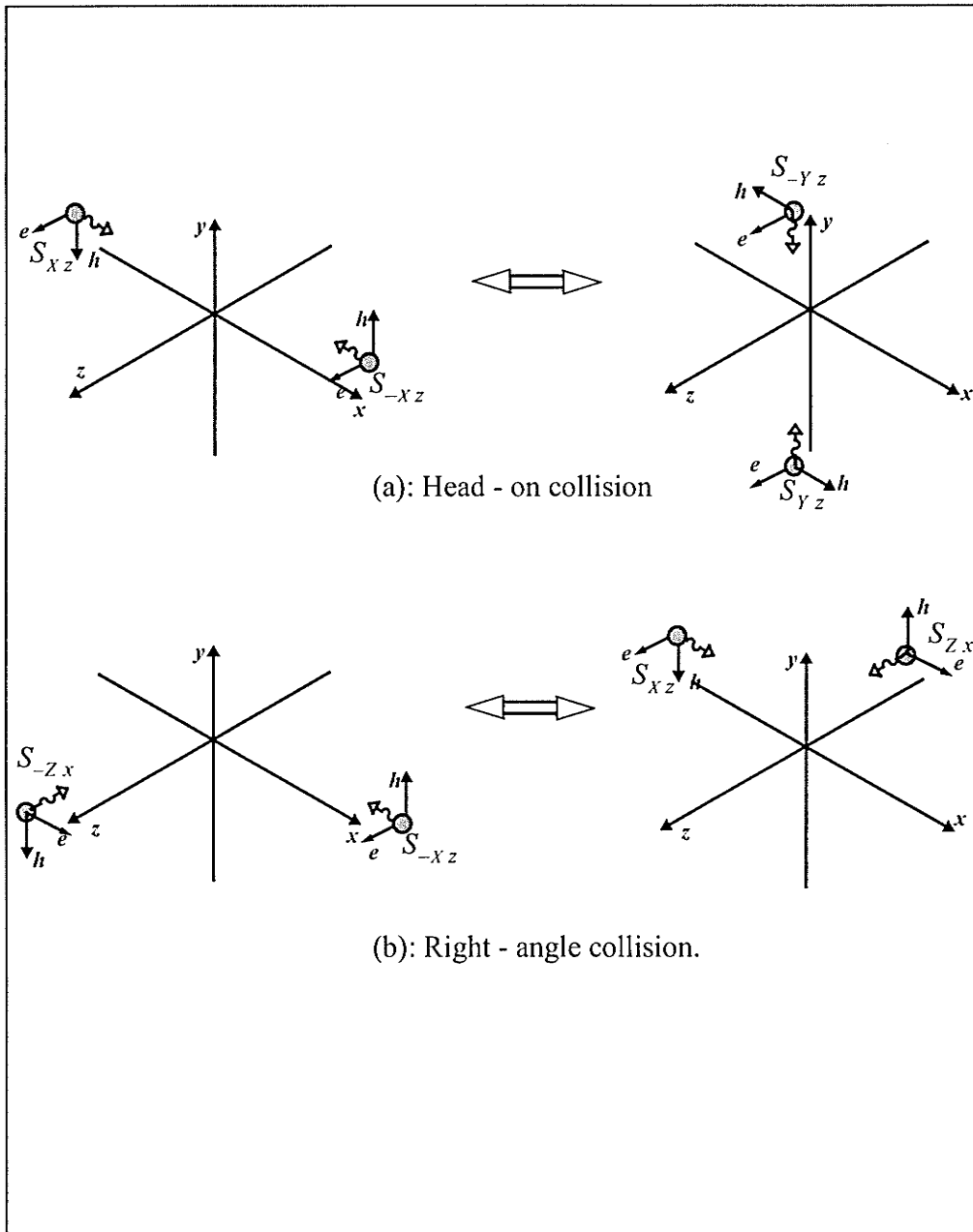
## Appendix A

The collision rules of the 3-*d* vector *LGA* model are listed below for the reference.

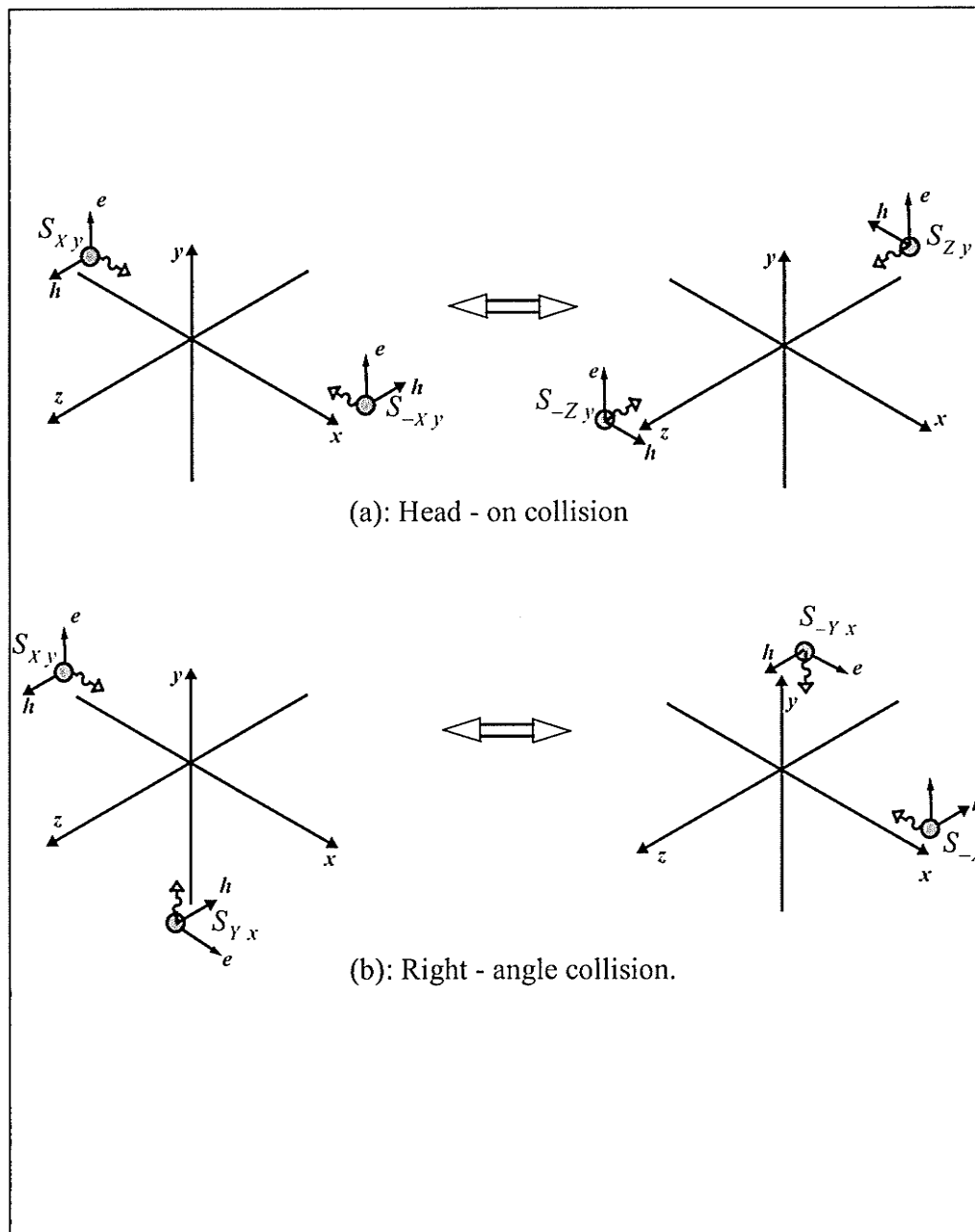




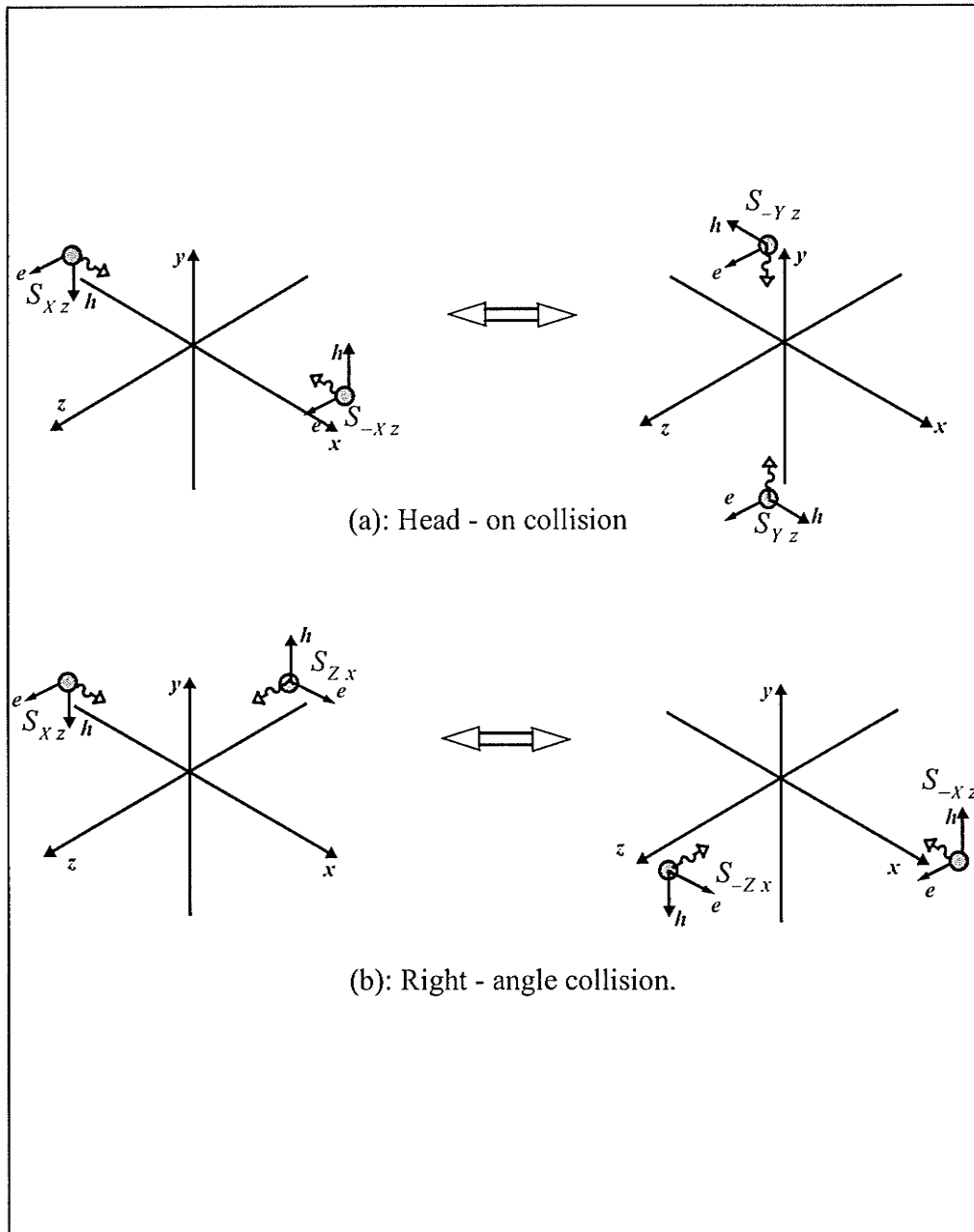
# APPENDIX A



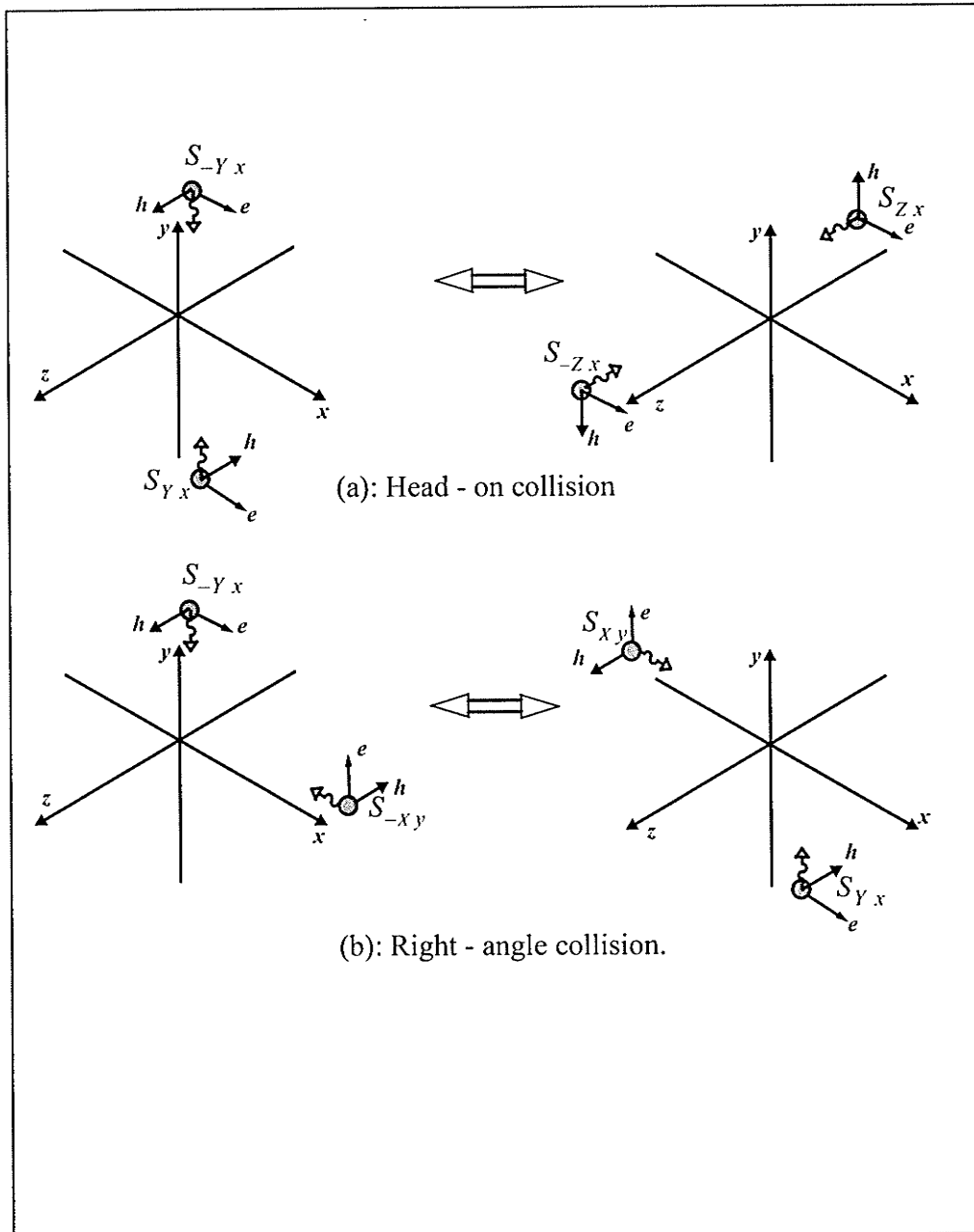
# APPENDIX A



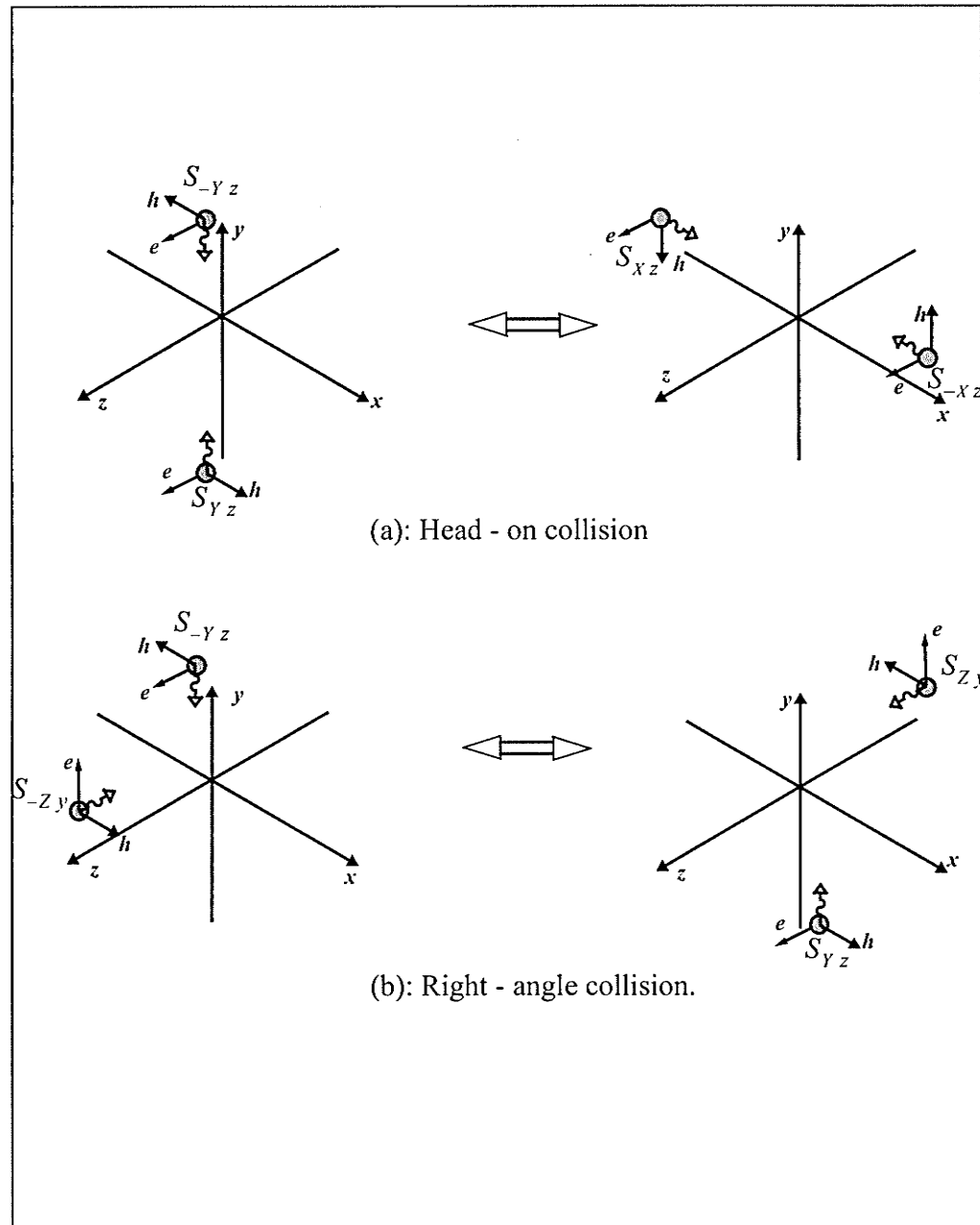
# APPENDIX A



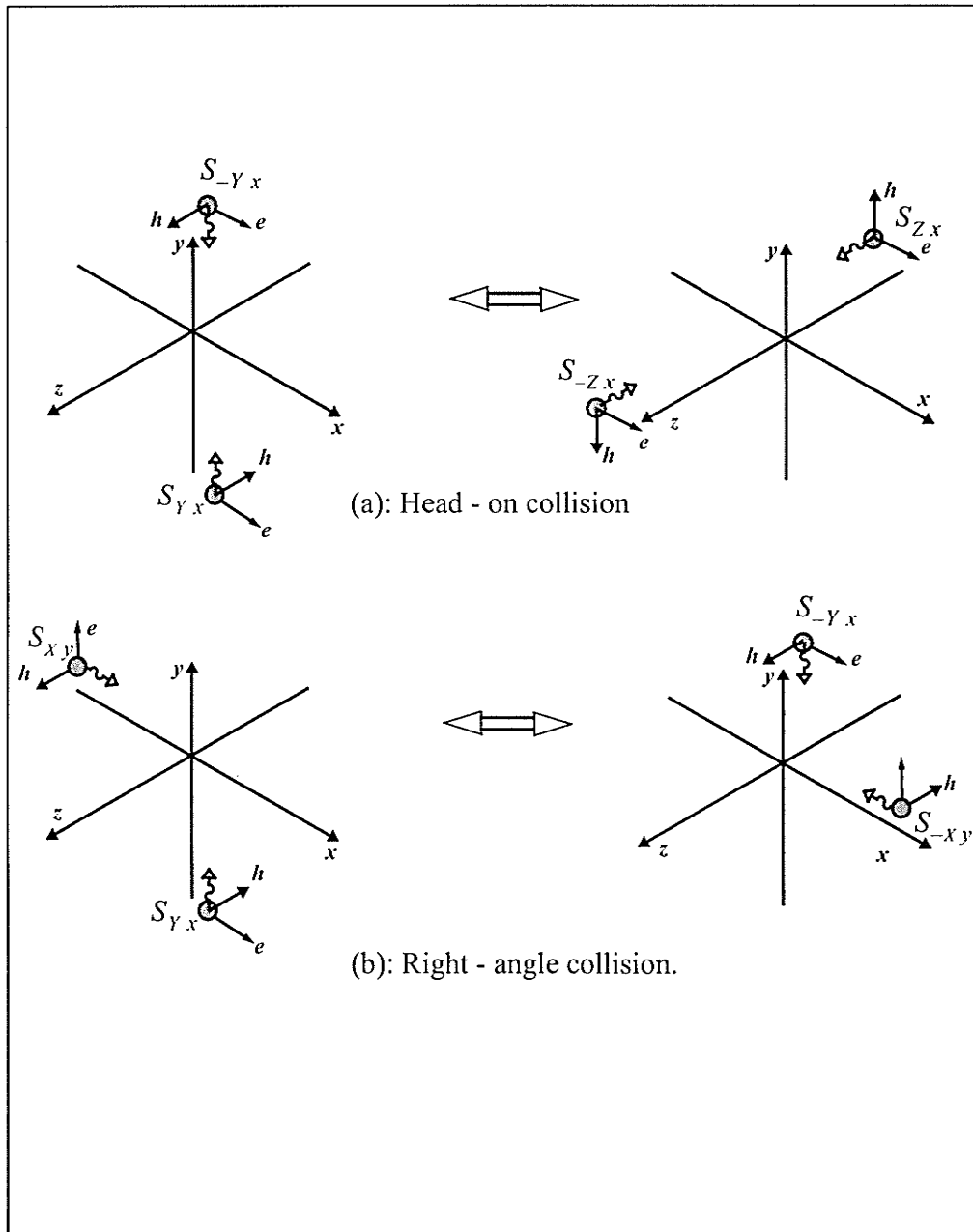
# APPENDIX A



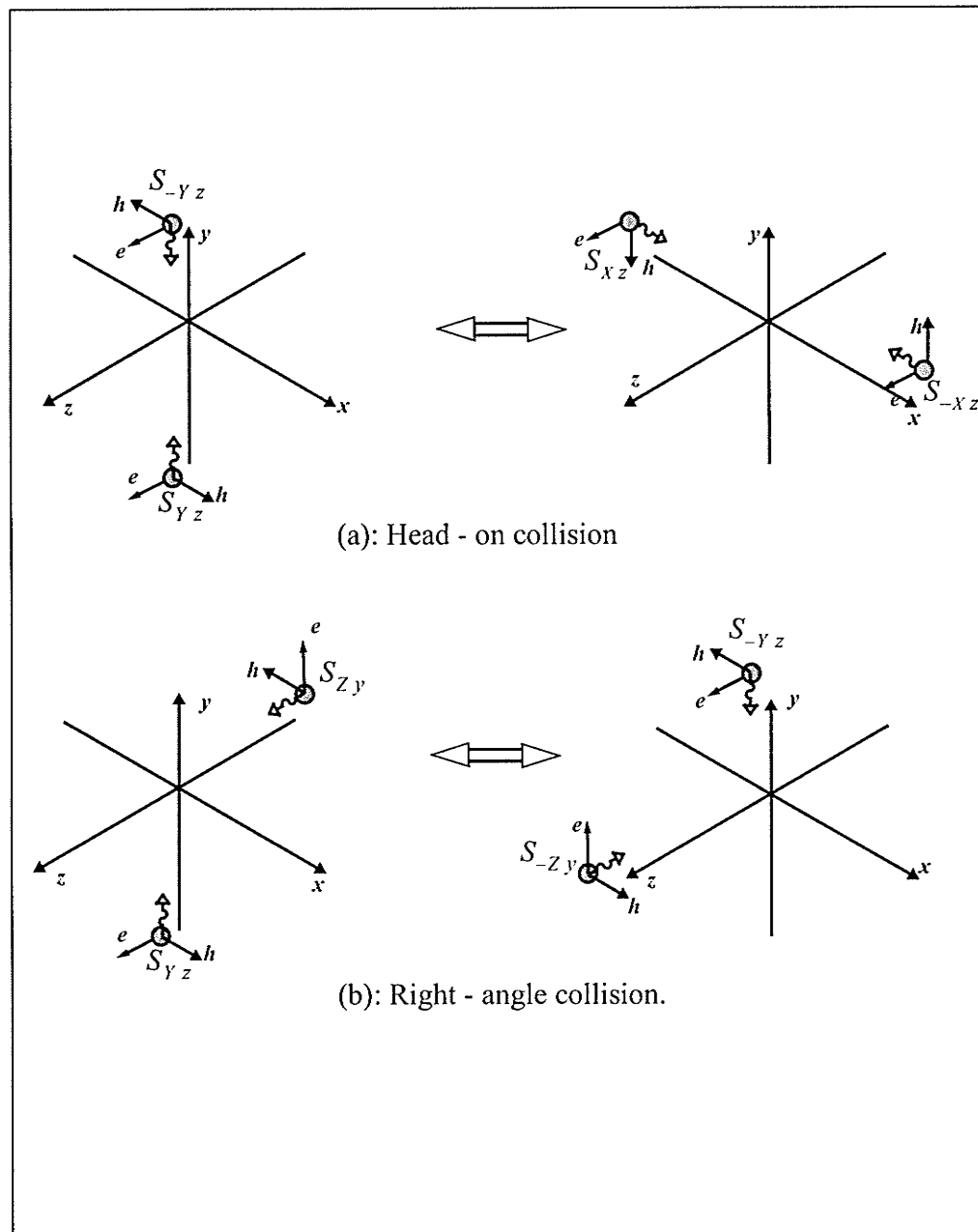
# APPENDIX A



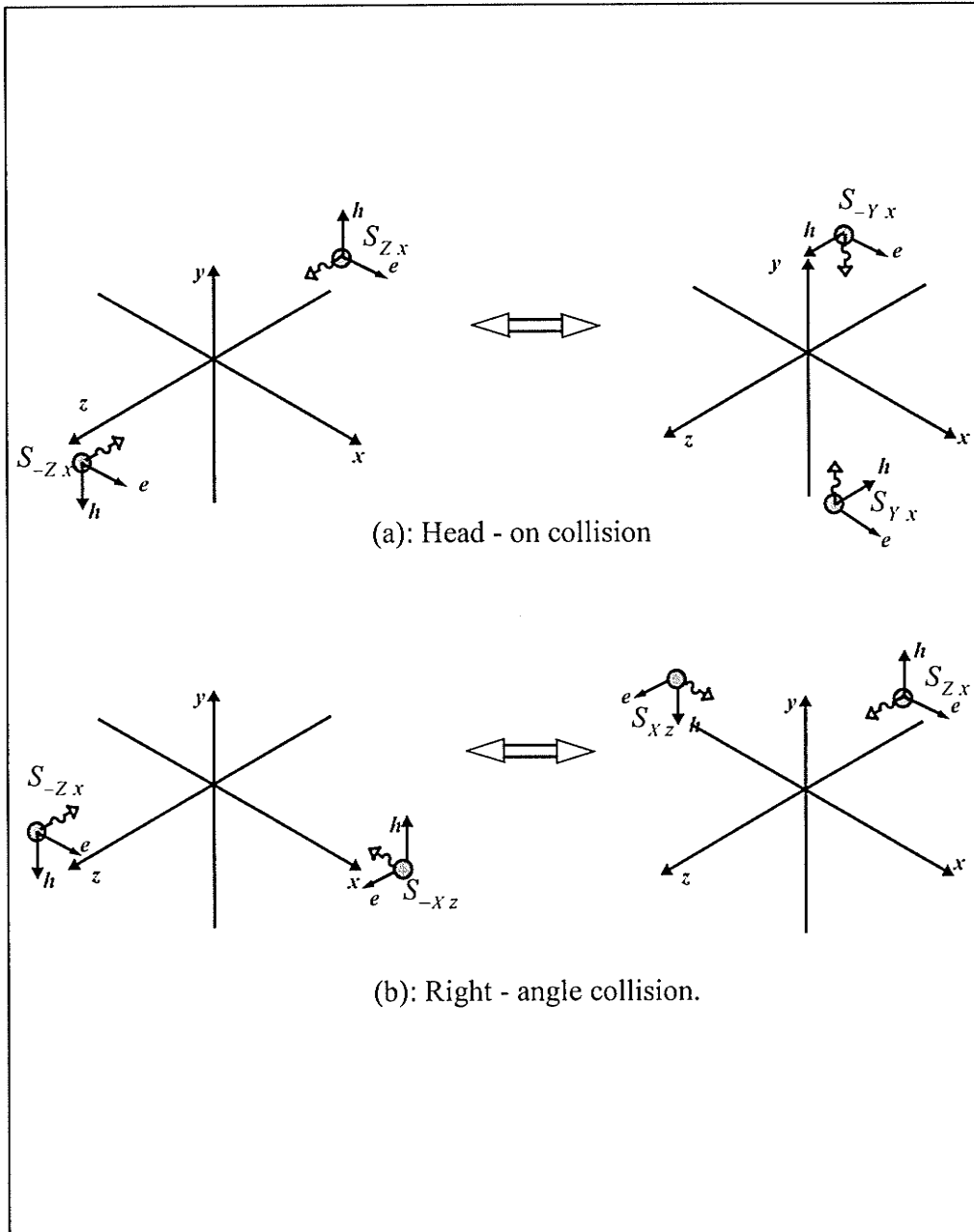
# APPENDIX A



# APPENDIX A

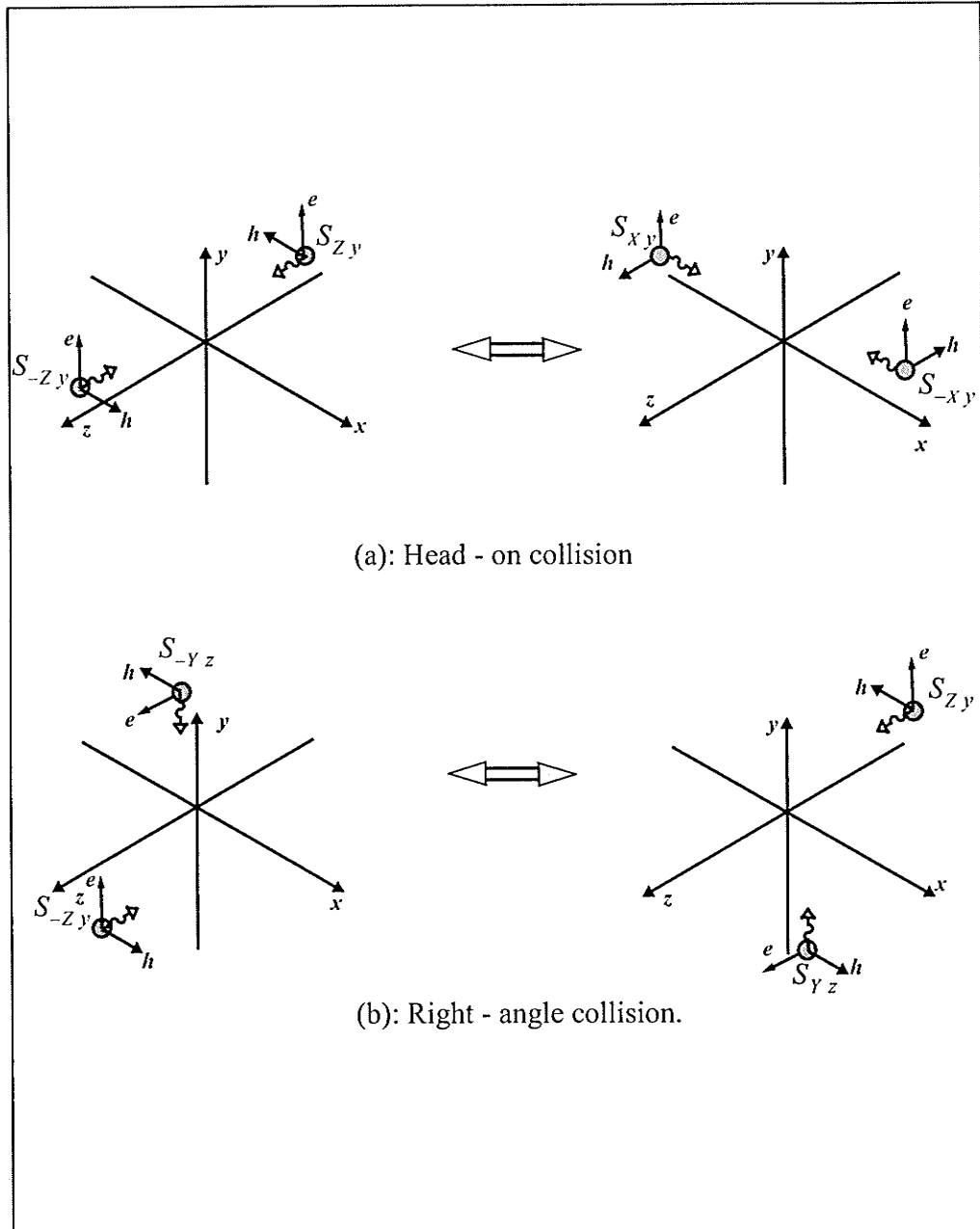


# APPENDIX A

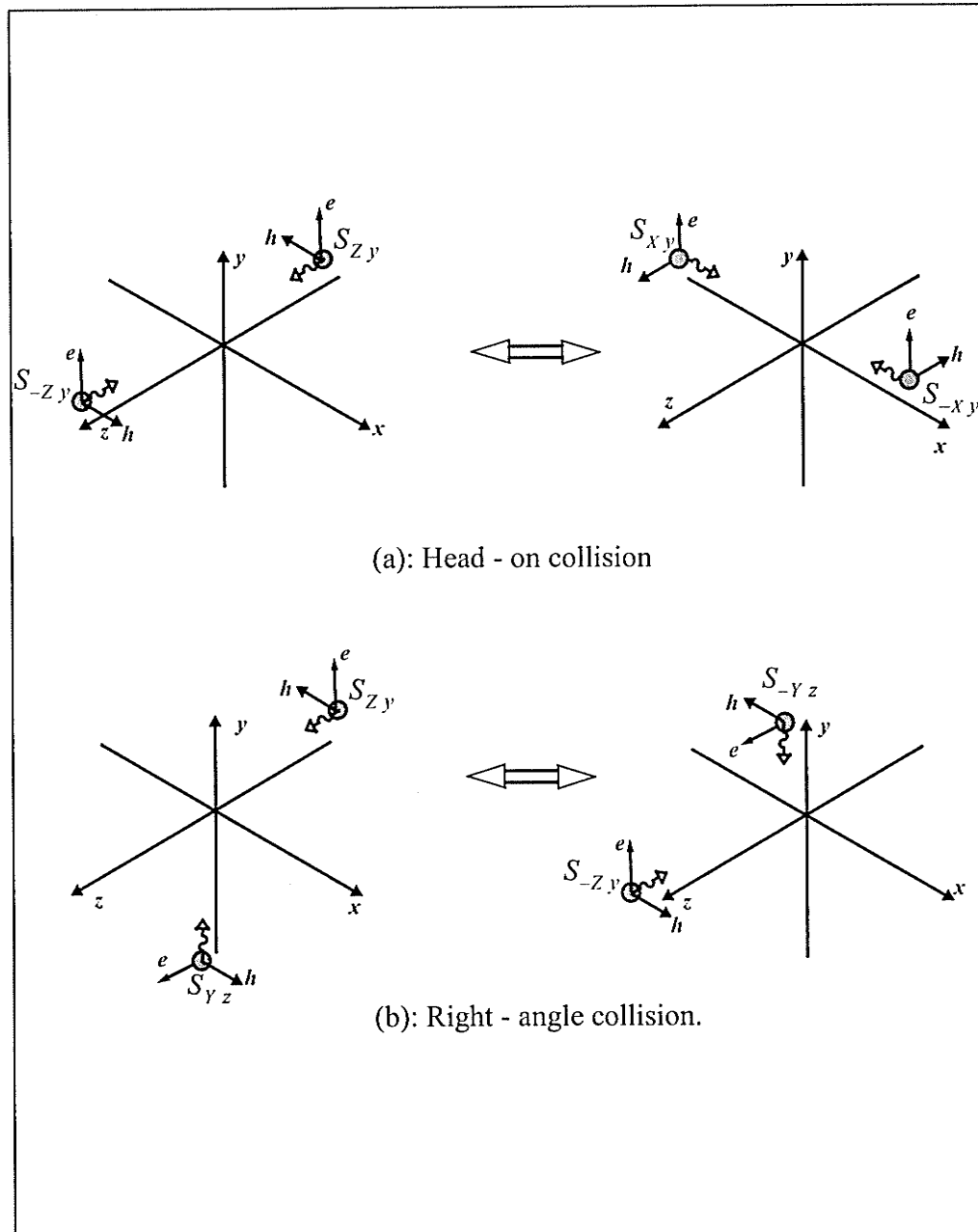




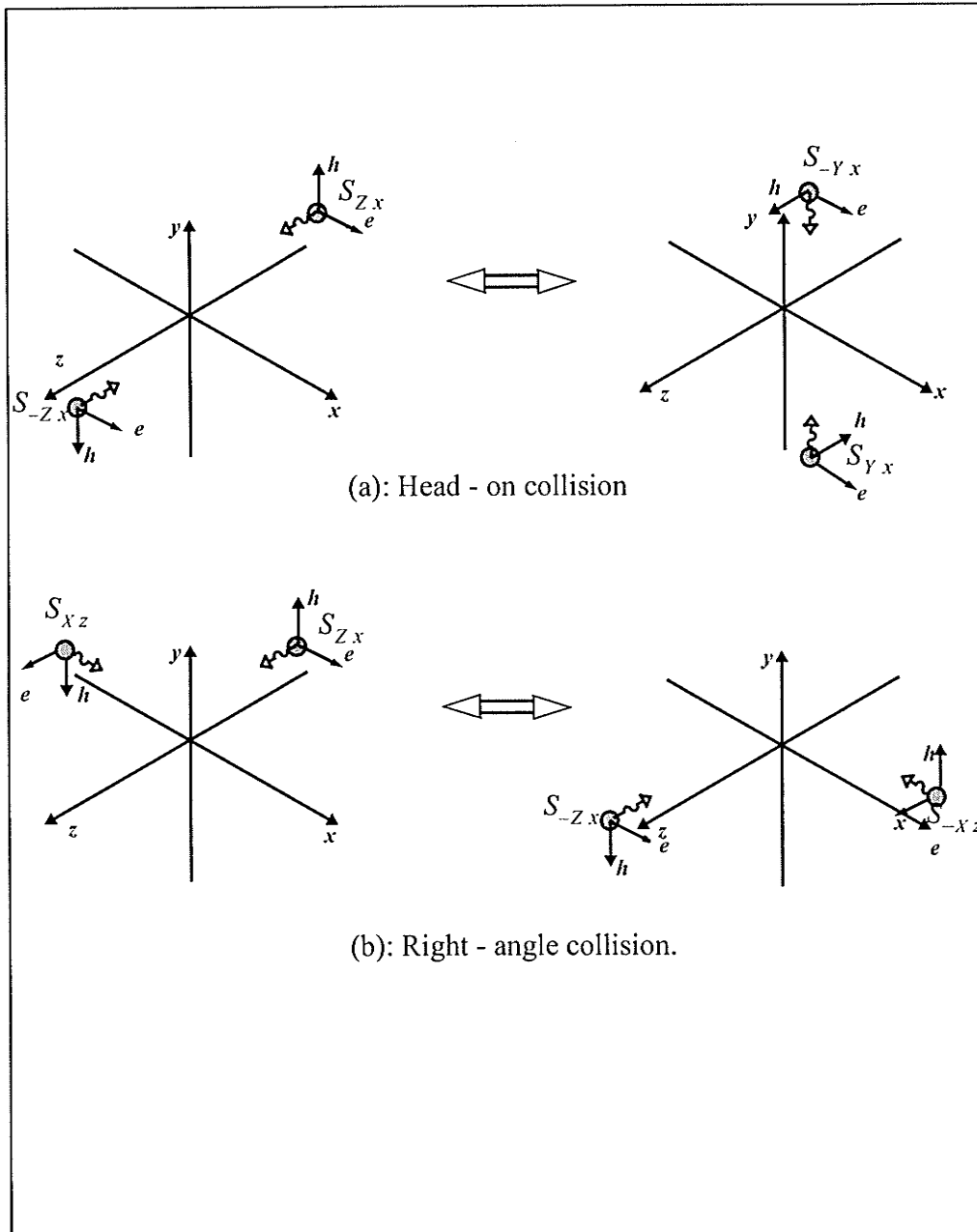
# APPENDIX A



# APPENDIX A



# APPENDIX A



## Appendix B Interaction Mixture Calculation

This appendix gives details of calculation of the interaction matrix which is given as Equations(4.33) and (4.34) in Section 4.2. The elements are defined as the differential of collision operators  $\Omega_{\pm J i}$  with respect to  $N_{\pm K m}$ :

$$(T_D)_{\pm K, m}^{\pm J, i} = \left( \frac{\partial \Omega_{\pm J i}}{\partial N_{\pm K m}} \right) \Big|_{N^\dagger = N^{eq}}, \quad (\text{B.1})$$

where if  $J \in (\pm X)$ ,  $i \in (y \cdot z)$ ,  $J \in (\pm Y)$ ,  $i \in (z \cdot x)$  and  $J \in (\pm Z)$ ,  $i \in (x \cdot y)$ . The  $N^\dagger$  stands for the complete set of variables  $N_{\pm K m}$ , and if at an equilibrium,  $N^\dagger = N^{eq} = f$  (background density).

Here the calculation for the elements of the first and sixth rows in the matrix  $T_D$  is given below as a reference.

1): The elements of the first row of  $T_D$  are related with the collision operator  $\Omega_{-Xy}$ .

From the expression of (4.13), that is,

$$\Omega_{-Xy} = \overline{N_{-Xy}} [N_{Zy} N_{-Zy} \overline{N_{Xy}} + N_{Xy} N_{Yx} \overline{N_{-Yx}}] - N_{-Xy} [\overline{N_{Zy} N_{-Zy} N_{Xy}} + \overline{N_{Xy} N_{Yx} N_{-Yx}}]. \quad (\text{B.2})$$

Using (B.2), the elements can be calculated below.

$$\begin{aligned} \left( \frac{\partial \Omega_{-Xy}}{\partial N_{-Xy}} \right) \Big|_{N^\dagger = f} &= -2f(1-f), & \left( \frac{\partial \Omega_{-Xy}}{\partial N_{-Xz}} \right) \Big|_{N^\dagger = f} &= 0, \\ \left( \frac{\partial \Omega_{-Xy}}{\partial N_{Xy}} \right) \Big|_{N^\dagger = f} &= 0, & \left( \frac{\partial \Omega_{-Xy}}{\partial N_{Xz}} \right) \Big|_{N^\dagger = f} &= 0, \end{aligned}$$

## APPENDIX B

$$\left( \frac{\partial \Omega_{-Xy}}{\partial N_{-Yx}} \right) \Big|_{N^* = f} = -f(1-f), \quad \left( \frac{\partial \Omega_{-Xy}}{\partial N_{-Yz}} \right) \Big|_{N^* = f} = 0,$$

$$\left( \frac{\partial \Omega_{-Xy}}{\partial N_{Yx}} \right) \Big|_{N^* = f} = 0, \quad \left( \frac{\partial \Omega_{-Xy}}{\partial N_{Yz}} \right) \Big|_{N^* = f} = 0,$$

$$\left( \frac{\partial \Omega_{-Xy}}{\partial N_{-Zx}} \right) \Big|_{N^* = f} = 0, \quad \left( \frac{\partial \Omega_{-Xy}}{\partial N_{-Zy}} \right) \Big|_{N^* = f} = f(1-f),$$

$$\left( \frac{\partial \Omega_{-Xy}}{\partial N_{Zy}} \right) \Big|_{N^* = f} = f(1-f), \quad \left( \frac{\partial \Omega_{-Xy}}{\partial N_{Zx}} \right) \Big|_{N^* = f} = 0.$$

Thus, the elements on the first row of  $T_D$  are obtained as:

$$f(1-f)(-2, 0, 0, 0, -1, 0, 1, 0, 0, 1, 1, 0)$$

2); For the elements of the sixth row of  $T_D$ , it follows from the collision operator

$\Omega_{-Yz}$  (4.18):

$$\Omega_{-Yz} = \overline{N_{-Yz}} [N_{Xz} \overline{N_{-Xz}} \overline{N_{Yz}} + N_{Zy} \overline{N_{Yz}} \overline{N_{-Zy}}] - N_{-Yz} [\overline{N_{Xz}} \overline{N_{-Xz}} N_{Yz} + \overline{N_{Yz}} \overline{N_{Zy}} N_{-Zy}]$$

(B.3)

that we have

$$\left( \frac{\partial \Omega_{-Yz}}{\partial N_{-Xy}} \right) \Big|_{N^* = f} = 0, \quad \left( \frac{\partial \Omega_{-Yz}}{\partial N_{-Xz}} \right) \Big|_{N^* = f} = f(1-f),$$

$$\left( \frac{\partial \Omega_{-Yz}}{\partial N_{Xy}} \right) \Big|_{N^* = f} = 0, \quad \left( \frac{\partial \Omega_{-Yz}}{\partial N_{Xz}} \right) \Big|_{N^* = f} = f(1-f),$$

## APPENDIX B

$$\left(\frac{\partial \Omega_{-Yz}}{\partial N_{-Yx}}\right)\bigg|_{N^* = f} = 0, \quad \left(\frac{\partial \Omega_{-Yz}}{\partial N_{-Yz}}\right)\bigg|_{N^* = f} = -2f(1-f),$$

$$\left(\frac{\partial \Omega_{-Yz}}{\partial N_{Yx}}\right)\bigg|_{N^* = f} = 0, \quad \left(\frac{\partial \Omega_{-Yz}}{\partial N_{Yz}}\right)\bigg|_{N^* = f} = 0,$$

$$\left(\frac{\partial \Omega_{-Yz}}{\partial N_{-Zx}}\right)\bigg|_{N^* = f} = 0, \quad \left(\frac{\partial \Omega_{-Yz}}{\partial N_{-Zy}}\right)\bigg|_{N^* = f} = -f(1-f),$$

$$\left(\frac{\partial \Omega_{-Yz}}{\partial N_{Zy}}\right)\bigg|_{N^* = f} = f(1-f), \quad \left(\frac{\partial \Omega_{-Yz}}{\partial N_{Zx}}\right)\bigg|_{N^* = f} = 0,$$

and the elements as:

$$f(1-f)(0, 1, 0, 1, 0, -2, 0, 0, 0, -1, 1, 0).$$

The other row elements can be straightforwardly calculated in the same way.